

American Journal of Science

DECEMBER 1974

THEORETICAL PREDICTION OF THE THERMODYNAMIC BEHAVIOR OF AQUEOUS ELECTROLYTES AT HIGH PRESSURES AND TEMPERATURES: I. SUMMARY OF THE THERMODYNAMIC/ELECTROSTATIC PROPERTIES OF THE SOLVENT

HAROLD C. HELGESON and DAVID H. KIRKHAM

Department of Geology and Geophysics, University of California,
Berkeley, California 94720

ABSTRACT. Thermodynamic/electrostatic properties of H₂O at high pressures and temperatures were calculated from regression equations representing dielectric constant data reported by Oshry (ms), Owen and others (1961), and Heger (ms) for temperatures and pressures from 0° to 550°C and 0.001 to 5 kb together with finite difference derivatives computed from specific volumes given by Burnham, Holloway, and Davis (1969b) for 20° to 900°C and 1 to 10 kb. Corresponding properties below a kilobar were computed with the aid of the equation of state developed by Keenan and others (1969), which describes the thermodynamic behavior of H₂O in close accord with the tolerances of the International Skeleton Tables of 1963. The results of the calculations are given in equations, tables, and diagrams depicting isotherms, isobars, and isopleths of specific volume, entropy, enthalpy, internal energy, Helmholtz and Gibbs free energies, fugacity, and heat capacity, together with the dielectric constant, coefficients of isobaric thermal expansion and isothermal compressibility, the Born (1920) free energy function, and their partial derivatives. Perturbation of the thermodynamic/electrostatic behavior of H₂O by the critical phenomenon leads to significant differences in the dependence of its properties on temperature, pressure, and density above and below ~ 400°C and ~ 1 to 2 kb. The calculations permit prediction of the consequences of these differences on the chemical interaction of minerals and aqueous electrolyte solutions in geochemical processes.

INTRODUCTION

Recent advances in solution chemistry, thermodynamics, and computer technology make it possible to describe quantitatively equilibrium and mass transfer among minerals and aqueous electrolytes in geochemical processes involving large numbers of components, phases, and chemical species at both high and low temperatures and pressures. The present series of communications is intended to provide a comprehensive set of equations and data to facilitate such calculations.

Theoretical and experimental studies of hydrothermal systems over the past 50 years leave little doubt that mineral solubilities and the chemical and thermodynamic behavior of solute species in aqueous electrolytes are controlled to a large extent by the thermodynamic/electrostatic properties of the solvent, which change dramatically with increasing temperature and pressure. The equations, tables, and diagrams presented below constitute an internally consistent summary of these properties, based on critical evaluation and regression of density and dielectric constant data reported in the literature for temperatures and

pressures from 0° to 900°C and 0.001 to 10 kb. These conditions bracket those found in the Earth from its surface to a lithostatic depth of ~ 35 km, which is equivalent in pressure to a hydrostatic depth of ~ 100 km. The temperature span ranges from the stability fields of ice I and VI to the low-pressure melting temperatures of hydrous silicate rocks.

The thermodynamic properties of H₂O have long been of interest to engineers responsible for power generation and in recent decades to geologists concerned with geochemical and geophysical processes at high temperatures and pressures. As a consequence, a plethora of steam tables and other compilations has appeared through the years, most of which cater to engineers and are too restricted in the scope of pressures, temperatures, and/or the properties considered to be generally applicable in science. Many of the compilations are based on conventions and expressed in units that are inconvenient in a geochemical context, some are insufficiently detailed, and none includes all properties of interest in solution chemistry. Among the more important of these is the dielectric constant and its partial derivatives with respect to pressure and temperature. The latter variables can be used in conjunction with expansibilities, compressibilities, and other thermodynamic properties of H₂O to compute electrostatic parameters in the Debye-Hückel theory, evaluate Born charging equations, and formulate algorithms and equations of state for predicting and correlating the thermodynamic properties of aqueous electrolytes at high pressures and temperatures.

REVIEW OF PREVIOUS WORK

A multitude of experimental and theoretical studies of the thermodynamic properties of steam, water, and ice has accumulated in the century and a half since Carnot (1824) published his famous memoir on the power of heat, but only in the last 50 years have systematic and coordinated efforts been made to compile accurate data of high precision in a comprehensive and organized program of research. Following the appearance of the International Critical Tables in 1928, the First International Conference on the Properties of Steam was organized to establish tolerances and compile a set of skeleton tables listing accepted values for the thermodynamic properties of H₂O. The skeleton tables compiled at this conference provided the basis for the ASME steam tables of 1930 (Keenan, 1930). Two years later, Mollier's (1932) tables and diagrams appeared almost simultaneously with those of Knoblauch and others (1932). At the Third International Conference on the Properties of Steam in 1934, agreement was reached on a revised and expanded set of skeleton tables and tolerances for temperatures ≤ 550°C and pressures ≤ 300 bars. Shortly thereafter, Keenan and Keyes (1936) produced the first comprehensive set of steam tables for temperatures and pressures from 0° to 871°C and 0 to 380 bars. The latter tables, which proved to be highly reliable and widely used, were based on a critical review of the literature and an equation of state derived from precise pressure-volume-temperature measurements from 0° to 460°C and 0 to 350 atm (Smith and Keyes,

1934; Keyes, Smith, and Gerry, 1936). These data, together with many others, were reported in Dorsey's (1940) exhaustive review and compilation of the properties of H_2O , which has been complemented recently by extensive critiques of the physical chemistry of water (Horne, 1969, 1972; Franks, 1972).

International conferences on the properties of steam have been held intermittently since 1934, but it was not until the sixth conference in 1963 that agreement was reached on a revised and enlarged set of skeleton tables extending from 0° to 800°C and from 0 to 1 kb. The advent of high-speed computers and the skeleton tables compiled at the third and sixth international conferences on the properties of steam generated a myriad of regression and interpolation formulas, equations of state, and steam tables, which have appeared in steady succession since World War II (for example, Callendar and Egerton, 1944, 1958; Schall, 1950; Dzung and Rohrbach, 1955; Vukalovich, 1958; Vukalovich and others, 1959; Nowak and Grosh, 1961; Bain, 1964; Juza, Kmoniček, and Šifner, 1966; Meyer and others, 1967; Schmidt, 1969; Papetti and Fujisaki, 1971; Barker and Henderson, 1972; Seegers and Greer, 1972). In recent years efforts have been made to extend the level of precision of pressure-volume-temperature measurements (for example, Owen, White, and Smith, 1956; Kell, 1967; Kell and Whalley, 1965; Kell, McLaurin, and Whalley, 1968; Millero, Curry, and Drost-Hansen, 1969; Rowe and Chou, 1970; Grindley and Lind, 1971; Gildseth, Habenschuss, and Spedding, 1972; Greene, Beachey, and Milne, 1972; Millero, Knox, and Emmet, 1972; Wang and Millero, 1973; Fine and Millero, 1973), and in 1965 the International Formulation Committee reached agreement on the form of the equations to be used by the International Conference on the Properties of Steam for computer representation of the skeleton tables (Internat. Formulation Comm., 1967, 1968).

Measurements of the specific volume of H_2O at high pressures and low temperatures have been carried out since the turn of the century (for example, Amagat, 1893; Bridgeman, 1913, 1931, 1935; Adams, 1931), but it was not until Kennedy (1950) applied modern technology to check and extend early reconnaissance measurements (Tamman and Rührenbeck, 1932; Goranson, 1938) that reliable data became available for pressures above a kilobar at high temperatures. Since then, numerous experimental and theoretical studies of the density of H_2O at high pressures and temperatures have appeared (for example, Kennedy, 1957; Kennedy, Knight, and Holser, 1958; Holser and Kennedy, 1958, 1959; Howard, 1961; Maier and Franck, 1966; Walsh and Rice, 1957; Rice and Walsh, 1957; Al'tshuler, Bakanova, and Trunin, 1958; Sharp, 1962; Köster and Franck, 1969; Grindley and Lind, 1971), but none has been as systematic and comprehensive as that reported by Burnham, Holloway, and Davis (1969a, and b). Repeated calculations of the fugacity and other properties of H_2O at high temperatures and pressures have been made from these various data (for example, Holser, 1954; Pistorius and Sharp, 1960, 1961; Anderson, 1964, 1967; Burnham, Holloway, and Davis, 1969b; Haas,

1970; Holloway, Egger, and Davis, 1971), most of which are in general (but not always close) agreement with one another.

In the same year that Burnham, Holloway and Davis' data became available, Keenan and others (1969) published an independent set of steam tables for the thermodynamic properties of H₂O to 1300°C and 1 kb based on critical evaluation of precise experimental data reported in the literature and a remarkably versatile "fundamental" equation for the Helmholtz free energy (relative to zero entropy of H₂O_{liquid} at the triple point) as a function of temperature and density. Also in the same year, Heger (ms) reported his measurements of the dielectric constant of H₂O at high temperatures and pressures. All three of these outstanding contributions have been of inestimable value to the present study.

The electrostatic properties of H₂O have received extensive experimental and theoretical attention through the years, particularly at low temperatures and pressures (for example, Wyman, 1930; Åkerlöf, 1932; Wyman and Ingalls, 1938; Kirkwood, 1939; Dorsey, 1940; Oster and Kirkwood, 1943; Malmberg and Maryott, 1956; Cole, 1960; Hasted, 1961, 1972; Vidulich and Kay, 1962; Vidulich, Evans, and Kay, 1967; Kay, Vidulich, and Pribadi, 1969). The dielectric constant of saturated water from 100°C to the critical temperature was measured by Oshry (ms; Åkerlöf and Oshry, 1950), and Fogo, Benson, and Copeland (1954) published values for steam from 377° to 395°C at densities from 0.1 to 0.5 g cm⁻³. In recent years, measurements of the dielectric constant at high pressures and low temperatures (for example, Kyropoulos, 1926; Lees, ms; Harris, Haycock, and Alder, 1953; Scaife, 1955; Owen and others, 1961) have been extended to high temperatures (Gier and Young, 1963; Heger, ms). Although considerable discrepancy exists among these various sets of data, they afford close estimates of the electrostatic behavior of H₂O in the supercritical region (Franck, 1956; Quist and Marshall, 1965; Franck, 1969; Jansoone and Franck, 1972). These estimates have been used in conjunction with viscosity and conductance measurements to compute activity product constants of H₂O, which are now available to 1000°C and 120 kb (David and Hamann, 1959, 1960; Franck, 1961; Dudziak and Franck, 1966; Holzapfel and Franck, 1966; Quist, 1970; Fisher and Barnes, 1972; Whitfield, 1972; Millero, Hoff, and Kahn, 1972). A number of the thermodynamic, transport, and electrostatic properties of H₂O at both low and high pressures and temperatures have been reviewed recently by Franck (1969), Kell (1972), and Tödheide (1972).

The outstanding progress made in the last decade toward documenting and expanding the state of knowledge concerning the thermodynamic/electrostatic behavior of H₂O at high pressures and temperatures will no doubt be considered in depth at the 1974 International Conference on the Properties of Steam. Hopefully, the members of that conference will expand the scope of the steam tables to include all properties of interest in solution chemistry, geology, and other scientific disciplines concerned with H₂O at high pressures and temperatures.

CONVENTIONS, UNITS, AND NOTATION

The standard state for H_2O adopted in this study is one of unit fugacity (f) of the *hypothetical* perfect gas at 1 bar and any specified temperature. Accordingly, the compressibility factor (z) and the fugacity coefficient (χ) of H_2O approach unity as $P \rightarrow 0$, and the activity (a) and fugacity of H_2O are equal at all pressures and temperatures. Because the fugacities and fugacity coefficients reported below for both the liquid and gas phase regions are based on the standard state properties of steam (that is, those of the hypothetical perfect gas at 1 bar), the activities of $\text{H}_2\text{O}_{\text{liquid}}$ and $\text{H}_2\text{O}_{\text{gas}}$ are equal at saturation. At 1 bar and temperatures below 100°C , the fugacity coefficient of H_2O corresponds to that of metastable steam, which becomes increasingly nonideal as temperature decreases. However, as temperature increases to $\sim 600^\circ\text{C}$ at 1 bar, $\chi \rightarrow 1$ as H_2O approaches ideality.

Owing to the critical phenomenon, no single standard state is equally convenient for simultaneous consideration of the liquid, gas, and supercritical phases of H_2O . Although designation of separate standard states for $\text{H}_2\text{O}_{\text{liquid}}$ and $\text{H}_2\text{O}_{\text{gas}}$ leads to dual activities and fugacities in the supercritical region, such a distinction is nevertheless advantageous in many geochemical calculations. For example, the standard state described above facilitates quantitative interpretation of univariant equilibria in the supercritical region, but solubility calculations can be simplified by adopting a standard state convention which is unrestricted with respect to both pressure and temperature. Under these circumstances, $a = 1$ and $f = f^\circ$ at all pressures and temperatures.

The standard state for H_2O most commonly encountered in solution chemistry specifies unit activity of the pure liquid at 1 bar. Activities of $\text{H}_2\text{O}_{\text{liquid}}$ consistent with this standard state can be computed from the apparent molal Gibbs free energies of formation (ΔG) given (and defined) below for 1 bar and temperatures $< 100^\circ\text{C}$ by first designating the corresponding fugacity reported for 1 bar as f° , which requires the activity of $\text{H}_2\text{O}_{\text{liquid}}$ to be unity at 1 bar. The activity of $\text{H}_2\text{O}_{\text{liquid}}$ at a higher pressure can then be computed from $\ln a = (\Delta G - \Delta G^\circ)/RT$ with ΔG° equal to the apparent standard molal Gibbs free energy of formation of $\text{H}_2\text{O}_{\text{liquid}}$ at unit pressure; that is, the values of ΔG reported below for 1 bar and temperatures $< 100^\circ\text{C}$. In certain cases, it may be advantageous to specify unit activity of H_2O at 1 bar and any temperature, which requires ΔG° to be equal to $\Delta G_{1 \text{ bar}}$ at all temperatures. Similarly, it may be convenient in solubility studies to adopt a standard state convention which requires the activity of $\text{H}_2\text{O}_{\text{liquid}}$ to be unity at all saturation pressures and temperatures. Under these conditions, $\Delta G_{\text{H}_2\text{O}, \text{liquid}}^\circ$ equals the values of ΔG for steam-saturated liquid H_2O . Values of ΔG° for these various standard states can be taken from table 29 or computed from equations presented below. Any liquid standard state is related to the

gas standard state adopted in this study by $RT \ln (a_{\text{H}_2\text{O}, \text{gas}}/a_{\text{H}_2\text{O}, \text{liquid}}) = (\Delta G_{\text{H}_2\text{O}, \text{liquid}}^\circ - \Delta G_{\text{H}_2\text{O}, \text{gas}}^\circ)$ at saturation.

The symbol P is used in this communication to designate pressure in preference to its lower case equivalent, which is commonly employed in gas chemistry to designate pressure in a one component system. All temperatures are thermodynamic (that is, the units are consistent with the celsius scale of temperature rather than the international practical temperature scale) expressed in degrees kelvin ($^\circ\text{K}$) or degrees centigrade ($^\circ\text{C}$) and designated by T and t, respectively. The symbols T_r and P_r refer to a reference temperature and pressure of 298.15 $^\circ\text{K}$ and 1 bar. Similarly, T_{tr} and P_{tr} stand for the triple point temperature and pressure (273.16 $^\circ\text{K}$ and 0.006113 bars). The subscript *triple* appended to a symbol indicates that it pertains to liquid H_2O at the triple point. Other subscripts include *c* or *critical* to refer to the critical point (374.136 $^\circ\text{C}$ and 220.88 bars), *sat* to designate saturated liquid along the vapor pressure curve, and P, T, P_r , T_r , P_{tr} , and T_{tr} to designate particular pressures and temperatures. The superscript $^\circ$ denotes standard state properties of H_2O for the convention adopted above. All other standard states discussed below are designated by the superscript $^\bullet$ to preclude confusion.

The values of entropy (S) and heat capacity (C_P or C_V) given in the tables and diagrams below are expressed in thermochemical calories (4.184 calories joule $^{-1}$) per mole per degree Kelvin (therm cal mole $^{-1}$ ($^\circ\text{K}$) $^{-1}$ or cal mole $^{-1}$ ($^\circ\text{K}$) $^{-1}$). Similarly, enthalpy (H) internal energy (E), and Gibbs (G) and Helmholtz (A) free energies are expressed in cal mole $^{-1}$ or kilocalories per mole (kcal mole $^{-1}$), which can be converted to joules per mole (j mole $^{-1}$), joules per gram (j g $^{-1}$), international calories per mole (int cal mole $^{-1}$), or int cal g $^{-1}$ with the aid of table 1. Volume (V) is expressed in cm 3 mole $^{-1}$ or cm 3 g $^{-1}$, which can also be converted to other units by applying conversion factors in table 1. Density (ρ) is given in g cm $^{-3}$, and the coefficients of isobaric thermal expansion (α) and isothermal compressibility (β) in ($^\circ\text{K}$) $^{-1}$ and bar $^{-1}$, respectively. The derivatives of α , β , and ϵ (the dielectric constant, which is dimensionless) are also expressed in reciprocal degrees kelvin and reciprocal bars to appropriate powers. Fugacity (f) is given in bars or kilobars. The fugacity coefficient (χ) is dimensionless ($\chi = f/P$), as is the compressibility factor ($z = PV/RT$) and activity ($a = f/f^\circ$). All molal properties given in the tables are referred to a molecular weight of H_2O equal to 18.0153 g mole $^{-1}$ consistent with the 1961 table of relative atomic weights based on $^{12}\text{C} = 12$ exactly. Values of the gas constant (R) with various dimensions are given in table 1 to facilitate thermodynamic calculations in alternate units.

All values shown in parentheses in the tables or represented by dashed lines in the figures given below represent interpolated, extrapolated, or otherwise more uncertain values. The number of decimal digits specified in the tables does not necessarily imply an absolute level of numerical uncertainty, which is discussed in the text accompanying the tables. In certain cases, relative uncertainties can be assessed from the

TABLE I
Conversion factors and values of the gas constant (R) in various units^a

	cm ³ g ⁻¹	cm ³ mole ⁻¹	j g ⁻¹ bar ⁻¹	j mole ⁻¹ bar ⁻¹	therm cal g ⁻¹ bar ⁻¹	therm cal mole ⁻¹ bar ⁻¹	int cal g ⁻¹ bar ⁻¹	int cal mole ⁻¹ bar ⁻¹
1 cm ³ g ⁻¹ =	1	18.0153	0.1	1.80153	0.023901	0.430584	0.023885	0.430295
1 cm ³ mole ⁻¹ =	0.05551	1	0.005551	0.1	0.001327	0.023901	0.001326	0.023885
1 j g ⁻¹ bar ⁻¹ =	10	180.1477						
1 j mole ⁻¹ bar ⁻¹ =	0.55508	10						
1 therm cal g ⁻¹ bar ⁻¹ =	41.8393	735.579						
1 therm cal mole ⁻¹ bar ⁻¹ =	2.32243	41.8393						
1 int cal g ⁻¹ bar ⁻¹ =	41.86728	754.148						
1 int cal mole ⁻¹ bar ⁻¹ =	2.32399	41.8673						

	j g ⁻¹	j mole ⁻¹	therm cal g ⁻¹	therm cal mole ⁻¹	int cal g ⁻¹	int cal mole ⁻¹
1 j g ⁻¹ =	1	18.0153	0.23901	4.30584	0.23885	4.30295
1 j mole ⁻¹ =	0.05551	1	0.01327	0.23901	0.01326	0.23885
1 therm cal g ⁻¹ =	4.1840	75.3760	1	18.0153	1.00067	18.02737
1 therm cal mole ⁻¹ =	0.23225	4.1840	0.05551	1	0.05555	1.00067
1 int cal g ⁻¹ =	4.1868	75.4265	0.99933	18.00323	1	18.0153
1 int cal mole ⁻¹ =	0.23240	4.1868	0.05547	0.99933	0.05551	1

R	units	R	units	R	units	R	units
0.46151	j g ⁻¹ (°K) ⁻¹	0.110306	therm cal g ⁻¹ (°K) ⁻¹	0.110232	int cal g ⁻¹ (°K) ⁻¹	4.6151	cm ³ bar g ⁻¹ (°K) ⁻¹
8.31424	j mole ⁻¹ (°K) ⁻¹	1.98719	therm cal mole ⁻¹ (°K) ⁻¹	1.98586	int cal mole ⁻¹ (°K) ⁻¹	83.14241	cm ³ bar mole ⁻¹ (°K) ⁻¹

^aThe molal units shown in the table are referred to a molecular mass of H₂O equal to 18.0153 g mole⁻¹, which is consistent with the 1961 table of relative atomic weights based on ¹²C = 12 exactly.

tables by noting differences in the number of decimals given for high and low temperatures and pressures. The labels *sat* or *saturation* refer to steam-saturated liquid H₂O.

Most steam tables published in the last 15 years, as well as the recent compilation by Burnham, Holloway, and Davis (1969b), are predicated on $S_{triple} = G_{triple} = 0$, which is the convention adopted by the 5th International Conference on the Properties of Steam. The values of H and S reported in steam tables are thus actually $H - H_{triple}$ and $S - S_{triple}$. Although the steam table convention facilitates engineering studies, it is not particularly convenient for geochemical calculations because the stipulation that $S_{triple} = G_{triple} = 0$ conflicts with standard state conventions used to compute and tabulate thermodynamic properties of minerals and gases in other widely used compilations (for example, Latimer, 1952; Wagman and others, 1965, 1966, 1968, 1969; Wagman and others, 1971; Parker, Wagman, and Evans, 1971; Stull and Prophet, 1971; Robie and Waldbaum, 1968). Entropies and enthalpies of H₂O based on the steam table convention can be converted to other reference systems simply by adding values of S_{triple} and H_{triple} consistent with the desired convention to the respective values of S and H reported in the steam tables. Similarly, because densities and volumes reported in steam tables are absolute values, internal energies based on other conventions can be computed directly from steam table data by specifying E_{triple} and evaluating

$$E - E_{triple} = H - H_{triple} + PV - P_{tr} V_{triple} \quad (1)$$

In contrast, calculation of corresponding Gibbs or Helmholtz free energies from values of H and S reported in steam tables requires specification of S_{triple} as well as G_{triple} or A_{triple} consistent with the desired convention. The extent to which the free energies of H₂O change with temperature depends on the magnitude of the entropy at the reference temperature and pressure, which can be demonstrated by writing

$$G - G_{triple} = H - H_{triple} - TS + T_{tr} S_{triple} \quad (2)$$

and

$$\begin{aligned} A - A_{triple} &= E - E_{triple} - TS + T_{tr} S_{triple} \\ &= G - G_{triple} - PV + P_{tr} V_{triple} \end{aligned} \quad (3)$$

which are not equivalent to

$$G = H - TS \quad (4)$$

and

$$A = E - TS \quad (5)$$

unless

$$S_{triple} = 0.$$

To facilitate geochemical calculations, the enthalpies, internal energies, and Gibbs and Helmholtz free energies of H₂O given in the tables and diagrams below are expressed as apparent molal enthalpies, internal energies, and Gibbs and Helmholtz free energies of formation from the

elements (ΔH , ΔE , ΔG , and ΔA) consistent with their standard molal counterparts at 298.15°K and 1 bar; that is,¹

$$\begin{aligned}\Delta H &\equiv \Delta H^{\bullet}_f + (H - H_{P_r, T_r}) \\ &= \Delta H^{\bullet}_f + (H - H_{triple}) - (H_{P_r, T_r} - H_{triple})\end{aligned}\quad (6)$$

$$\begin{aligned}\Delta E &= \Delta E^{\bullet}_f + (E - E_{P_r, T_r}) \\ &= \Delta E^{\bullet}_f + (E - E_{triple}) - (E_{P_r, T_r} - E_{triple})\end{aligned}\quad (7)$$

$$\begin{aligned}\Delta G &= \Delta G^{\bullet}_f + (G - G_{P_r, T_r}) \\ &= \Delta G^{\bullet}_f + (G - G_{triple}) - (G_{P_r, T_r} - G_{triple})\end{aligned}\quad (8)$$

and

$$\begin{aligned}\Delta A &= \Delta A^{\bullet}_f + (A - A_{P_r, T_r}) \\ &= \Delta A^{\bullet}_f + (A - A_{triple}) - (A_{P_r, T_r} - A_{triple})\end{aligned}\quad (9)$$

where ΔH^{\bullet}_f , ΔE^{\bullet}_f , ΔG^{\bullet}_f , and ΔA^{\bullet}_f refer to the standard molal enthalpy, internal energy, Gibbs free energy, and enthalpy of formation of liquid H₂O from its elements in their stable form at 298.15°K (T_r) and one bar (P_r). The superscript \bullet is used in equations (6) through (9) rather than \circ to distinguish the standard state properties given by Wagman and others (1968) for liquid H₂O from those of the gas standard state adopted in this study. The values of ΔH^{\bullet}_f and ΔG^{\bullet}_f employed below are given in table 2 together with corresponding values of ΔE^{\bullet}_f and ΔA^{\bullet}_f computed from

$$\Delta E^{\bullet}_f = \Delta H^{\bullet}_f - P_r \Delta V^{\bullet}_f \quad (10)$$

and

$$\Delta A^{\bullet}_f = \Delta G^{\bullet}_f - P_r \Delta V^{\bullet}_f \quad (11)$$

using $V^{\circ}_{O_2} = V^{\circ}_{H_2} = V_{ideal\ gas} = 24,465\text{ cm}^3\text{ mole}^{-1}$. The entropies and heat capacities reported below are third law molal properties consistent with

$$\begin{aligned}S &= -\left(\frac{\partial \Delta G}{\partial T}\right)_P = -\left(\frac{\partial \Delta A}{\partial T}\right)_V = S^{\bullet} + (S - S_{P_r, T_r}) \\ &= S^{\bullet} + (S - S_{triple}) - (S_{P_r, T_r} - S_{triple})\end{aligned}\quad (12)$$

and

$$C_P = \left(\frac{\partial \Delta H}{\partial T}\right)_P = T \left(\frac{\partial S}{\partial T}\right)_P \quad (13)$$

where S^{\bullet} represents the standard molal third law entropy of liquid H₂O at 298.15°K and one bar given by Wagman and others (1968).

Conversion of the apparent molal enthalpies, internal energies, and free energies as well as the third law molal entropies given below to corresponding values based on the steam table convention can be made with

¹ Use of the word apparent in referring to ΔH , ΔE , ΔG , and ΔA was suggested by Benson (1968) to preclude confusion with corresponding properties of formation from the elements at high pressures and temperatures such as those tabulated by Robie and Waldbaum (1968). The latter properties include provision for changes in the thermodynamic properties of the elements with increasing pressure and temperature, which cancel in chemical reactions.

the aid of the properties of liquid H₂O given in table 2 for the triple point and 298.15°K and 1 bar. Corresponding values of heat capacity and volume are also given in table 2 along with the respective differences in the thermodynamic properties of liquid H₂O caused by increasing temperature and pressure from T_{tr} and P_{tr} to T_r and P_r.

VOLUME

The volume of H₂O in cm³ mole⁻¹ is given in table 3 and plotted in figures 1 and 2 for temperatures and pressures to 900°C and 10 kb.

TABLE 2

Thermodynamic properties of liquid H₂O at the triple point and corresponding values of the properties at 298.15°K (T_r) and 1 bar (P_r) consistent with the standard state for liquid H₂O adopted by Wagman and others (1968) and the definitions represented by equations (6) through (9), (12), and (13)^a

Property	j g ⁻¹	therm cal mole ⁻¹	Property	j g ⁻¹ (°K) ⁻¹	therm cal mole ⁻¹
$\Delta H_{\underline{f}}^{\circ}$	-15,866	-68,315 ^b	$\Delta A_{\underline{f}}^{\circ}$	-12,962	-55,812 ^c
$H_{P_r, T_r} - H_{\underline{triple}}$	104.89 ^d	451.63	$A_{P_r, T_r} - A_{\underline{triple}}$	-92.28 ^{e, g}	-397.32
$\Delta H_{\underline{triple}}$	-15,971	-68,767	$\Delta A_{\underline{triple}}$	-12,870	-55,415
$\Delta E_{\underline{f}}^{\circ}$	-15,662	-67,436 ^c	$\Delta G_{\underline{f}}^{\circ}$	-13,165	-56,687 ^b
$E_{P_r, T_r} - E_{\underline{triple}}$	104.79 ^{e, h}	451.20	$G_{P_r, T_r} - G_{\underline{triple}}$	-92.18 ^{e, f}	-396.89
$\Delta E_{\underline{triple}}$	-15,766	-67,887	$\Delta G_{\underline{triple}}$	-13,073	-56,290
S [*]	3.8808 ^l	16.71 ^{b, m}	V [*]	0.100296 ^{d, i, k}	0.43186 ^j
$S_{P_r, T_r} - S_{\underline{triple}}$	0.3664 ^{d, l}	1.5776 ^m	$V_{P_r, T_r} - V_{\underline{triple}}$	0.00028 ^{e, i}	0.00119 ^j
$S_{\underline{triple}}$	3.5144 ^l	15.132 ^m	$V_{\underline{triple}}$	0.10002 ^{d, i}	0.43067 ^j
C _P ^o	4.183 ^{d, l}	18.01 ^m	C _V ^o	4.141 ^{d, l}	17.83 ^m

^a $\Delta H_{\underline{triple}}$, $\Delta E_{\underline{triple}}$, $\Delta A_{\underline{triple}}$, and $\Delta G_{\underline{triple}}$ correspond, respectively, to the standard enthalpy, internal energy, and Helmholtz and Gibbs free energies of formation of one mole of liquid H₂O from its elements in their stable form at 298.15°K and one bar ($\Delta H_{\underline{f}}^{\circ}$, $\Delta E_{\underline{f}}^{\circ}$, $\Delta A_{\underline{f}}^{\circ}$, and $\Delta G_{\underline{f}}^{\circ}$) plus the change in the respective properties of liquid H₂O ($H_{P_r, T_r} - H_{\underline{triple}}$, $E_{P_r, T_r} - E_{\underline{triple}}$, $A_{P_r, T_r} - A_{\underline{triple}}$, and $G_{P_r, T_r} - G_{\underline{triple}}$) caused by decreasing the temperature and pressure to 273.16°K and 0.006113 bars at the triple point (eqs 6 through 9). S_{triple} represents the molal third law entropy of liquid H₂O at the triple point computed from equation (12) and the values of S^{*} and $S_{P_r, T_r} - S_{\underline{triple}}$ given above.

^bWagman and others (1968). ^ccomputed from equations (10) and (11). ^dKeenan and others (1969) and Schmidt (1969). ^ecalculated from data given in the sources referenced in footnote d. ^fEquation (2). ^gEquation (3). ^hEquation (1). ⁱj g⁻¹ bar⁻¹. ^jtherm cal mole⁻¹ bar⁻¹. ^kKell (1967). ^lj gm⁻¹ (°K)⁻¹. ^mtherm cal mole⁻¹ (°K)⁻¹.

The values shown for pressures \leq a kilobar were computed from the Helmholtz function derived by Keenan and others (1969), which can be written as

$$\psi = \psi_o + RT (\ln \rho + \rho Q) \quad (14)$$

where

$$\psi_o = \left(\sum_{i=1}^6 C_i / \tau^{i-1} \right) + C_7 \ln T + C_8 \ln (T/\tau) \quad (15)$$

and

$$Q = (\tau - \tau_c) \sum_{j=1}^7 (\tau - \tau_{aj})^{j-2} \left(\sum_{i=1}^8 A_{ij} (\rho - \rho_{aj})^{i-1} + e^{-4.8\rho} \sum_{i=9}^{10} A_{ij} \rho^{i-9} \right) \quad (16)$$

where ρ refers to the density of H_2O in $g\ cm^{-3}$, T denotes temperature in $^{\circ}K$, R stands for the gas constant in $\text{joules } g^{-1} (^{\circ}K)^{-1}$ (table 1), $\tau = 1000/T$, $\tau_c = 1000/T_{critical} = 1.544912$, $\tau_{aj} = \tau_c$ for $j = i$ and 2.5 for $j > 1$, $\rho_{aj} = 0.634$ for $j = 1$ and 1.0 for $j > 1$, C_i and A_{ij} represent arrays of coefficients given in table 4, and

$$\psi = A - A_{triple} + S_{triple} (T - T_{tr}) \quad (17)$$

where A is the Helmholtz free energy in $\text{joules } g^{-1}$ of H_2O at the temperature and pressure of interest, A_{triple} refers to the Helmholtz free energy in $\text{joules } g^{-1}$ of liquid H_2O at the triple point (273.16 $^{\circ}K$ and 0.006113 bars), and S_{triple} stands for the third law entropy in $\text{joules } g^{-1} (^{\circ}K)^{-1}$ of the liquid at the triple point. It follows from equations (14), (17), and the relation

$$dA = -SdT - PdV = -SdT + \frac{P}{\rho^2} d\rho \quad (18)$$

that

$$\begin{aligned} P &= - \left(\frac{\partial A}{\partial V} \right)_T = \rho^2 \left(\frac{\partial A}{\partial \rho} \right)_T = \rho^2 \left(\frac{\partial \psi}{\partial \rho} \right)_T \\ &= \rho RT \left(1 + \rho Q + \rho^2 \left(\frac{\partial Q}{\partial \rho} \right)_T \right) \end{aligned} \quad (19)$$

where P refers to pressure in bars, V is the specific volume of H_2O in $cm^3\ g^{-1}$, and $(\partial Q/\partial \rho)_T$ corresponds to the partial derivative of equation (16) with respect to density at constant temperature (eq A-22 in the app).

Equation (19) represents experimental pressure–volume–temperature data for H_2O to 0.1 percent or better from 0 $^{\circ}$ to 800 $^{\circ}C$ and 0 $^{\circ}$ to 1 kb, but at temperatures below 220 $^{\circ}C$ the uncertainty is 0.01 percent (Keenan

TABLE 3
Molal volume (V) in cm³ mole⁻¹ computed from equations (19)
through (21)—see figures 1, 2, and 4

t (°C)	PRESSURE, KB											
	SAT	0.5	1	2	3	4	5	6	7	8	9	10
25	18.0681	17.6886	17.3547	16.84	16.41	16.05	15.72	15.45	15.22	15.01	14.79	14.61
50	18.2340	17.8610	17.5303	17.02	16.59	16.23	15.91	15.62	15.39	15.17	14.97	14.79
75	18.4820	18.0933	17.7526	17.22	16.18	16.42	16.09	15.80	15.55	15.34	15.13	14.96
100	18.7991	18.3778	18.0161	17.44	16.98	16.61	16.28	15.98	15.73	15.50	15.30	15.11
125	19.1851	18.7147	18.3211	17.70	17.21	16.82	16.48	16.17	15.91	15.67	15.46	15.27
150	19.6455	19.1075	18.6697	18.00	17.46	17.04	16.69	16.37	16.09	15.85	15.63	15.42
175	20.1901	19.5606	19.0638	18.33	17.73	17.28	16.91	16.57	16.28	16.03	15.79	15.58
200	20.8344	20.0807	19.5054	18.69	18.03	17.53	17.13	16.78	16.48	16.21	15.97	15.74
225	21.6039	20.6782	19.9976	19.08	18.34	17.80	17.37	17.00	16.68	16.40	16.14	15.90
250	22.5416	21.3703	20.5457	19.50	18.68	18.08	17.62	17.23	16.89	16.59	16.32	16.07
275	23.7224	22.1850	21.1593	19.95	19.05	18.38	17.88	17.46	17.10	16.79	16.51	16.25
300	25.2858	23.1669	21.8528	20.43	19.43	18.69	18.14	17.70	17.32	16.99	16.70	16.42
325	27.5307	24.3871	22.6469	20.95	19.83	19.02	18.43	17.95	17.54	17.20	16.89	16.60
350	31.3508	25.9614	23.5689	21.51	20.26	19.37	18.72	18.20	17.77	17.41	17.08	16.77
375		28.0920	24.6535	22.12	20.71	19.73	19.02	18.47	18.01	17.62	17.27	16.95
400		31.1824	25.9406	22.79	21.19	20.11	19.34	18.75	18.26	17.84	17.47	17.13
425		36.1590	27.4745	23.52	21.70	20.51	19.67	19.03	18.51	18.07	17.67	17.31
450		44.7894	29.3033	24.31	22.24	20.93	20.02	19.33	18.77	18.30	17.88	17.49
475		57.1878	31.4791	25.18	22.81	21.36	20.37	19.63	19.04	18.53	18.09	17.68
500		70.1236	34.0536	26.13	23.41	21.82	20.74	19.95	19.31	18.77	18.30	17.86
525		81.8168	37.0572	27.15	24.05	22.29	21.12	20.27	19.59	19.02	18.52	18.05
550		92.2038	40.4681	28.25	24.71	22.77	21.52	20.60	19.87	19.27	18.73	18.24
575		101.5571	44.1991	29.43	25.40	23.28	21.92	20.94	20.17	19.52	18.96	18.43
600		110.1153	48.1255	30.67	26.13	23.79	22.33	21.28	20.46	19.78	19.18	18.63
625		118.0515	52.1293	31.98	26.89	24.33	22.75	21.64	20.76	20.04	19.41	18.84
650		125.4894	56.1235	33.35	27.67	24.88	23.18	22.00	21.07	20.31	19.65	19.04
675		132.5197	60.0537	34.77	28.48	25.44	23.63	22.36	21.38	20.58	19.89	19.25
700		139.2110	63.6502	36.24	29.31	26.02	24.08	22.74	21.70	20.85	20.13	19.47
725		145.6166	67.6192	37.74	30.16	26.62	24.54	23.12	22.02	21.13	20.37	19.69
750		151.7790	71.2367	39.26	31.04	27.23	25.01	23.50	22.35	21.41	20.62	19.91
775		157.7331	74.7445	40.81	31.94	27.85	25.49	23.90	22.68	21.70	20.87	20.13
800		163.5079	78.1479	42.36	32.86	28.49	25.98	24.30	23.02	21.99	21.12	20.35
825		169.1279	81.4536	43.92	33.80	29.14	26.47	24.70	23.36	22.28	21.37	20.57
850		174.6138	84.6695	45.48	34.75	29.79	26.97	25.10	23.71	22.58	21.63	20.80
875		179.9838	87.8033	47.03	35.71	30.44	27.46	25.51	24.06	22.89	21.90	21.02
900		185.2535	90.8630	48.57	36.66	31.09	27.94	25.91	24.41	23.20	22.18	21.26

TABLE 4
 A_{ij} , C_i , and F_i coefficients for equations (15), (16), and (20)
after Keenan and others (1969)

i	j						
	1	2	3	4	5	6	7
1	29.492937	-5.1985860	6.8335354	-0.1564104	-6.3972405	-3.9661401	-0.69048554
2	-132.13917	7.7779182	-26.149751	-0.72546108	26.409282	15.453061	2.7407416
3	274.64632	-33.301902	65.326396	-9.2734289	-47.740374	-29.142470	-5.1028070
4	-360.93828	-16.254622	-26.181978	4.3125840	56.323130	29.568796	3.9636085
5	342.18431	-177.31074	0	0	0	0	0
6	-244.50042	127.48742	0	0	0	0	0
7	155.18535	137.46153	0	0	0	0	0
8	5.9728487	155.97836	0	0	0	0	0
9	-410.30848	337.31180	-137.46618	6.7874983	136.87317	79.847970	13.041253
10	-416.05860	-209.88866	-733.96848	10.401717	645.81880	399.17570	71.531353

$C_1 = 1857.065$	$C_5 = -20.5516$	$F_1 = -741.9242$	$F_5 = 0.1094098$
$C_2 = 3229.12$	$C_6 = 4.85233$	$F_2 = -29.72100$	$F_6 = 0.439993$
$C_3 = -419.465$	$C_7 = 46.0$	$F_3 = -11.55286$	$F_7 = 0.2520658$
$C_4 = 36.6649$	$C_8 = -1011.249$	$F_4 = -0.8685635$	$F_8 = 0.05218684$

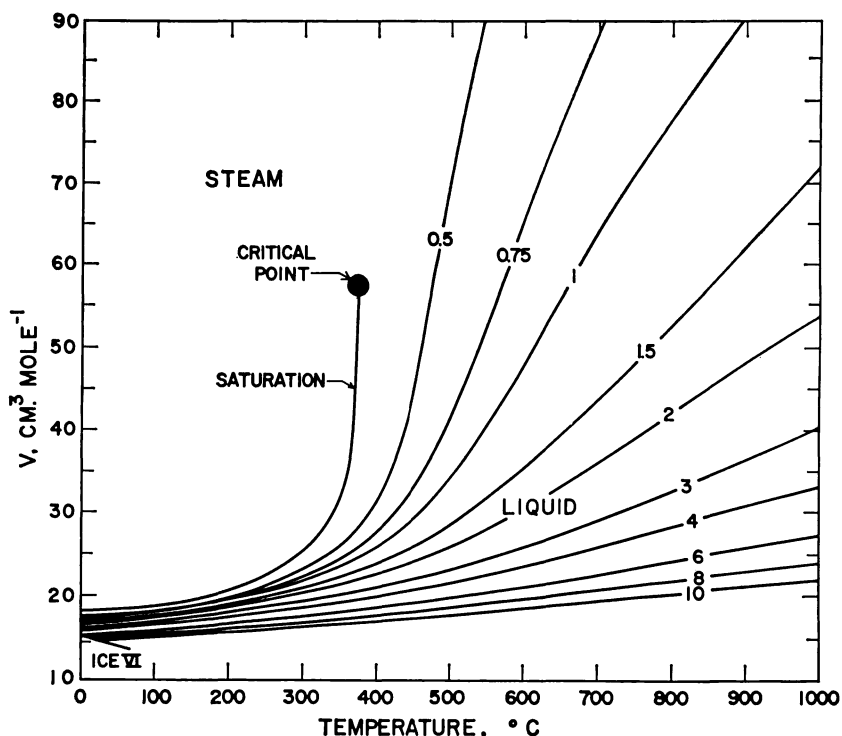


Fig. 1. Molal volume (table 3) as a function of temperature at constant pressure (labeled in kb) computed from equations (19) through (21) and the coefficients in tables 4 through 6.

and others, 1969) which is comparable to that reported by Kell and Whalley (1965) and Fine and Millero (1973). Even more accurate representation (to within 0.008 percent) of the saturation curve is afforded by

$$P_{sat} = P_c \exp \left(10^{-5\tau}(t_c - t) \sum_{i=1}^8 F_i (0.65 - 0.01t)^{i-1} \right) \quad (20)$$

where P_{sat} stands for saturation pressure, $P_c = P_{critical} = 220.88$ bars, τ is again $1000/T$ (where T is in $^{\circ}\text{K}$), t represents temperature in $^{\circ}\text{C}$, $t_c = t_{critical} = 374.136^{\circ}\text{C}$, and F_i refers to an array of coefficients in table 4 (Keenan and others, 1969).

Equations (19) and (20) were used together with iterative computer techniques to calculate the molal volumes shown in table 3 and figures 1 and 2 for pressures \leq a kilobar. The volumes shown for pressures above a kilobar were computed from a modification of the regression poly-

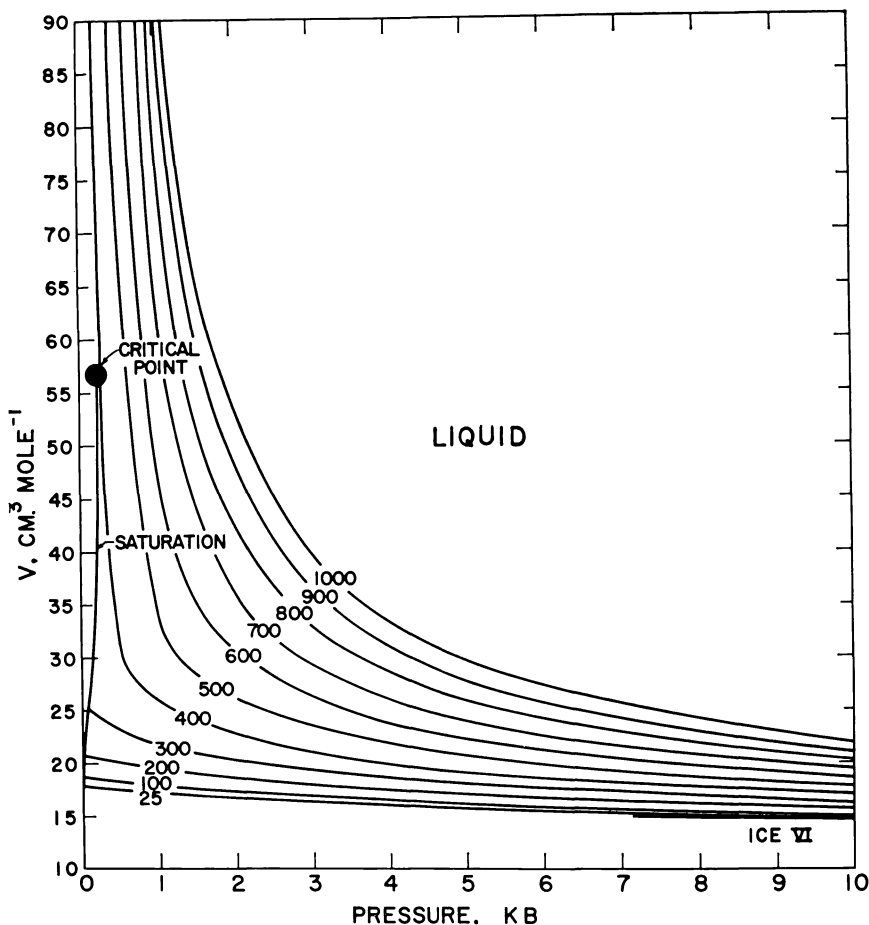


Fig. 2. Molal volume (table 3) as a function of pressure at constant temperature (labeled in °C) computed from equations (19) through (21) and the coefficients in tables 4 through 6.

nomial employed by Burnham, Holloway, and Davis (1969b), which can be written as

$$V = \sum_{i=0}^i \sum_{j=0}^{i-i} a_{ij} t^i P^{rj-1} \quad (21)$$

where V is again the specific volume of H₂O in cm³ g⁻¹, P stands for pressure in bars, t refers to temperature in °C, r is a switch constant equal to 1 or -1 (see below), and a_{ij} refers to the arrays of fit coefficients in tables 5 and 6. Owing to the critical phenomenon and the extrapolation procedure employed in computing volumes beyond the upper pressure-

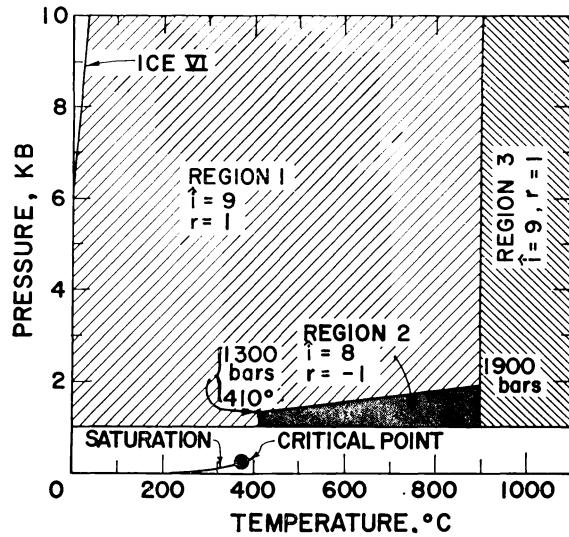


Fig. 3. Regions of pressure and temperature represented by alternate statements of equation (21) with the values of i and r shown above (Burnham, Hollaway, and Davis, 1969).

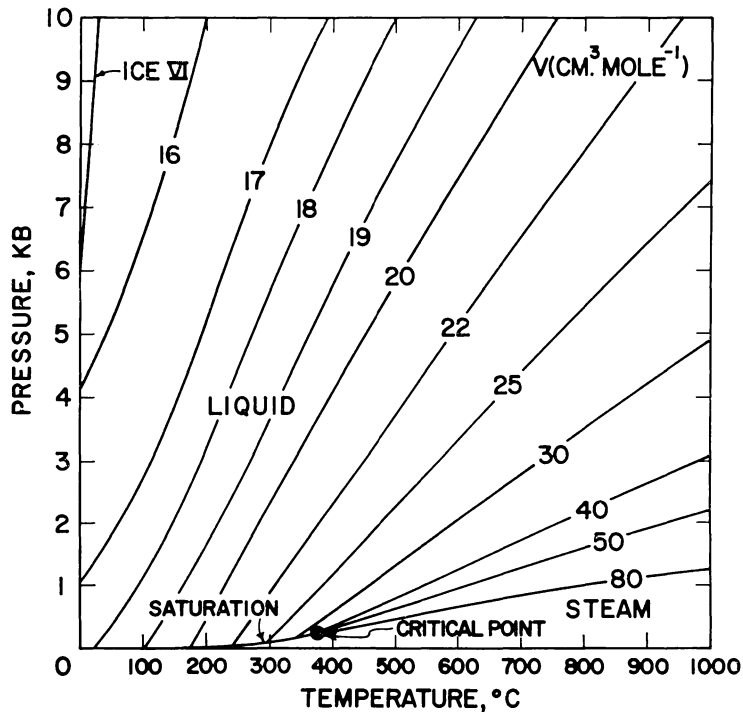


Fig. 4. Isochores (labeled in $\text{cm}^3 \text{mole}^{-1}$) as a function of pressure and temperature (table 3 and figs. 1 and 2).

temperature limits of their measurements (8400 bars and 900°C), Burnham, Holloway, and Davis (1969b) used separate statements of equation (21) to represent the specific volume of H₂O in different pressure-temperature regions. These regions (numbered 1, 2, and 3) and the values of i and r in the statement of equation (21) appropriate to each are shown in figure 3. The a_{ij} coefficients for regions 1 and 2 are given in tables 5 and 6, respectively, but the corresponding coefficients for region 3 were omitted from this communication because they are based entirely on extrapolation of measurements at lower temperatures.

Specific volumes computed from equation (21) are reported to be within 0.3 percent of the measured volumes (Burnham, Holloway, and Davis, 1969b), but more recent measurements indicate that the uncertainty at high pressures and temperatures may be as high as ± 0.6 percent (C. W. Burnham, personal commun.). Comparison of specific volumes computed from equation (21) with those reported by Grindley and Lind (1971) for temperatures from 25° to 150°C reveals discrepancies ranging from 0.2 percent or less at 2 kb to 0.6 percent or less at 8 kb. The values given by Grindley and Lind are consistently lower than those computed from equation (21). Similarly, the specific volumes reported by Burnham, Holloway, and Davis (1969b) at high pressures and temperatures are slightly lower than those measured recently (C. W. Burnham and V. Wall, personal commun.), but at temperatures below 150°C, the latter measurements are in close agreement with those reported by Grindley and Lind (V. Wall, personal commun.). It thus appears that a slight (≤ 0.6 percent) but systematic error is inherent in densities computed from equation (21) and the coefficients in tables 5 and 6. The possible effect of this error on the calculations presented below is included in the overall uncertainties assigned to the results of the calculations.

It can be seen in figures 1 and 2 that the volume of H₂O forms a hyperbolic surface in pressure-volume-temperature space. However, at 10 kb the volume of H₂O increases only of the order of 7 cm³ mole⁻¹ as temperature increases from 30° to 1000°C, which is approximately twice the increase associated with decreasing pressure from 10 kb to 1 bar at $\sim 30^\circ\text{C}$. Note in figure 4 that the isochores for water take on a slight sigmoid shape as temperature decreases, and their curvature increases as they approach the melting curves of the ice polymorphs.

COMPRESSIBILITY AND THERMAL EXPANSION

The coefficient of isothermal compressibility (β) of H₂O can be computed for pressures \leq a kilobar by differentiating equation (19) with respect to density at constant temperature. The resulting expression appears as

$$\begin{aligned} \beta^{-1} &= \rho \left(\frac{\partial P}{\partial \rho} \right)_T \\ &= P + \rho^2 RT \left(Q + 3\rho \left(\frac{\partial Q}{\partial \rho} \right)_T + \rho^2 \left(\frac{\partial^2 Q}{\partial \rho^2} \right)_T \right) \end{aligned} \quad (22)$$

which can in turn be differentiated to give

$$\begin{aligned} \left(\frac{\partial\beta}{\partial P}\right)_T &= \beta^2 \left(2\beta P - 3 - \rho^3\beta RT \left(4 \left(\frac{\partial Q}{\partial\rho}\right)_T \right. \right. \\ &\quad \left. \left. + 5\rho \left(\frac{\partial^2 Q}{\partial\rho^2}\right)_T + \rho^2 \left(\frac{\partial^3 Q}{\partial\rho^3}\right)_T \right) \right) \end{aligned} \quad (23)$$

and

$$\begin{aligned} \left(\frac{\partial\beta}{\partial T}\right)_P &= - \left(\frac{\partial\alpha}{\partial P}\right)_T = (1 - \beta P) \left(2\alpha\beta - \frac{\beta}{T} \right) \\ &\quad - \beta^2\rho^2 RT \left(\left(\frac{\partial Q}{\partial T}\right)_P + 3\rho \left(\frac{\partial}{\partial T} \left(\frac{\partial Q}{\partial\rho}\right)_T\right)_P \right) \\ &\quad - 3\rho\alpha \left(\frac{\partial Q}{\partial\rho}\right)_T + \rho^2 \left(\frac{\partial}{\partial T} \left(\frac{\partial^2 Q}{\partial\rho^2}\right)_T\right)_P \\ &\quad - 2\rho^2\alpha \left(\frac{\partial^2 Q}{\partial\rho^2}\right)_T \end{aligned} \quad (24)$$

where $(\partial Q/\partial T)_P$, $(\partial Q/\partial\rho)_T$, $(\partial^2 Q/\partial\rho^2)_T$, $(\partial^3 Q/\partial\rho^3)_T$, $(\partial(\partial Q/\partial\rho)_T/\partial T)_P$, and $(\partial(\partial^2 Q/\partial\rho^2)_T/\partial T)_P$ correspond to partial derivatives of equation (16) given in the appendix (eqs A-8, A-22, A-23, A-24, A-35, and A-39), and α represents the coefficient of isobaric thermal expansion, which can be computed for pressures \leq a kilobar from

$$\begin{aligned} \alpha &= -\frac{1}{\rho} \left(\frac{\partial\rho}{\partial T}\right)_P = \frac{\beta P}{T} \\ &\quad + \rho RT\beta \left(\rho \left(\frac{\partial Q}{\partial T}\right)_\rho + \rho^2 \left(\frac{\partial}{\partial T} \left(\frac{\partial Q}{\partial\rho}\right)_T\right)_\rho \right) \end{aligned} \quad (25)$$

Equation (25) is the result of combining the partial derivative of equation (19) with respect to temperature at constant density with the identity,

$$\left(\frac{\partial P}{\partial T}\right)_\rho = \frac{\alpha}{\beta}, \quad (26)$$

which leads to

$$\begin{aligned} \left(\frac{\partial\alpha}{\partial T}\right)_P &= \frac{\alpha}{\beta} \left(\frac{\partial\beta}{\partial T}\right)_P - \frac{2\beta P}{T^2} + \frac{\alpha}{T} (1 - \alpha T + \beta P) \\ &\quad + \rho RT\beta \left(\rho \left(\frac{\partial}{\partial T} \left(\frac{\partial Q}{\partial T}\right)_\rho\right)_P - \rho\alpha \left(\frac{\partial Q}{\partial T}\right)_\rho + \right. \end{aligned}$$

$$+ \left(\frac{\partial \left(\frac{\partial \left(\frac{\partial Q}{\partial \rho} \right)_T}{\partial T} \right)_\rho}{\partial T} \right)_P - 2\rho^2 \alpha \left(\frac{\partial \left(\frac{\partial Q}{\partial \rho} \right)_T}{\partial T} \right)_\rho \quad (27)$$

where $(\partial Q/\partial T)_\rho$, $(\partial(\partial Q/\partial T)_\rho/\partial T)_P$, $(\partial(\partial Q/\partial \rho)_T/\partial T)_\rho$, and $(\partial(\partial(\partial Q/\partial \rho)_T/\partial T)_\rho/\partial T)_P$ represent additional partial derivatives of equation (16) given in the appendix (eqs A-43, A-45, A-46, and A-47). Equations (19), (20), (22), and (25) were used to compute the values of α and β for pressures \leq a kilobar in tables 7 and 8, which are represented by the curves in figures 5 through 8.

TABLE 7
Coefficient of isobaric thermal expansion (α) in $(^\circ\text{K})^{-1} \times 10^5$
computed from equations (25), (33), and (39) and the values
of V in table 3—see figures 5, 6, and 16

t (°C)	PRESSURE, KB								
	SAT	0.5	1	2	3	4	5	6	7
25	25.53	30.99	34.30	38.4	40.6	42.3	43.4	43.9	44.2
50	46.24	45.80	45.76	44.5	44.6	44.8	44.7	44.5	44.3
75	61.39	57.21	54.79	50.4	48.8	47.7	46.7	45.8	45.0
100	74.86	67.55	63.03	56.1	52.9	50.6	48.8	47.2	46.0
125	88.36	77.84	71.27	61.6	56.7	53.5	50.9	48.7	47.0
150	102.71	88.36	79.51	67.0	60.4	56.1	52.8	50.1	48.0
175	118.70	99.24	87.61	72.4	63.9	58.5	54.5	51.4	48.8
200	137.62	110.87	95.60	77.8	67.2	60.7	56.1	52.4	49.6
225	161.75	124.03	103.80	83.1	70.4	62.7	57.4	53.3	50.1
250	195.13	139.93	112.71	88.3	73.5	64.6	58.6	54.1	50.6
275	245.37	160.30	123.00	93.5	76.5	66.4	59.8	54.8	51.0
300	329.48	187.56	135.41	98.7	79.4	68.2	60.9	55.5	51.4
325	499.05	225.16	150.64	103.9	82.4	70.0	62.0	56.2	51.8
350	1038.30	278.55	169.21	109.4	85.5	71.9	63.2	57.0	52.2
375		358.22	191.25	115.3	88.6	73.8	64.5	57.9	52.8
400		488.47	216.32	121.5	91.8	75.8	65.9	58.8	53.4
425		715.91	243.57	128.0	95.1	77.9	67.3	59.8	54.0
450		973.36	272.09	134.9	98.4	79.9	68.7	60.8	54.7
475		923.47	300.82	141.9	101.5	81.8	70.0	61.8	55.4
500		707.36	327.40	148.9	104.3	83.4	71.1	62.6	55.9
525		537.73	347.20	156.7	107.2	85.7			
550		426.21	354.86	161.6	109.8	87.0			
575		351.40	348.44	165.3	111.9	88.0			
600		298.71	331.01	167.7	113.5	88.8	(74.8)	(65.6)	(58.2)
625		259.87	307.74	168.8	114.6	89.3			
650		230.18	282.87	168.5	115.2	89.6			
675		206.79	258.89	167.1	115.2	89.7			
700		187.93	236.91	164.5	114.8	89.7	(75.3)	(66.1)	(58.4)
725		172.44	217.29	161.1	114.2	89.7			
750		159.52	200.01	157.0	113.3	89.8			
775		148.61	184.87	152.5	112.4	89.8			
800		139.29	171.64	147.6	111.4	89.9	(76.1)	(67.7)	(60.2)
825		131.26	160.06						
850		124.28	149.92						
875		118.18	141.02						
900		112.80	133.17						

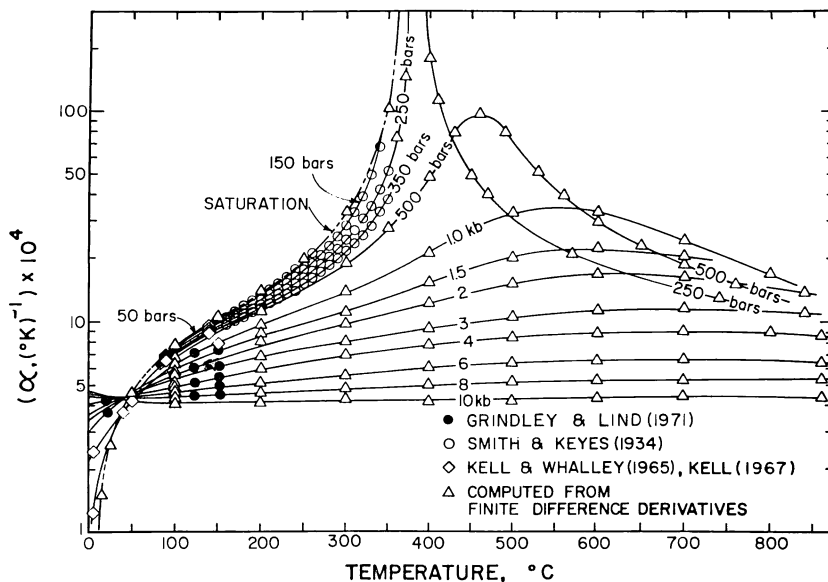


Fig. 5. Coefficient of isobaric thermal expansion (table 7) as a function of temperature at constant pressure (labeled in bars and kb) computed from equations (19) through (21), (25), (33), and (39) and coefficients in tables 4, 5, 6, 9, and 10 (curves). The symbols represent values taken from the literature or computed from finite difference derivatives of specific volumes given by Schmidt (1969), Burnham, Holloway, and Davis (1969b), and Keenan and others (1969).

Because equation (19) so closely represents the dependence of density on pressure and temperature below a kilobar (Keenan and others, 1969), minimal uncertainties attend calculation of β , $(\partial\beta/\partial P)_T$, $(\partial\beta/\partial T)_P$, α , and $(\partial\alpha/\partial T)_P$ for pressures \leq a kilobar from equations (22) through (25) and (27). It can be seen in figures 5 through 8 that the calculated values of α and β are in close agreement with corresponding coefficients of isothermal compressibility and isobaric thermal expansion reported in the literature. Values of β computed from equation (22) for temperatures from 25° to 100°C and pressures from 1 to 1000 bars are within 1 percent or less of those derived from sound velocity data by Fine and Millero (1973), except for pressures at or near a kilobar where the difference is 4 percent or less. Similar comparison of expansibilities computed from equation (25) with those reported by Fine and Millero (1973) yields corresponding differences of 1 percent and 2 percent, respectively. The expansibilities and compressibilities given by Fine and Millero are within \sim 1 percent or less of those reported by Kell and Whalley (1965). It can also be seen in figures 5 through 8 that the values of α and β computed from equations (22) and (25) are in close agreement with corresponding values calculated from finite differences in specific volume $((\Delta V/\Delta T)_P/V$ and $(-\Delta V/\Delta P)_T/V$). As shown below, equations (23), (24), and (27) afford similar agreement with their finite difference counterparts

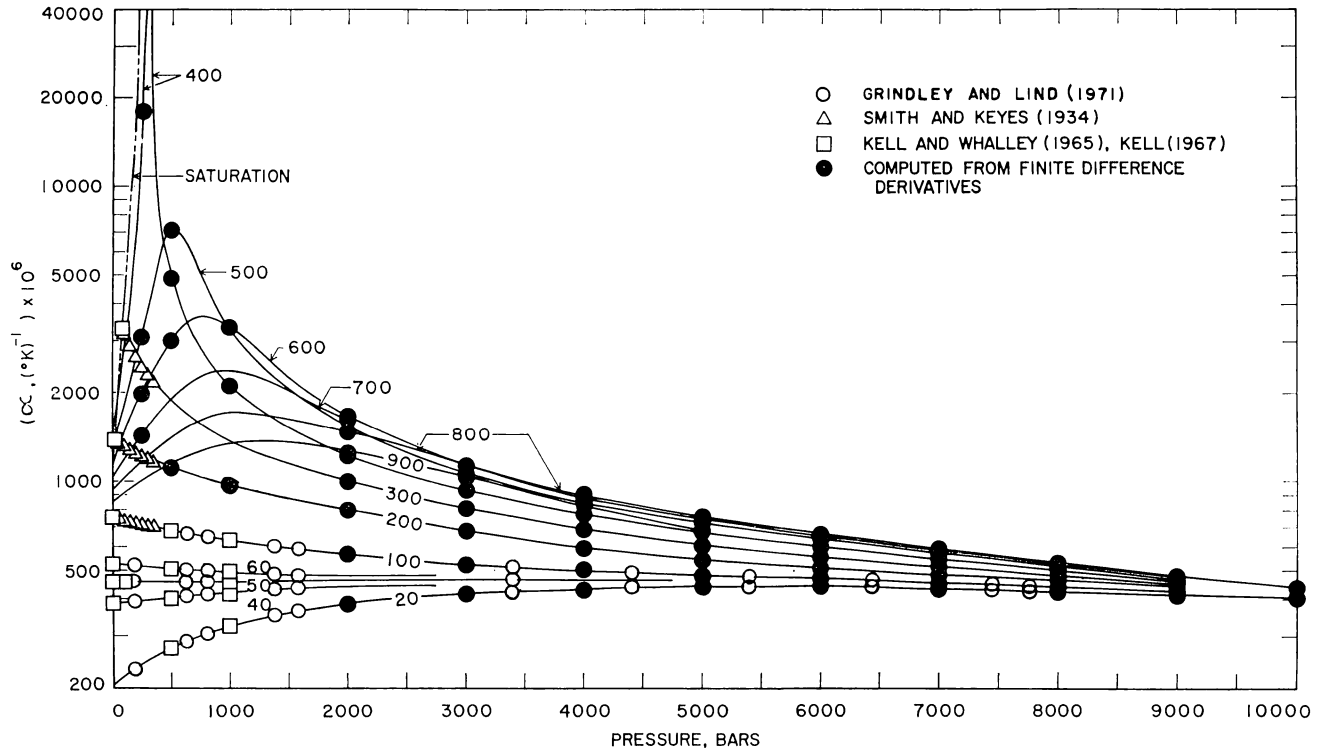


Fig. 6. Coefficient of isobaric thermal expansion (table 7) as a function of pressure at constant temperature (labeled in $^\circ C$) computed from equations (19) through (21), (25), (33), and (39) and coefficients in tables 4, 5, 6, 9, and 10 (curves). The symbols represent values taken from the literature or computed from finite difference derivatives of specific volumes given by Schmidt (1969), Burnham, Holloway, and Davis (1969b), and Keenan and others (1969).

$((\Delta(-\Delta V/\Delta P)_T/V)/\Delta P)_T$, $(\Delta(-\Delta V/\Delta P)_T/V)/\Delta T)_P$, and $(\Delta((\Delta V/\Delta T)_P/V)/\Delta T)_P$.

In principle, the compressibility and thermal expansion of H₂O at pressures above a kilobar can be computed from the isothermal and isobaric partial derivatives of equation (21), which can be written as

$$\left(\frac{\partial V}{\partial P}\right)_T = -V\beta = \sum_{i=0}^i \sum_{j=0}^{i-i} (rj-1) a_{ij} t^i P^{rj-2} \quad (28)$$

and

$$\left(\frac{\partial V}{\partial T}\right)_P = V\alpha = \sum_{i=0}^i \sum_{j=0}^{i-i} i a_{ij} t^{i-1} P^{rj-1} \quad (29)$$

TABLE 8

Coefficient of isothermal compressibility (β) in $\text{bar}^{-1} \times 10^6$ computed from equations (22), (32), and (38) and the values of V in table 3—see figures 7, 8, and 17^a

t (°C)	PRESSURE, KB									
	SAT	0.5	1	2	3	4	5	6	7	8
25	45.60	39.91	36.57	30.0	25.3	21.6	18.8	16.7	15.2	14.1
50	44.36	38.95	36.07	29.8	25.1	21.6	18.8	16.7	15.2	14.1
75	45.89	39.86	36.44	30.0	25.2	21.7	18.9	16.8	15.3	14.2
100	49.50	42.11	37.70	30.8	25.6	22.0	19.2	17.1	15.5	14.4
125	55.12	45.60	39.82	32.0	26.4	22.6	19.7	17.5	15.9	14.6
150	63.09	50.41	42.83	34.0	27.5	23.3	20.3	18.0	16.3	15.0
175	74.24	56.82	46.82	36.6	29.0	24.3	21.0	18.6	16.8	15.4
200	90.09	65.35	52.02	39.7	30.9	25.5	21.9	19.3	17.3	15.8
225	113.48	76.87	58.73	43.6	33.1	27.0	23.0	20.1	18.0	16.4
250	149.96	92.75	67.45	48.1	35.7	28.6	24.1	21.0	18.7	17.0
275	211.54	115.26	78.84	53.3	38.6	30.4	25.4	22.0	19.5	17.7
300	329.06	148.27	93.85	59.3	41.9	32.5	26.9	23.1	20.4	18.4
325	607.65	198.70	113.72	66.3	45.6	34.8	28.5	24.3	21.4	19.2
350	1698.85	280.16	140.04	74.3	49.8	37.3	30.2	25.6	22.5	20.1
375		423.17	174.66	83.6	54.3	40.0	32.1	27.1	23.6	21.1
400		707.68	219.66	94.3	59.3	42.9	34.1	28.6	24.8	22.1
425		1349.14	277.43	106.7	64.8	46.1	36.2	30.2	26.1	23.2
450		2525.76	350.85	120.9	70.7	49.4	38.5	31.9	27.5	24.4
475		3289.09	442.71	137.1	77.1	53.0	40.9	33.7	29.0	25.6
500		3266.80	553.11	155.4	84.0	56.7	43.4	35.6	30.5	26.9
525		3043.18	674.90							
550		2839.08	792.51	189.8	99.9	67.7	48.6	39.9	(33.3)	(29.2)
575		2680.23	889.54							
600		2558.34	958.68	230.0	116.5	76.3	54.0	43.8	(36.5)	(31.9)
625		2463.48	1002.28							
650		2388.27	1026.73	269.1	133.9	85.5	59.5	47.8	(39.7)	(34.5)
675		2327.61	1038.30							
700		2277.93	1041.66	305.5	151.2	94.7	65.1	51.8	(43.0)	(37.2)
725		2236.74	1040.01							
750		2202.21	1035.45	337.3	167.3	103.8	70.5	55.7	(46.1)	(40.0)
775		2173.01	1029.28							
800		2148.12	1022.36	363.7	181.6	112.6	75.8	59.5	(49.3)	(43.0)
825		2126.74	1015.20							
850		2108.27	1008.12							
875		2092.22	1001.31							
900		2078.18	994.87							

^aValues given for temperatures and pressures above 500°C and 6 kb are based on graphic interpolation (see text).

However, evaluation of equations (28) and (29) with the fit coefficients in tables 5 and 6 (which were derived from those obtained by Burnham, Holloway, and Davis, 1969b) from regression of their experimental specific volume measurements with equation 21) yields partial derivatives that differ significantly from corresponding finite difference derivatives $((\Delta V/\Delta P)_T$ and $(\Delta V/\Delta T)_P$) computed directly from the smoothed specific volumes generated by the regression polynomial. Equations (28) and (29) and the coefficients in tables 5 and 6 also yield values of $(\partial V/\partial P)_T$ and $(\partial V/\partial T)_P$ between 1 and 2 kb which are inconsistent with those computed from equations (22) and (25) for pressures \leq a kilobar. Regression of the experimental data with equation (21) apparently led to an overfit of the specific volume measurements in certain parts of the regions depicted in figure 3, and an underfit in others. Linear regression of asymptotic surfaces may lead to errors in derivatives caused by overfitting which are not manifest in the fits of the integral function. In this case the fit coefficients for equation (21) in tables 5 and 6 yield specific volumes to within 0.6 percent of the measured values (see above), but uncertainties in the partial derivatives generated by equations (28) and (29) are as much as two or more orders of magnitude greater at the boundaries of the fit regions.

The coefficients of isothermal compressibility and isobaric thermal expansion of H_2O exhibit dramatic saddle-shaped pressure-temperature configurations with "pommels" at the critical point, where $-(\partial V/\partial P)_T = (\partial V/\partial T)_P = \alpha = \beta = \infty$. To overcome difficulties inherent in achieving accurate algebraic representation of these complicated surfaces with analytic derivatives of specific volume regression polynomials, finite difference derivatives were first computed from specific volumes generated by equation (21) at closely spaced intervals from 0.001 to 10 kb and 20° to 900°C. The computed values of V were used in preference to the experimental measurements to minimize the effect of experimental uncertainty on the finite difference derivatives. The spacing of the intervals was determined by the requirement that the percent change in specific volume be substantially greater than the percent uncertainty in the specific volumes but small enough to yield close approximations of the true derivatives at the midpoints of the intervals. After sorting to eliminate obvious aberrations caused by asymmetry in a number of the finite differences, the values of both $(\Delta V/\Delta P)_T$ and $(\Delta V/\Delta T)_P$ (or corresponding values of α and β computed from the finite difference derivatives) were regressed simultaneously with appropriate derivative polynomials generated from a single integral equation. In an effort to identify the best algebraic expression for this purpose, various polynomials were used to regress the finite difference values as a function of pressure and temperature or density and temperature, but none fit all the values adequately over the entire pressure-temperature range represented by regions 1 and 2 in figure 3. The best fit for the combined regions was obtained by in-

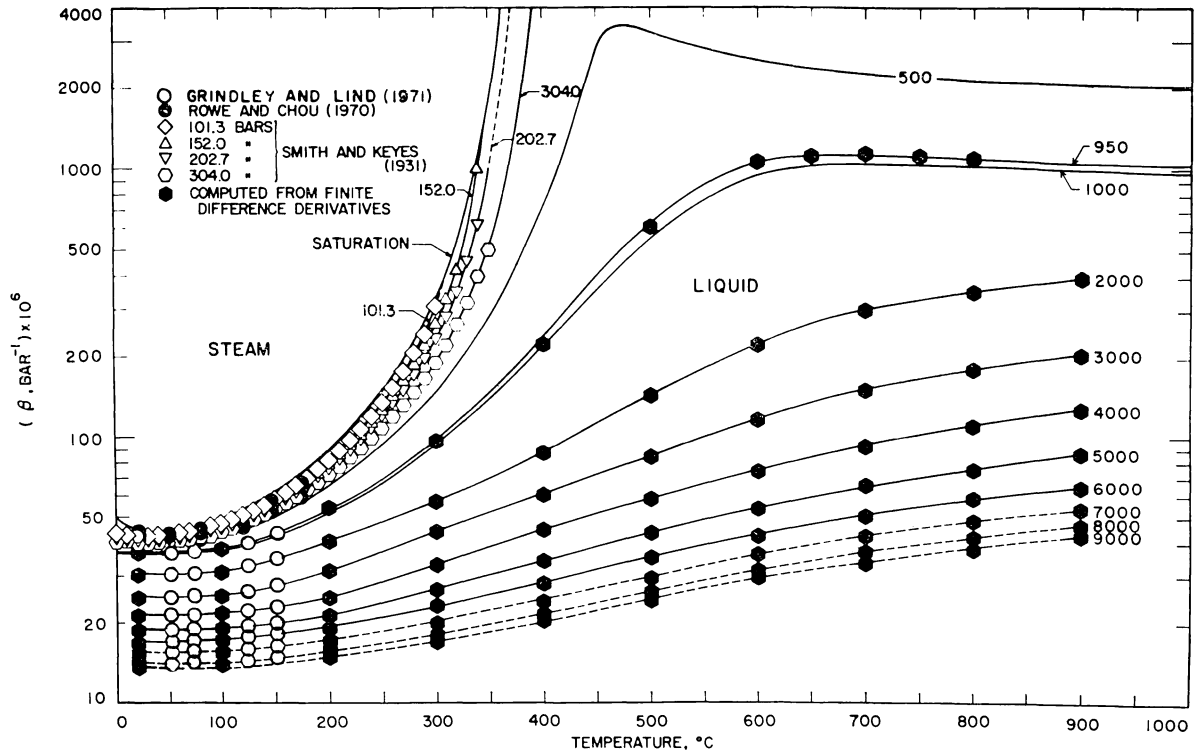


Fig. 7. Coefficient of isothermal compressibility (table 8) as a function of temperature at constant pressure (labeled in bars) computed from equations (19) through (22), (32), and (38) and coefficients in tables 4, 5, 6, 9, and 10 (solid curves). The symbols represent values taken from the literature or computed from finite difference derivatives of specific volumes given by Schmidt (1969), Burnham, Holloway, and Davis (1969b), and Keenan and others (1969). The dashed curves are based on smooth graphic interpolation of the finite difference β values.

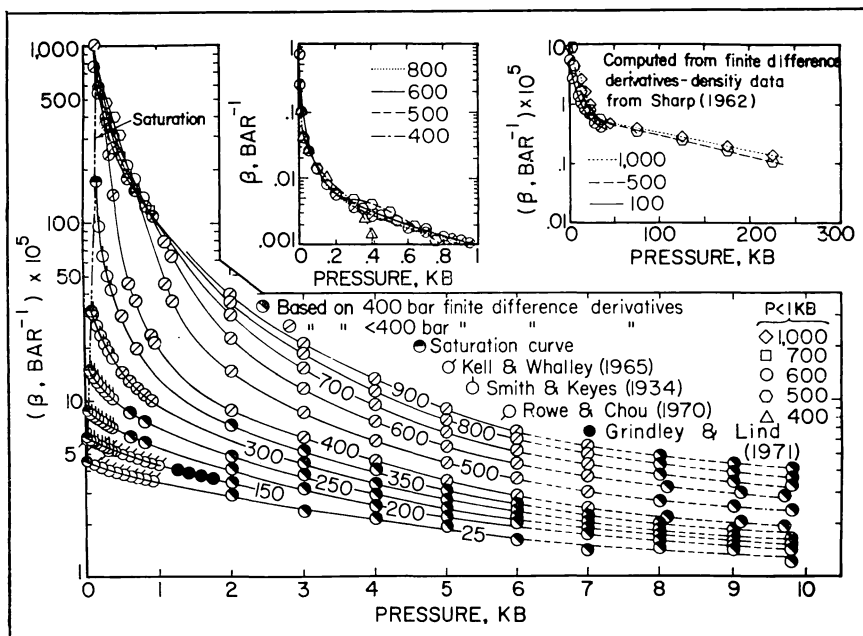


Fig. 8. Coefficient of isothermal compressibility (table 8) as a function of pressure and at constant temperature (labeled in °C) computed from equations (19) through (22), (32), and (38) and coefficients in tables 4, 5, 6, 9, and 10 (solid curves). The symbols represent values taken from the literature or computed from finite difference derivatives of specific volumes given by Schmidt (1969), Burnham, Holloway, and Davis (1969b), and Keenan and others (1969). The dashed curves are based on smooth graphic interpolation of the finite difference β values.

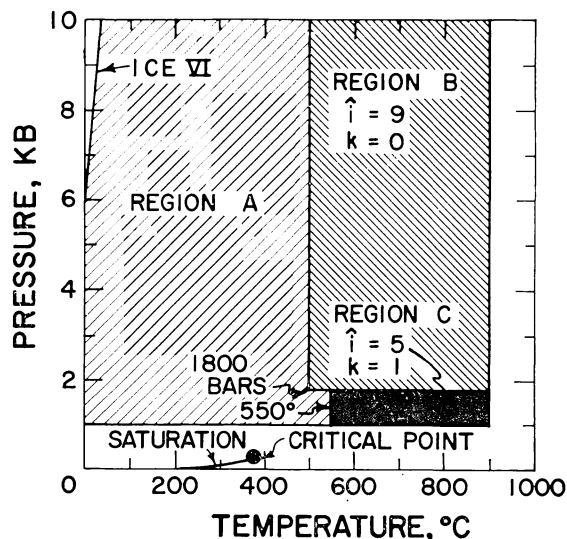


Fig. 9. Regions of pressure and temperature represented by equations (32) through (37) for region A and alternate statements of equations (38) through (43) for regions B and C.

dependent nonlinear regression of the finite difference α and β values with exponential functions of the form

$$\beta = \exp\left(\sum_{i=0}^3 \sum_{j=0}^{7-i} b_{ij} T^i P^j\right) \quad (30)$$

and

$$\alpha = \exp\left(\sum_{i=0}^3 \sum_{j=0}^{7-i} c_{ij} T^i P^j\right) \quad (31)$$

which for the most part rendered residuals in α of less than 1 percent and residuals in β of less than 5 percent. However, at pressures < 1500 bars the residuals increased and reached 10 to 15 percent at the low-pressure boundary of the fit region. The failure of these functions at pressures from 1000 to 1500 bars together with unacceptable discrepancies in the cross derivatives and correspondingly large uncertainties in $(\partial\beta/\partial P)_T$ and $(\partial\alpha/\partial T)_P$ computed from the partial derivatives of equations (30) and (31) forced rejection of these expressions as adequate representatives of α and β .

Further numerical analysis with other functions of temperature and density led to the decision to subdivide the region of pressure and temperature in a fashion similar to that chosen by Burnham, Holloway, and Davis (1969b) for specific volume (fig. 3). Comparative overlapping regression of $(\Delta V/\Delta P)_T$ and $(\Delta V/\Delta T)_P$ in alternate subdivisions with and without including data for pressures \leq a kilobar indicated that all the finite difference derivatives and corresponding values of α and β could be represented with adequate accuracy by separate polynomials describing these variables in the three regions of pressure-temperature space labeled A, B, and C in figure 9. The best fits in region A were obtained with

$$\beta^{-1} = \sum_{j=0}^5 \sum_{i=0}^{8-j} j B_{ij} T^i \rho^j \quad (32)$$

and

$$\alpha = \beta \sum_{j=0}^5 \sum_{i=0}^{8-j} i B_{ij} T^{i-1} \rho^j \quad (33)$$

which are consistent with

$$P = \sum_{j=0}^5 \sum_{i=0}^{8-j} B_{ij} T^i \rho^j \quad (34)$$

where B_{ij} stands for the coefficients given in table 9 for region A in figure 9. Differentiating equation (32) with respect to pressure at constant temperature leads to

$$\left(\frac{\partial\beta}{\partial P}\right)_T = -\beta^3 \sum_{j=0}^5 \sum_{i=0}^{8-j} j^2 B_{ij} T^i \rho^j \quad (35)$$

and the corresponding partial derivative with respect to temperature at constant pressure can be written as

$$\left(\frac{\partial\beta}{\partial T}\right)_P = -\left(\frac{\partial\alpha}{\partial P}\right)_T = -\beta^2 \sum_{j=0}^5 \sum_{i=0}^{8-j} j B_{ij} (iT^{i-1} \rho^j - jT^i \rho^j \alpha) \quad (36)$$

TABLE 9
Coefficients for equations (32) and (33) in region A of figure 9

$B_{ij} = \hat{B}_{ij} \times 10^{B_{ij}^*}$						
\hat{B}_{ij}						
i	j					
	0	1	2	3	4	5
0	0.	5.541654961	-5.647694994	1.391084523	9.314051406	-4.224085781
1	2.001619452	-6.480330829	7.804635059	-4.149778955	8.284235229	-3.173272705
2	-8.445248783	2.599081364	-2.997059355	1.567146158	-3.437390375	1.864672542
3	1.849203613	-5.126544377	5.215914752	-2.327295430	4.123082012	-1.650956925
4	-2.344156348	5.544129599	-4.597168845	1.520379055	-1.562138539	
5	1.782166279	-3.321663469	1.982307354	-3.619181443		
6	-8.063473576	1.021229414	-3.272068272			
7	2.064415341	-1.237172220				
8	-2.498805152					

B_{ij}^*						
i	j					
	0	1	2	3	4	5
0	0	6	6	6	5	5
1	4	4	4	4	3	1
2	1	2	2	2	1	0
3	-1	-1	-1	-1	-2	-3
4	-4	-4	-4	-4	-5	
5	-7	-7	-7	-8		
6	-11	-10	-11			
7	-14	-14				
8	-18					

Similarly, the partial derivative of equation (33) with respect to temperature at constant pressure is given by

$$\left(\frac{\partial\alpha}{\partial T}\right)_P = \frac{\alpha}{\beta}\left(\frac{\partial\beta}{\partial T}\right)_P + \beta \sum_{j=0}^5 \sum_{i=0}^{8-j} i B_{ij} ((i-1)T^{i-2} \rho^j - jT^{i-1} \rho^j \alpha) \tag{37}$$

The finite difference derivatives in regions B and C of figure 9 can be represented closely by equations of the form

$$\left(\frac{\partial V}{\partial P}\right)_T = -\beta V = \sum_{i=0}^i \sum_{j=0}^{i+k-i} j D_{ij} T^i P^{j-1} \tag{38}$$

and

$$\left(\frac{\partial V}{\partial T}\right)_P = \alpha V = \sum_{i=0}^i \sum_{j=0}^{i+k-i} i D_{ij} T^{i-1} P^j \tag{39}$$

which are consistent with

$$V = \sum_{i=0}^i \sum_{j=0}^{i+k-i} D_{ij} T^i P^j \tag{40}$$

where D_{ij} , i , and k refer to the arrays of fit coefficients and integer constants given in table 10 for regions B and C in figure 9. It follows from equation (38) that we can write

$$\left(\frac{\partial\beta}{\partial P}\right)_T = \beta^2 - \rho \sum_{i=0}^i \sum_{j=0}^{i+k-i} j(j-1)D_{ij} T^i P^{j-2} \tag{41}$$

and

$$\left(\frac{\partial\beta}{\partial T}\right)_P = -\left(\frac{\partial\alpha}{\partial P}\right)_T = -\alpha\beta - \rho \sum_{i=0}^i \sum_{j=0}^{i+k-i} ijD_{ij} T^{i-1} P^{j-1} \tag{42}$$

Similarly, the partial derivative of equation (39) with respect to temperature at constant pressure leads to

$$\left(\frac{\partial\alpha}{\partial T}\right)_P = -\alpha^2 + \rho \sum_{i=0}^i \sum_{j=0}^{i+k-i} i(i-1)D_{ij} T^{i-2} P^{j-1} \tag{43}$$

The coefficients in equations (32) through (37) for region A in figure 9 (table 9) and those in table 10 for alternate statements of equations (38) through (43) for regions B and C were obtained by simultaneous linear regression of $(-\Delta V/\Delta P)_T/V$ and $(\Delta V/\Delta T)_P/V$ with equations (32) and (33), and $(\Delta V/\Delta P)_T$ and $(\Delta V/\Delta T)_P$ with equations (38) and (39). The values of V employed in the calculations were computed from equation (21). The number of finite difference derivatives considered in the regression analysis of the regions varied from 100 to 300, depending on the region. The limits of the summation terms in equations (32) through (37) and (38) through (43) were defined by comparative regression of the finite difference data with polynomials of alternate degree in an effort to preclude overfit and insure partial derivatives consistent with their finite difference counterparts. Overlapping regression of the fit regions and incorporation of data for pressures below a kilobar in fitting regions A and C in figure 9 minimized inter-regional discontinuities in the computed values of α , β , and their partial derivatives as functions of temperature and pressure. In most cases the inter-regional discrepancies in α are less than 1 percent,

TABLE 10
Coefficients for equations (38) and (39) in regions B and C of figure 9
($i = 9$ and $k = 0$ for region B, and $i = 5$ and $k = 1$ for region C)

$$D_{ij} = \hat{D}_{ij} \times 10^6 i!$$

\hat{D}_{ij} for region B					
i	j				
	0	1	2	3	4
0	0.	-1.506919791	1.407973492	-7.507571325	2.471604632
1	-1.73752824	2.810937616	7.031625811	-5.954625622	2.223890468
2	4.503625642	-7.193725721	5.156729178	-1.997843646	4.203016232
3	1.986537032	-1.133016027	5.705056876	-1.410074499	1.247849426
4	-5.376132969	-1.172816191	3.305071187	3.521599490	-9.298387117
5	1.484839030	-3.468262960	-6.1135922413	7.391640366	-1.171172984
6	-1.126923624	7.595081341	-1.272723651	-1.546104985	
7	-8.992177755	-4.338459618	1.368240982		
8	1.459740213	6.914686939			
9	-4.903210863				

\hat{D}_{ij} for region C				
i	j			
	0	1	2	3
0	0.	4.668287584	-7.085868594	2.111356062
1	-7.041518081	2.955659758	2.779240901	-1.768464908
2	2.151504359	-1.525948185	4.132847534	9.211139144
3	-2.773357282	2.067817026	-2.526689074	-1.019479759
4	1.650848239	-1.137352755	1.051203720	
5	-3.731274546	2.162263675		

\hat{D}_{ij} for region B					
i	j				
	5	6	7	8	9
0	-5.205698231	7.023757340	-5.865613363	2.757432199	-5.572007869
1	-4.458179301	4.957412121	-2.879352320	6.815947672	
2	-4.702839663	2.617250953	-5.673263000		
3	-2.017582894	-1.207488032			
4	3.676616808				

\hat{D}_{ij} for region C						
i	j					
	4	5	6			
0	7.954938710	-4.642576017	6.177986362			
1	3.383614741	-2.222308253				
2	-1.082504726					

D_{ij}^a for region B										
i	j									
	0	1	2	3	4	5	6	7	8	9
0	0	-3	-6	-10	-13	-17	-21	-25	-29	-34
1	-4	-8	-10	-13	-16	-20	-24	-28	-33	
2	-6	-9	-12	-15	-19	-23	-27	-32		
3	-8	-11	-15	-18	-22	-27	-31			
4	-11	-15	-18	-22	-26	-30				
5	-13	-17	-21	-25	-29					
6	-16	-20	-24	-28						
7	-20	-23	-27							
8	-22	-27								
9	-26									

D_{ij}^a for region C							
i	j						
	0	1	2	3	4	5	6
0	0	-3	-5	-8	-12	-15	-19
1	-1	-4	-7	-10	-14	-18	
2	-3	-6	-11	-14	-17		
3	-6	-9	-13	-17			
4	-9	-12	-16				
5	-13	-16					

and those in β are less than 4 percent. However, corresponding discrepancies in the partial derivatives of α and β are generally larger (see below).

Equations (32) and (33) fit the finite difference values of α and β in region A of figure 9 to within 3 percent, except for three residuals less than 4 percent and four less than 8 percent. With the exception of two residuals less than 4 percent, equation (38) represents $(\Delta V/\Delta P)_T$ in region B of figure 9 to within 2 percent at pressures ≤ 6 kb. Above 6 kb in region B, the regression equation yields residuals in excess of minimal requirements for dependable partial differentiation. Most of the residuals above 6 kb in region B are of the order of 5 percent or less, seven are between 5 and 10 percent, and one is greater than 10 percent. Although these latter residuals are not excessive, their distribution is nonrandom, which precludes general application of equation (38) and the fit coefficients in table 10 for pressures above 6 kb in region B. The uncertainty in both α and β in region C is less than 4 percent, except four residuals in β which are less than 8 percent. Equation (39) reproduces the values of $(\Delta V/\Delta T)_P$ in both regions B and C to within 1 percent from 1 to 10 kb, with the exception of ten residuals which are less than 3 percent. Except as noted above and in the vicinity of the region boundaries, the residuals in all of the fits approximate random distributions. Values of α and β calculated from equations (32) and (33) for temperatures $\leq 150^\circ\text{C}$ and pressures $>$ a kilobar are within 4 percent of those computed by Grindley and Lind (1971). The two sets of values diverge from one another with increasing pressure above ~ 3 kb. At higher pressures, the values of α computed by Grindley and Lind are slightly lower and those of β slightly higher than the corresponding values computed in this study. Although equations (34) and (40) yield values of V in good accord with those generated by equation (21), the latter expression is more convenient to use and affords more accurate representation of the experimental specific volumes of H_2O reported by Burnham, Holloway, and Davis (1969a). Simultaneous regression of β^{-1} , α , and P with equations (32) through (34), and V , $(\Delta V/\Delta P)_T$ and $(\Delta V/\Delta T)_P$ with equations (38) through (40) rendered essentially the same results as those obtained without including P , V , and equations (34) and (40).

Values of α and β computed from equations (21), (32), (33), (38), and (39) for pressures greater than a kilobar in regions A, B, and C of figure 9 are given in tables 7 and 8 together with those calculated from equations (22) and (25) for pressures \leq a kilobar. The close agreement of the computed values (solid curves) with their finite difference counterparts and those calculated by Grindley and Lind (1971) is apparent in figures 5 through 8, where α and β are plotted as functions of temperature and pressure. The coefficients for region A were used to compute the values for α and β at 500°C and pressures $>$ a kilobar. The dashed curves in figure 8 and the parenthetical values in table 8 above 500°C and 6 kb represent graphic extrapolations of the computed values below 6 kb, extended through the high-pressure finite difference β values. As indicated above, equation (38) and the fit coefficients in table 10 are not suitable

for accurate representation of β in this region of temperature-pressure space.

The dependence of β on pressure above 10 kb is depicted in the upper right inset diagram of figure 8, where finite difference values of β computed from specific volumes generated by Sharp (1962) from shock wave data are plotted for pressures to 225 kb at 500° and 1000°C. The curves in the upper right inset diagram of figure 8, like those for 600° to 900°C at pressures above 6 kb in figures 7 and 8, were not computed but represent smooth graphic interpolations of the finite difference values of β .

It can be seen in figure 5 that the logarithm of α exhibits a reverse sigmoid isobaric dependence on temperature at pressures and temperatures below ~ 2 kb and the critical temperature; that is, as temperature increases at constant pressure from 0° to 374°C at low pressures, $\log \alpha$ first increases to a decreasing degree and then to an increasing degree. At the critical point, α approaches infinity. For pressures greater than the critical pressure, the isobars in figure 5 exhibit extrema that dampen and shift progressively to higher temperatures with increasing pressure to ~ 6 kb, above which the extrema disappear. At pressures from ~ 2 to 5 kb, $\log \alpha$ increases to a decreasing degree as temperature increases isobarically from 0° to $\sim 700^\circ\text{C}$, but at higher pressures the isobars exhibit minima below 100°C. At temperatures below $\sim 50^\circ\text{C}$, α increases as pressure increases isothermally, but between $\sim 50^\circ\text{C}$ and the critical temperature α decreases with increasing pressure at constant temperature (fig. 6). The difference in the dependence of α on pressure above and below $\sim 50^\circ\text{C}$ can be attributed to the effect of temperature on the structural order of liquid H_2O . At temperatures above the critical temperature, the isotherms in figure 6 exhibit extrema below ~ 2 kb, which dampen and shift to higher pressures with increasing temperature.

In contrast to the behavior of α , β decreases monotonically as pressure increases isothermally at all temperatures (fig. 8), changing from $> 4 \times 10^{-5} \text{ bar}^{-1}$ at 1 bar to $< 1 \times 10^{-6} \text{ bar}^{-1}$ between 200 and 300 kb. Where the extrema in the isobaric temperature dependence of β dampen with increasing pressure and disappear above a kilobar (fig. 7), the extrema in the α isobars persist to much higher pressures (fig. 5). Nevertheless, the magnitude of the change in α and β is of the same order of magnitude for a temperature increase from 0° to 900°C at high pressures (figs. 5 and 7).

Partial derivatives of α and β calculated for pressures \leq a kilobar from equations (23), (24), and (27) together with those for higher pressures computed from alternate statements of equations (35) through (37) and (41) through (43) for the various regions in figure 9 are given in tables 11 through 13 and plotted as curves in figures 10 through 15, where they can be compared with their finite difference counterparts (designated by the symbols). The values of V , α , and β required for the calculations were computed in the manner described above.

It can be seen in figures 10 through 13 that the calculated dependence of $(\partial\beta/\partial P)_T$ and $(\partial\alpha/\partial T)_P$ on temperature and pressure is in reasonably close agreement with that defined by the finite difference derivatives (figs. 10 through 13), which are uncertain to a comparable extent. The computed values of $(\partial\beta/\partial P)_T$ and $(\partial\alpha/\partial T)_P$ differ from their finite difference counterparts by less than ~ 10 to 20 percent, which corresponds to the maximum inter-regional discrepancy in the calculated values of $(\partial\beta/\partial P)_T$ at the boundary separating regions A and B in figure 9 above 4 kb (indicated by the zigzag segments of the 4.5 and 5.5 isobars in the inset diagram of fig. 10). For the most part, uncertainties in the values of $(\partial\beta/\partial P)_T$ and $(\partial\alpha/\partial T)_P$ computed for region A of figure 9 are of the order of 5 to 10 percent or less, which also corresponds to the uncertainty in the cross derivatives in all of the regions (figs. 14 and 15).

The configuration of the 850°C isotherm in the inset diagram of figure 13 is apparently the result of an overfit of α as a function of pres-

TABLE 11
Partial derivative of the coefficient of isothermal compressibility with respect to pressure at constant temperature in $\text{bar}^{-2} \times 10^9$ computed from equations (23), (35), and (41) and the values of V and β in tables 3 and 8—see figures 10 and 11

t (°C)	PRESSURE, KB									
	SAT	0.5	1	2	3	4	5	6	7	8
25	-15.66	-8.32	-5.48	-5.2	-4.5	-3.4	-2.4	-1.8	-1.3	-1.0
50	-15.17	-7.61	-4.33	-5.5	-4.4	-3.3	-2.4	-1.7	-1.3	-1.0
75	-16.66	-8.73	-5.38	-5.8	-4.4	-3.3	-2.4	-1.7	-1.3	-1.0
100	-20.20	-10.95	-7.23	-6.3	-4.6	-3.3	-2.4	-1.8	-1.4	-1.1
125	-26.18	-14.19	-9.58	-7.0	-4.8	-3.5	-2.5	-1.9	-1.4	-1.1
150	-35.71	-18.72	-12.49	-7.9	-5.3	-3.7	-2.7	-2.0	-1.5	-1.2
175	-51.18	-25.14	-16.17	-9.2	-5.9	-4.0	-2.8	-2.1	-1.6	-1.3
200	-77.56	-34.48	-20.99	-11.0	-6.6	-4.4	-3.1	-2.2	-1.7	-1.3
225	-126.08	-48.67	-27.52	-13.2	-7.6	-4.8	-3.4	-2.4	-1.8	-1.4
250	-225.07	-71.26	-36.64	-16.1	-8.8	-5.4	-3.7	-2.6	-2.0	-1.5
275	-458.96	-109.23	-49.69	-19.8	-10.2	-6.1	-4.0	-2.9	-2.1	-1.7
300	-1149.55	-177.26	-68.70	-24.3	-11.9	-6.8	-4.5	-3.1	-2.3	-1.8
325	-4157.99	-309.25	-96.73	-30.0	-14.0	-7.7	-4.9	-3.4	-2.5	-1.9
350	-36533.97	-593.80	-138.31	-37.1	-16.3	-8.7	-5.5	-3.7	-2.7	-2.1
375		-1301.64	-200.02	-46.0	-19.1	-9.9	-6.0	-4.1	-3.0	-2.2
400		-3408.99	-291.82	-57.0	-22.2	-11.1	-6.7	-4.5	-3.2	-2.4
425		-10301.90	-428.91	-70.7	-25.8	-12.5	-7.4	-4.9	-3.5	-2.6
450		-21635.72	-632.16	-87.5	-29.9	-14.0	-8.1	-5.3	-3.7	-2.8
475		-17449.07	-919.85	(-107.8)	(-34.6)	(-15.7)	(-8.9)	(-5.7)	(-4.0)	(-2.9)
500		-9634.83	-1281.11	(-131.9)	(-39.8)	(-17.5)	(-9.7)	(-6.2)	(-4.3)	(-3.1)
525		-6409.38	-1642.09							
550		-5247.95	-1888.38							
575		-4771.15	-1964.67							
600		-4540.93	-1913.62							
625		-4412.99	-1806.70							
650		-4333.65	-1690.38							
675		-4280.30	-1584.32							
700		-4242.27	-1494.07							
725		-4214.01	-1419.51							
750		-4192.36	-1358.69							
775		-4175.38	-1309.26							
800		-4161.80	-1269.07							
825		-4150.78	-1236.26							
850		-4141.68	-1209.35							
875		-4134.06	-1187.13							
900		-4127.57	-1168.66							

sure at temperatures $\cong 650^\circ\text{C}$, where the uncertainty in $(\partial\alpha/\partial T)_P$ is large. For this reason, values of $(\partial\alpha/\partial T)_P$ are not given in table 13 for temperatures $> 500^\circ\text{C}$ at pressures $>$ a kilobar. The appearance of the isobars for 2, 5, and 10 kb in figure 12 also suggests overfit, but the similar configurations of the isobars for 1 and 2 kb imply that all the undulations in $(\partial\alpha/\partial T)_P$ as an isobaric function of temperature cannot be ascribed to

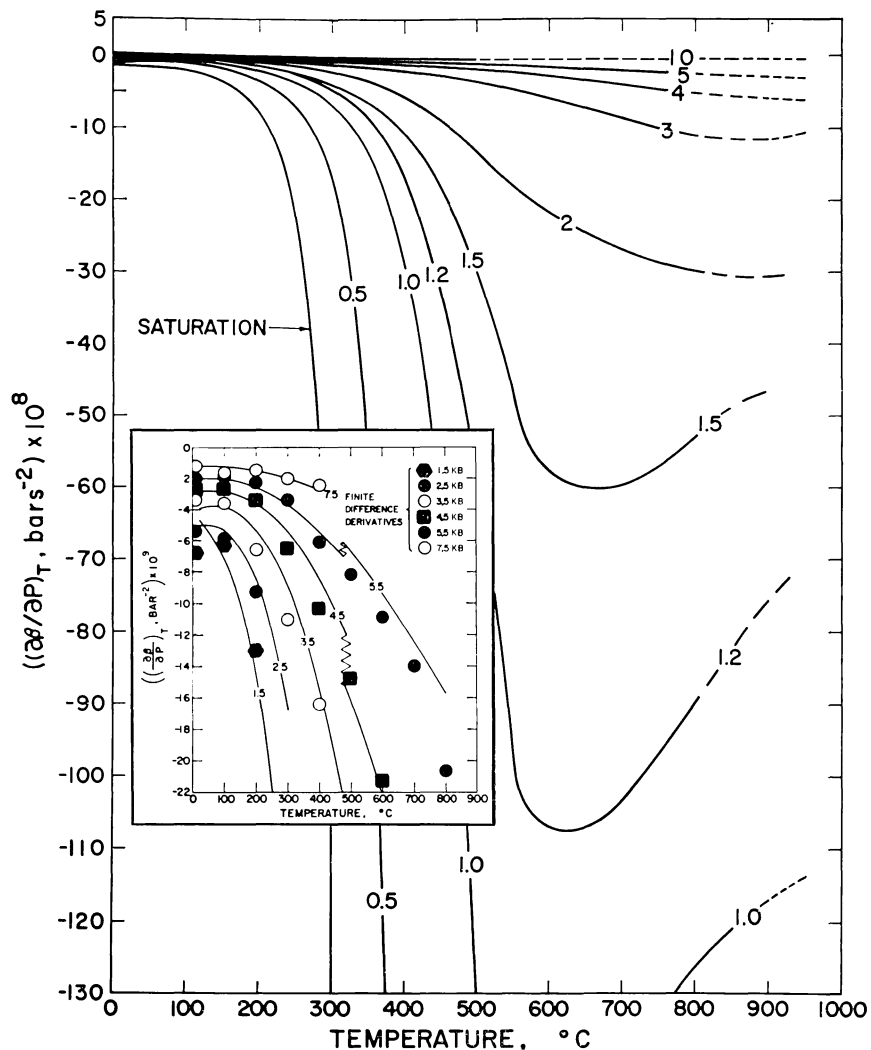


Fig. 10. Partial derivative of the coefficient of isothermal compressibility with respect to pressure at constant temperature (table 11) as a function of temperature at constant pressure (labeled in kb) computed from equations (19) through (23), (32), (35), (38), and (41) and coefficients in tables 4, 5, 6, 9, and 10 (curves). The symbols in the inset diagram represent finite difference derivatives calculated from the finite difference values of β plotted in figures 7 and 8.

regression vagaries. In contrast to the higher pressure isobars, the 1 kb curve was calculated from equation (27). Although no evidence of overfit is apparent in the computed curves of $(\partial\beta/\partial T)_P$ in figures 14 and 15, values of $(\partial\beta/\partial T)_P$ for temperatures $> 500^\circ\text{C}$ at pressures > 1 kb have been omitted from table 12 because of the failure of equation (38) to represent adequately the finite difference values of β at high pressures and temperatures (see above). This observation, coupled with the inter-regional discrepancies in $(\partial\beta/\partial P)_T$ in figure 10, also required omission of values of $(\partial\beta/\partial P)_T$ from table 11 for temperatures $> 500^\circ\text{C}$ at pressures $> a$ kilobar.

It can be seen in figure 11 that $(\partial\beta/\partial P)_T$ increases dramatically with increasing pressure at constant temperature. As pressure approaches 10 kb, $(\partial\beta/\partial P)_T \rightarrow (\partial^2\beta/\partial P^2)_T \rightarrow 0$ at all temperatures. Similarly, $(\partial\beta/\partial P)_T$ becomes a small negative number and $(\partial(\partial\beta/\partial P)_T/\partial T)_P \rightarrow 0$ as temperature decreases isobarically below $\sim 200^\circ\text{C}$ at all pressures (fig. 10). The critical phenomenon causes $(\partial\beta/\partial P)_T$ to minimize with increasing tem-

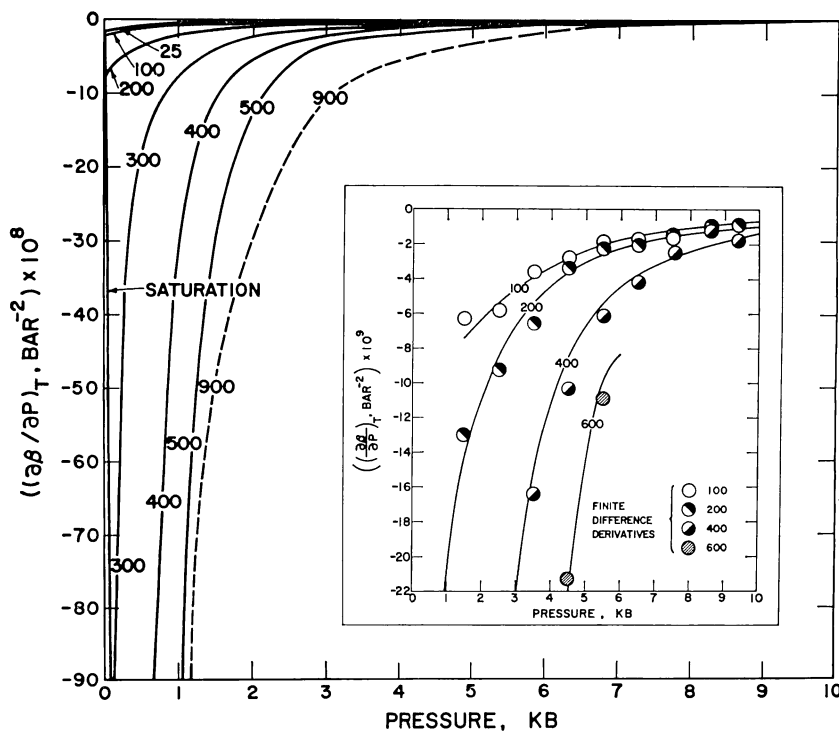


Fig. 11. Partial derivative of the coefficient of isothermal compressibility with respect to pressure at constant temperature (table 11) as a function of pressure at constant temperature (labeled in $^\circ\text{C}$) computed from equations (19) through (23), (32), (35), and (41) and coefficients in tables 4, 5, 6, 9, and 10 (curves). The symbols in the inset diagram represent finite difference derivatives calculated from the finite difference values of β plotted in figures 7 and 8.

perature at constant pressure ≤ 3 kb, and the temperature corresponding to the minimum in the isobars increases with increasing pressure (fig. 10). Note in figures 14 and 15 that $(\partial\beta/\partial T)_P$ is small and negative at all pressures below $\sim 30^\circ$ to 50°C but increases rapidly and maximizes with increasing temperature at constant pressure. At pressures \leq a kilobar, further increase in temperature at constant pressure causes $(\partial\beta/\partial T)_P$ again to pass through zero and minimize at high temperatures. At higher pressures the high-temperature minimum disappears, as does the low-pressure extremum in the isothermal pressure dependence of $(\partial\beta/\partial T)_P$ as temperature decreases (fig. 16). In contrast, it can be seen in figure 12 that the isobaric maxima in $(\partial\alpha/\partial T)_P$ as a function of temperature at pressure ≤ 2 kb are complemented by minima at higher temperatures, all of which dampen and disappear at higher pressures where $(\partial^2\alpha/\partial T^2)_P$ becomes small. As pressure increases isothermally, $(\partial\alpha/\partial T)_P \rightarrow (\partial(\partial\alpha/$

TABLE 12

Partial derivative of the coefficient of isothermal compressibility with respect to temperature at constant pressure in $\text{bar}^{-1} (\text{°K})^{-1} \times 10^8$ computed from equations (24), (36), and (42) and the values of V , α , and β in tables 3, 7, and 8—see figures 14 and 15

t (°C)	PRESSURE, KB									
	SAT	0.5	1	2	3	4	5	6	7	8
25	-12.38	-9.11	-3.75	-2.1	-2.2	-1.4	-0.8	-0.4	-0.2	-0.2
50	1.33	0.46	-0.29	0.2	-0.3	-0.1	0.1	0.2	0.3	0.2
75	10.53	6.48	3.26	2.2	1.4	1.1	1.0	0.8	0.7	0.6
100	18.44	11.49	6.77	4.2	2.8	2.1	1.7	1.4	1.2	1.0
125	27.00	16.47	10.22	6.2	4.1	3.0	2.4	1.9	1.5	1.3
150	37.95	22.18	13.91	8.3	5.3	3.9	3.0	2.4	1.9	1.6
175	53.72	29.45	18.21	10.6	6.6	4.7	3.6	2.8	2.3	1.9
200	78.49	39.39	23.55	13.2	7.9	5.5	4.1	3.2	2.6	2.1
225	120.67	53.64	30.48	16.0	9.3	6.3	4.6	3.6	2.9	2.4
250	199.64	74.87	39.68	19.1	10.7	7.0	5.1	4.0	3.2	2.6
275	368.11	107.72	52.08	22.6	12.1	7.8	5.6	4.3	3.5	2.9
300	808.94	160.75	68.82	26.3	13.7	8.6	6.1	4.7	3.8	3.1
325	2474.81	251.22	91.23	30.4	15.2	9.3	6.6	5.0	4.0	3.4
350	17421.98	419.05	120.56	34.9	16.9	10.1	7.1	5.4	4.3	3.6
375		772.55	157.77	40.0	18.5	10.9	7.6	5.8	4.6	3.9
400		1639.66	203.81	45.6	20.3	11.8	8.1	6.1	4.9	4.2
425		3741.13	260.33	52.0	22.2	12.6	8.6	6.5	5.2	4.4
450		4831.26	329.07	59.3	24.1	13.4	9.1	6.8	5.5	4.7
475		1076.18	406.24	(67.2)	(26.0)	(14.2)	(9.5)	(7.2)	(5.8)	(5.0)
500		-770.92	472.33	(75.8)	(27.9)	(14.9)	(9.9)	(7.5)	(6.1)	(5.2)
525		-900.62	491.07							
550		-723.48	438.04							
575		-554.18	333.40							
600		-427.69	221.75							
625		-336.07	131.55							
650		-268.95	68.35							
675		-218.72	27.26							
700		-180.33	1.73							
725		-150.40	-13.52							
750		-126.68	-22.16							
775		-107.60	-26.60							
800		-92.08	-28.43							
825		-79.33	-28.64							
850		-68.76	-27.87							
875		-59.95	-26.55							
900		-52.56	-24.93							

$\partial T)_P/\partial P)_T \rightarrow 0$ at all temperatures (fig. 13). Below $\sim 500^\circ\text{C}$, $(\partial\alpha/\partial T)_P$ is positive, except at high pressures and low temperatures.

The effect of the critical phenomenon and low-temperature structural contributions to the expansibility and compressibility of H_2O are also apparent in figures 16 and 17, where isopleths of α and β are plotted as functions of pressure and temperature. It can be seen that $(\partial P/\partial T)_\alpha$ is negative at low temperatures for $\alpha < 4.3 \times 10^{-4} (\text{°K})^{-1}$, but at higher temperatures the isopleths curve around the "infinite peak" of the critical point in an elliptical pattern which widens progressively with increasing

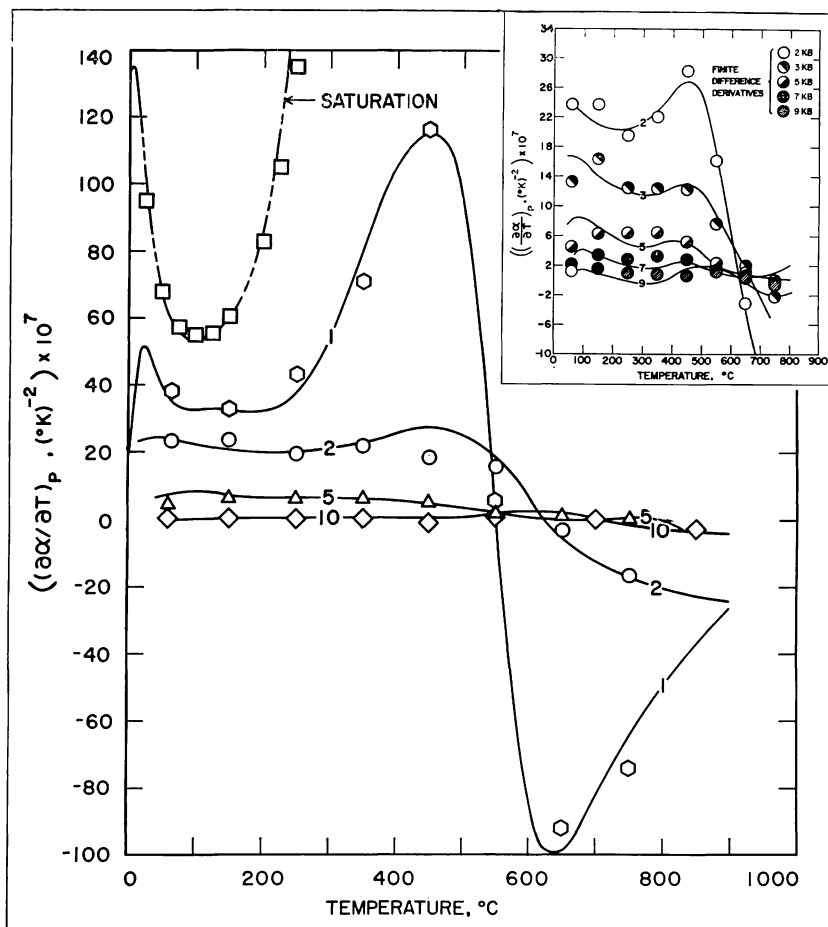


Fig. 12. Partial derivative of the coefficient of isobaric thermal expansion with respect to temperature at constant pressure (table 13) as a function of temperature at constant pressure (labeled in kb) computed from equations (19) through (21), (25), (27), (33), (37), (39), and (43) and coefficients in tables 4, 5, 6, 9, and 10 (curves). The symbols in the inset diagram represent finite difference derivatives calculated from the finite difference values of α plotted in figures 5 and 6.

pressure and temperature. At the critical point, $\alpha = \beta = (\partial\alpha/\partial T)_P = (\partial\beta/\partial P)_T = (\partial\beta/\partial T)_P = -(\partial\alpha/\partial P)_T = \infty$. However, as the thermodynamic behavior of H₂O approaches ideality with decreasing pressure, and $\alpha \rightarrow 1/T$, $\beta \rightarrow 1/P$. Hence, as $P \rightarrow 0$, $\beta \rightarrow (\partial\beta/\partial P)_T \rightarrow \infty$. As a consequence, the isopleths for $\beta \leq 10^{-3}$ bar⁻¹ in figure 17 do not close around the infinite critical peak as the isopleths for α do in figure 16. Instead, the isopleths at high temperatures and low pressures in figure 17 coincide with isobaric contours along an infinite "cliff" at low pressures and high temperatures. The infinite critical peak is perched on the slope of the

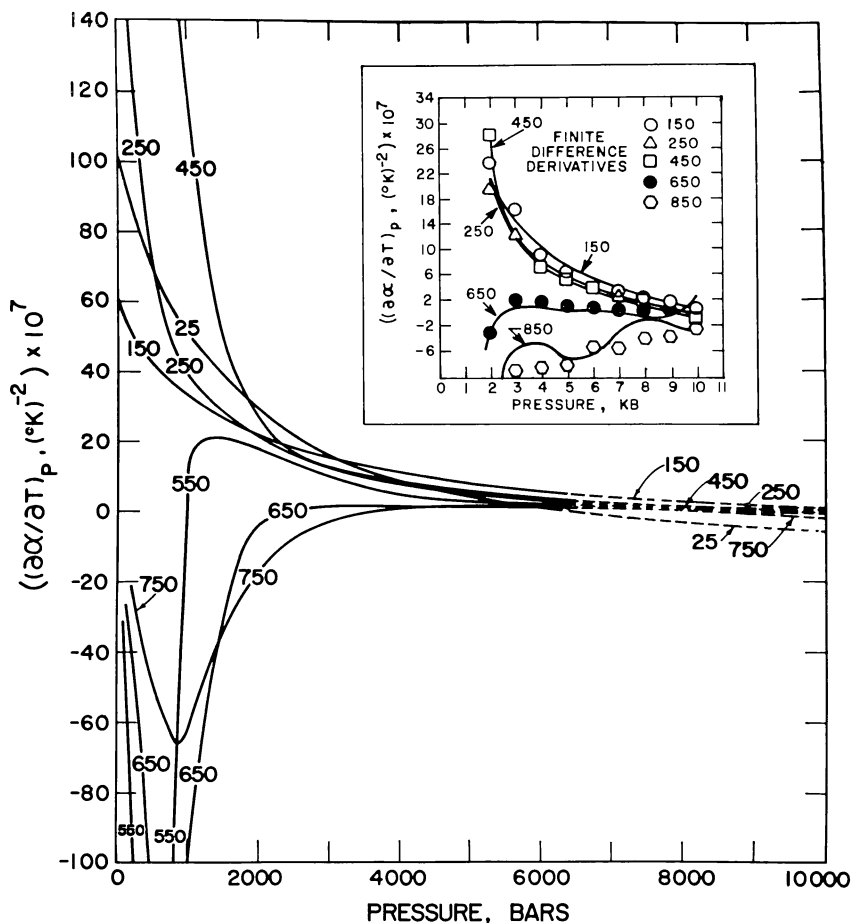


Fig. 13. Partial derivative of the coefficient of isobaric thermal expansion with respect to temperature at constant pressure (table 13) as a function of pressure at constant temperature (labeled in °C) computed from equations (19) through (21), (25), (27), (33), (37), (39), and (43) and coefficients in tables 4, 5, 6, 9, and 10 (curves). The symbols in the inset diagram represent finite difference derivatives calculated from the finite difference values of α plotted in figures 5 and 6.

cliff and separated from its summit by a minimum corresponding to $\beta > 10^{-3} \text{ bar}^{-1}$. As a consequence it fails to show up in figure 17.

The minimum in the isobaric temperature dependence of β at low temperatures (fig. 7) caused by structural ordering of the water dipoles results in corresponding minima in the isopleths for β below 100°C and $\sim 2 \text{ kb}$ in figure 17. No such minima occur in the case of α , but the latter variable becomes negative in the vicinity of the triple point, where β is positive and equal to its value at $\sim 500^\circ\text{C}$ and 5 kb . Increasing orientation of water dipoles with decreasing temperature thus has a dramatically different effect on α and β , and this difference persists to high pressures.

DIELECTRIC CONSTANT

Experimental values of the dielectric constant (ϵ) of H_2O are available at intervals ranging from a few degrees and bars along the satura-

TABLE 13

Partial derivative of the coefficient of isobaric thermal expansion with respect to temperature at constant pressure in $(^\circ\text{K})^{-2} \times 10^7$ computed from equations (27), (37), and (43) and the values of V and α in tables 3 and 7—see figures 12 and 13

t ($^\circ\text{C}$)	PRESSURE, KB									
	SAT	0.5	1	2	3	4	5	6	7	8
25	101.96	69.82	51.56	24.1	15.4	8.7	3.9	0.6	-1.6	-3.4
50	68.17	50.48	39.88	24.2	16.8	11.2	7.0	4.0	1.9	0.2
75	55.57	42.42	33.64	23.4	16.7	12.0	8.3	5.6	3.6	2.0
100	53.29	40.93	32.79	22.4	16.1	11.8	8.6	6.1	4.2	2.8
125	55.46	41.54	33.05	21.6	15.3	11.2	8.2	5.9	4.2	2.8
150	60.54	42.65	32.73	20.9	14.4	10.4	7.6	5.5	3.8	2.5
175	69.80	44.66	32.08	20.5	13.5	9.6	6.9	4.8	3.3	2.1
200	86.69	48.93	32.11	20.3	12.8	8.7	6.1	4.2	2.7	1.6
225	117.28	57.15	33.81	20.3	12.1	8.0	5.4	3.6	2.2	1.1
250	173.68	71.19	37.93	20.5	11.7	7.5	4.9	3.2	1.8	0.8
275	285.40	93.38	44.90	20.8	11.4	7.1	4.6	2.9	1.6	0.6
300	547.08	126.95	54.83	21.3	11.4	7.0	4.5	2.8	1.6	0.5
325	1415.93	177.30	67.37	22.1	11.6	7.0	4.6	2.9	1.7	0.6
350	8078.16	256.26	81.34	23.0	11.9	7.3	4.8	3.2	1.9	0.8
375		396.13	94.69	24.1	12.2	7.5	5.1	3.4	2.1	1.1
400		680.35	105.24	25.2	12.5	7.7	5.3	3.7	2.4	1.3
425		1137.94	112.11	26.2	12.6	7.8	5.4	3.8	2.5	1.4
450		569.16	115.44	26.9	12.3	7.5	5.2	3.6	2.5	1.4
475		-775.34	112.92	(27.0)	(11.5)	(6.7)	(4.6)	(3.2)	(2.1)	(1.2)
500		-814.69	96.58	(26.0)	(9.9)	(5.5)	(3.6)	(2.4)	(1.5)	(0.7)
525		-547.52	57.91							
550		-360.14	1.93							
575		-247.84	-50.99							
600		-179.01	-84.80							
625		-134.70	-98.50							
650		-104.72	-98.82							
675		-83.55	-92.36							
700		-68.06	-83.26							
725		-56.38	-73.71							
750		-47.36	-64.69							
775		-40.24	-56.58							
800		-34.53	-49.46							
825		-29.88	-43.29							
850		-26.05	-37.97							
875		-22.87	-33.39							
900		-20.20	-29.45							

tion curve to intervals of 50°C and 250 bars above the critical point in the shaded pressure-temperature region of figure 18. Of the many low temperature data in the literature, the values of the dielectric constant given by Owen and others (1961) from 0° to 70°C and 0.001 to 1 kb appear to be most consistent with those measured by Oshry (ms) along the saturation curve and Heger (ms) at high pressures and temperatures. For this reason, the data of Owen and others (1961) were "accepted" in this study in preference to those of Malmberg and Maryott (1956) and others. The experimental data given by Oshry in his dissertation were used instead of the smooth values generated by Åkerlof and Oshry (1950) from Oshry's data because the latter paper contains several errors and inconsistencies.

Numerous attempts were made during the course of the present study to fit the data taken from Oshry (ms), Owen and others (1961), and Heger (ms) at close pressure-temperature intervals in the shaded region of figure 18 with the Kirkwood equation (Kirkwood, 1939; Oster and Kirkwood, 1943), which Kirkwood derived from an extension of Onsager's theory of dielectric polarization to compute dielectric constants of polar liquids. The Kirkwood equation can be written as

$$\epsilon = \frac{1 + 9\Gamma + 2(2 + (1 + 9\Gamma)^2)^{1/2}}{4} \quad (44)$$

where

$$\Gamma = \frac{4\pi N^\circ \rho}{3M_w} \left(\omega + \frac{10^{-36} \mu^2 g}{3kT} \right) \quad (45)$$

in which $\pi = 3.14159265$, N° stands for Avogadro's number (6.02252×10^{23} mole⁻¹), ρ again refers to the density of H₂O in g cm⁻³, M_w designates the molecular weight of H₂O (18.0153 g mole⁻¹), k is Boltzman's constant (1.38054×10^{-16} erg (°K)⁻¹), ω represents the polarizability (1.58×10^{-24} cm³ mole⁻¹) and μ the dipole moment of the H₂O molecule, T stands for temperature in °K, and g is the Kirkwood correlation factor (which provides for molecular orientation).

Franck's (1956) early estimates of the dielectric constant at high pressures and temperatures are based on graphic fits of the Kirkwood equation to data given by Wyman (1930), Wyman and Engalls (1938), Åkerlof and Oshry (1950), and Fogo, Benson, and Copeland (1954). Franck's graphic fits have since been superseded by regression calculations with the Kirkwood equation (Quist and Marshall, 1965).

Because the dependence of $\mu^2 g$ on temperature and pressure (or density) cannot be determined independently, $\mu^2 g$ must be represented by an empirical function of these variables to obtain fits of dielectric constant data with equation (39). In fitting equation (44) to the values of the dielectric constant given by Fogo, Benson, and Copeland (1954), Wyman and Ingalls (1938), Owen and others (1961), Lees (ms), Åkerlof

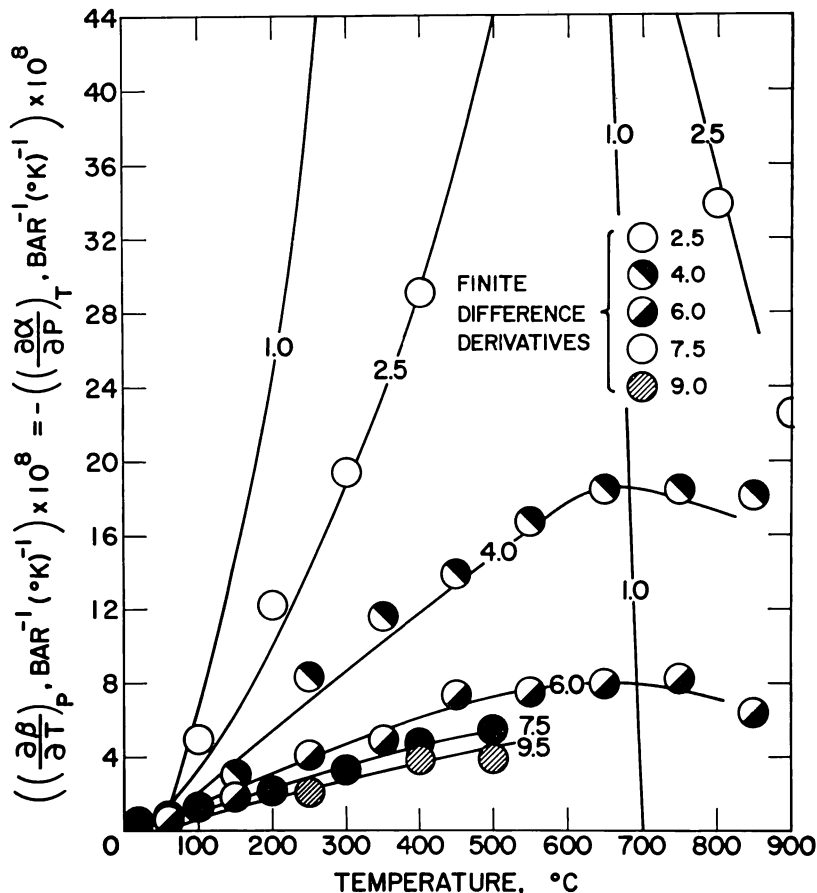


Fig. 14. Partial derivative of the coefficient of isothermal compressibility with respect to temperature at constant pressure (table 12) as a function of temperature at constant pressure (labeled in kb) computed from equations (19) through (22), (24), (25), (32), (33), (36), (38), (39), and (42) and coefficients in tables 4, 9, and 10 (curves). The symbols represent finite difference derivatives calculated from the finite difference values of α and β plotted in figures 5 through 8.

and Oshry (1950), and Gier and Young (1963)², Quist and Marshall (1965) represented μ^2g with a power function of density and temperature of the form

$$\mu^2g = 3.50 + \rho(\hat{A}_1 + \hat{A}_2 \rho + \hat{A}_3 \rho^2) f(T) \quad (46)$$

where \hat{A}_1 , \hat{A}_2 , and \hat{A}_3 represent fit coefficients, and $f(T)$ stands for a density-independent power function of temperature. In trial and error re-

² All these data, which apply to pressures ranging up to ~ 12 kb at 50°C and below, 2 kb from 50° to 350°C , and a few hundred bars from 350° to 393°C , are not consistent with one another. Many of them have since been superseded by Heger's (ms) study, which is internally consistent.

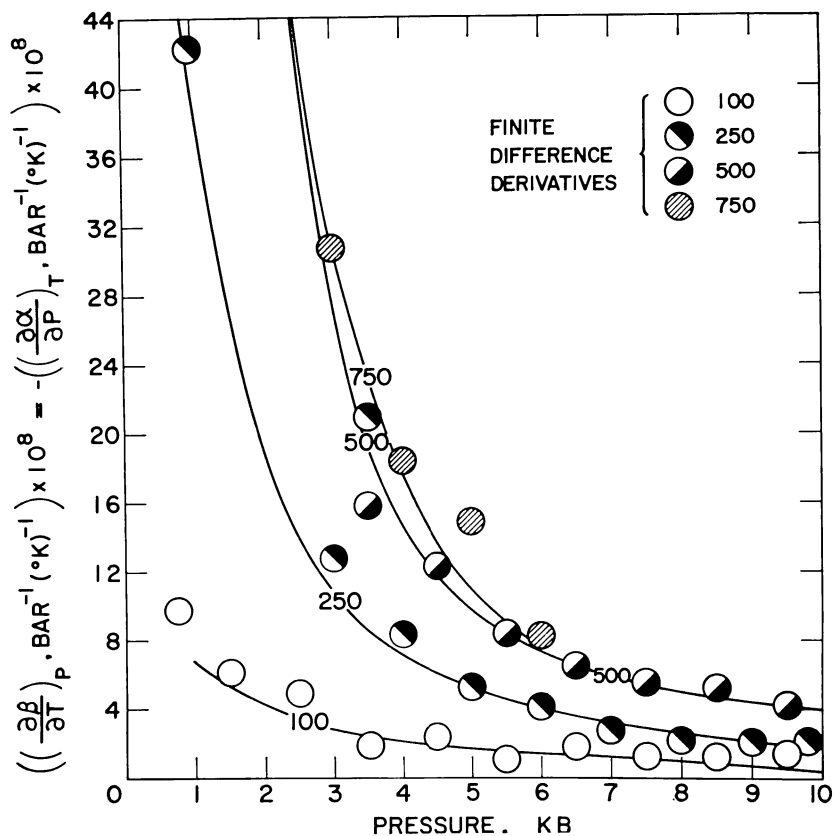


Fig. 15. Partial derivative of the coefficient of isothermal compressibility with respect to temperature at constant pressure (table 12) as a function of pressure at constant temperature (labeled in °C) computed from equations (19) through (22), (24), (25), (32), (33), (36), (38), (39), and (42) and coefficients in tables 4, 9, and 10 (curves). The symbols represent finite difference derivatives calculated from the finite difference values of α and β plotted in figures 5 through 8.

gression, Quist and Marshall permitted $f(T)$ to take any of three alternate forms ($f(T) = T^{-0.5}$, $f(T) = T^{-\hat{A}_4}$, or $f(T) = e^{-\hat{A}_4 T}$), each of which rendered equivalent fits of the data.

Regression of Heger's (ms) data in the present study with equations (44) through (46) using the alternate forms of $f(T)$ suggested by Quist and Marshall resulted in acceptable fits of the data at high temperatures and pressures, which is not surprising because Quist and Marshall's computed values of ϵ are in reasonable agreement with Heger's experimental data. However, as might be expected from Quist and Marshall's experience and the fact that alternate regression of Heger's data in the present study using different expressions for $f(T)$ failed to identify any one of the functions as better than another, composite fits of equations (44)

TABLE 14
Coefficients for equation (47)

$$\underline{e}_{ij} = \hat{e}_{ij} \times 10^{\underline{e}^*_{ij}}$$

		\hat{e}_{ij}				
j	i					
	0	1	2	3	4	
0	4.39109592	-2.33277456	4.61662109	-4.03643333	1.31604037	
1	-2.18995148	1.00498361	-1.35650709	5.94046919		
2	1.82898246	-2.08896146	1.60491325			
3	1.54886800	-6.13941874				
4	-6.13542375					

		\underline{e}^*_{ij}				
j	i					
	0	1	2	3	4	
0	2	0	-3	-6	4	
1	2	0	-3	-7		
2	1	-1	-4			
3	2	-2				
4	1					

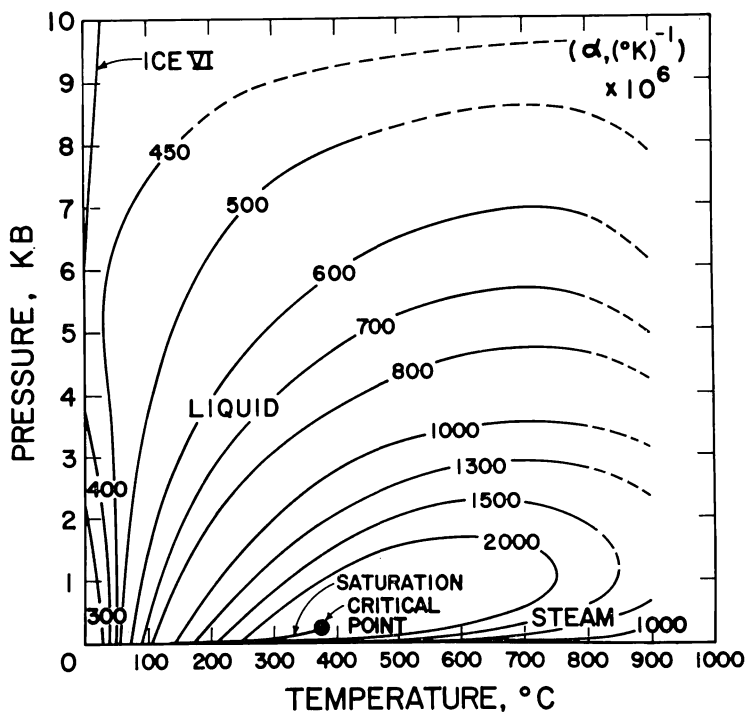


Fig. 16. Isopleths of α (labeled in $(^\circ\text{K})^{-1}$) as a function of pressure and temperature (table 7 and figs. 5 and 6).

through (46) to all of the data reported by Owen and others (1961), Oshry (ms), and Heger (ms) resulted in relatively poor fits with nonrandom trends of residuals. The magnitude and distribution of the residuals introduced unacceptable uncertainties in the partial derivatives of the dielectric constant computed from the partial derivatives of equation (44). Repeated attempts to obtain close fits of both the high- and low-temperature data with the Kirkwood equation by representing μ^2g with higher order power functions of density, with and without cross terms in density and temperature as well as modified alternate $f(T)$ functions, led to little improvement in the fits and eventually to the conclusion that (despite its theoretical origins) the Kirkwood equation is not suitable for comprehensive and accurate representation of the dielectric constant and its partial derivatives over the range of pressures and temperatures considered in this study.

In contrast to the Kirkwood equation, a simple fourth degree power function of temperature and density rendered close fits of all the experimental data as well as a random distribution of residuals over the entire shaded region of figure 18. This expression can be written as

$$\epsilon = \sum_{i=0}^4 \sum_{j=0}^{4-i} e_{ij} T^i \rho^j \quad (47)$$

where e_{ij} stands for the array of fit coefficients given in table 14. Values of the dielectric constant computed from equation (47) and the values of V calculated above are given in table 15 and plotted as solid curves representing ϵ or $\ln \epsilon$ in figures 19, 20, and 22 through 24, where they can be compared with the experimental values represented by the symbols.

Equation (47) fits the experimental data obtained by Oshry (ms), Owen and others (1961), and Heger (ms) to within 1 percent over most of the shaded region shown in figure 18. Only at the high temperature end of the saturation curve where Oshry's data exhibit excessive scatter (fig. 19) is the uncertainty greater, approaching 5 percent near the critical point where the dielectric constant is small. The maximum experimental uncertainty in the data ranges from < 0.1 percent for those of Owen and others to < 1 percent for the values of $\epsilon > 10$ and < 3 percent for the values of $\epsilon < 10$ given by Heger (ms). The maximum experimental uncertainty in Oshry's data for temperatures $< 350^\circ\text{C}$ is of the order of 1 to 2 percent.

It is apparent in figures 19, 20, and 22 through 24 that equation (47) not only affords accurate representation of the experimental data, but it also permits reasonable extrapolations of ϵ from 100° to 0°C at pressures

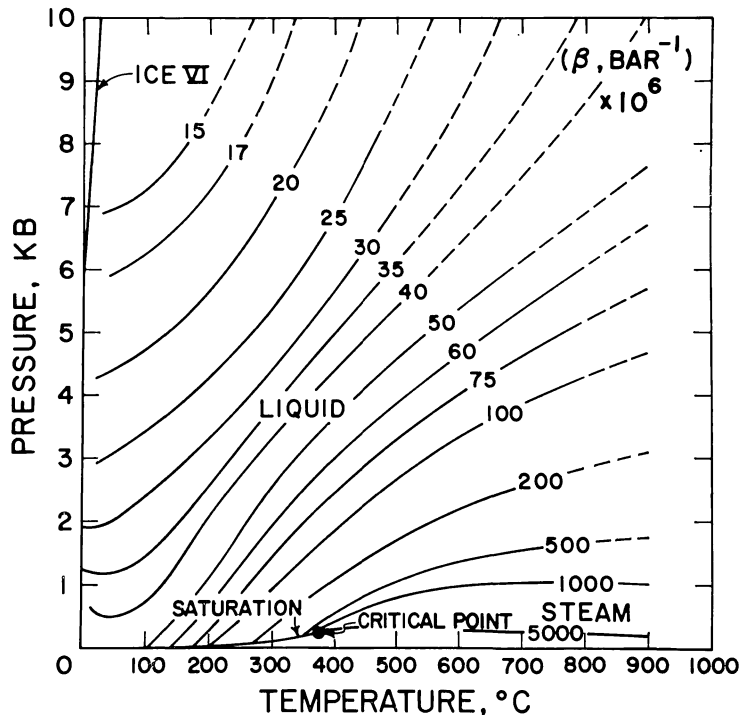


Fig. 17. Isopleths of β (labeled in bar^{-1}) as functions of pressure and temperature (table 8 and figs. 7 and 8).

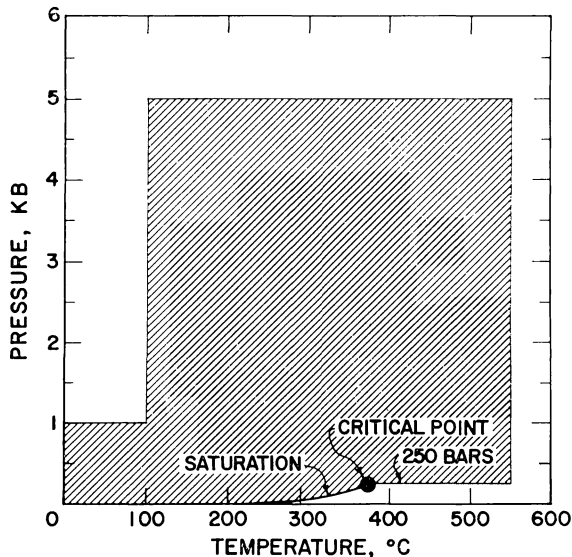


Fig. 18. Pressure-temperature region represented by dielectric constant data (Oshry, ms; Owen and others, 1961; Heger, ms) regressed with equation (44) to define the fit coefficients in table 14.

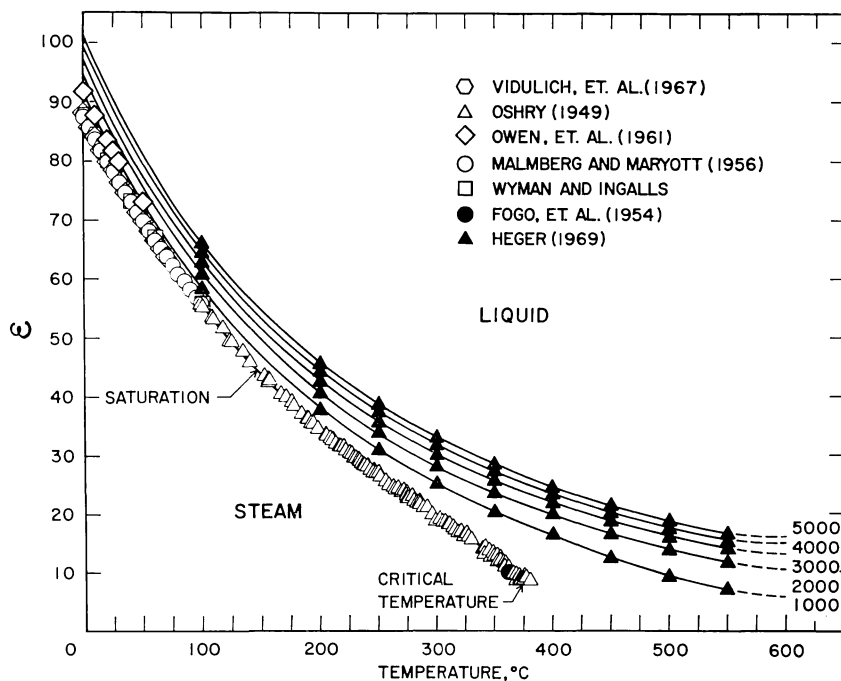


Fig. 19. Dielectric constant (table 15) as a function of temperature at constant pressure (labeled in bars) computed from equations (19) through (21) and (47) and coefficients in tables 4, 5, 6, and 14 (curves). The symbols represent values taken from the literature.

from 1 to 5 kb, and from 550°C to 600°C at pressures from 250 bars to 5 kb. However, such is not the case above 600°C, which precludes use of equation (47) and the fit coefficients in table 14 to compute extrapolated dielectric constants at higher temperatures.

It can be seen in figure 19 that the dielectric constant of H₂O decreases rapidly from values ranging from 88 to 100 at 0°C to < 20 at 600°C as temperature increases at constant pressure. In contrast, as pressure increases to 5 kb at constant temperature (fig. 20), the dielectric constant increases of the order of 10 to 15 units. Isopleths of the dielectric constant are shown in figure 21, where it can be deduced that $(\partial P/\partial T)_\epsilon$ changes from ~ 500 bar $(^\circ\text{K})^{-1}$ at 0°C to < 5 bar $(^\circ\text{K})^{-1}$ at high temperatures and low pressures.

The dashed curves in figures 19, 20, and 22 through 24 were drawn through interpolated values of the dielectric constant computed by Quist and Marshall (1965) at high temperatures and pressures; they do not represent extrapolations computed from equation (47) and the coefficients in table 14, which are inapplicable above 600°C. It can be seen that Quist and Marshall's values are reasonably consistent with Heger's data and the computed curves below 600°C. Nevertheless, owing to small discrepancies, composite regression of their values with those below 600°C

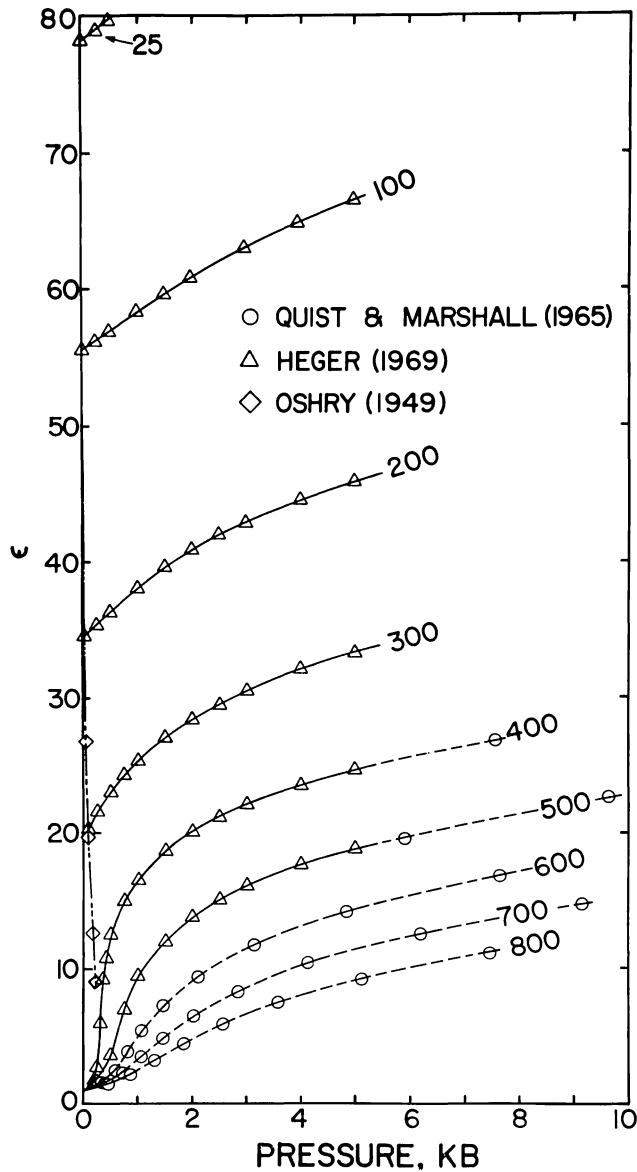


Fig. 20. Dielectric constant (table 15) as a function of pressure at constant temperature (labeled in °C) computed from equations (19) through (21) and (47) and coefficients in tables 4, 5, 6, and 14 (solid curves). The symbols correspond to values taken from the literature, and the dashed curves represent smooth graphic interpolation of Quist and Marshall's (1965) values for pressures > 5 kb and temperatures > 600°C.

yields an unacceptable fit of equation (47), and finite difference derivatives $((\Delta\varepsilon/\Delta T)_P$ and $(\Delta\varepsilon/\Delta P)_T$) calculated from Quist and Marshall's values are not consistent with those computed from Heger's experimental data at lower temperatures. Partial derivatives obtained by differentiating the functions used by Quist and Marshall (eqs 44 through 46) are similarly inconsistent, but, in contrast, partial differentiation of equation (47) yields derivatives in close agreement with their finite difference counterparts below 550°C (see below).

The dependence of $\ln \varepsilon$ on temperature and pressure is depicted in figures 22 and 23. The solid curves in these figures were generated by equation (47), and the symbols represent experimental data (or computed values in the case of those taken from Quist and Marshall). It can be seen in figure 22 that the near linear dependence of $\ln \varepsilon$ on temperature at constant pressure below $\sim 100^\circ\text{C}$ (Gurney, 1953) becomes substantially nonlinear at higher temperatures. In contrast, $\ln \varepsilon$ as a function of pressure at constant temperature approaches linearity at high pressures and temperatures, but it is also nearly linear at low temperatures (fig. 23).

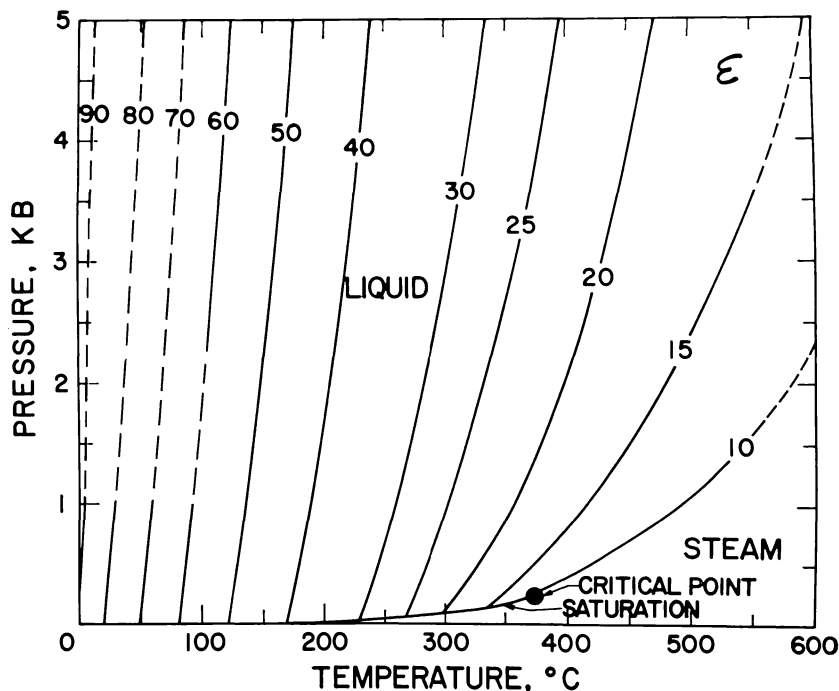


Fig. 21. Isopleths of ε (indicated by the labels on the curves) as a function of pressure and temperature (table 15 and figures 19 and 20).

The relation of the dielectric constant to specific volume is depicted in figure 24, where it can be seen that $(\partial \ln \epsilon / \partial \ln V)_T$ is essentially independent of both density and temperature. Under these conditions $(\partial \ln \epsilon / \partial P)_T$ is nearly proportional to the coefficient of isothermal compressibility.

The partial derivatives of equation (47) with respect to temperature and pressure can be written as

$$\left(\frac{\partial \epsilon}{\partial P}\right)_T = \epsilon \left(\frac{\partial \ln \epsilon}{\partial P}\right)_T = \beta \sum_{i=0}^4 \sum_{j=0}^{4-i} j e_{ij} T^i \rho^j \quad (48)$$

$$\left(\frac{\partial \epsilon}{\partial T}\right)_P = \epsilon \left(\frac{\partial \ln \epsilon}{\partial T}\right)_P = \sum_{i=0}^4 \sum_{j=0}^{4-i} e_{ij} \rho^j (iT^{i-1} - j\alpha T^i) \quad (49)$$

where α and β again stand for the coefficients of isobaric thermal expansion and isothermal compressibility. Values of $(\partial \ln \epsilon / \partial P)_T$ and $(\partial \ln \epsilon / \partial T)_P$ computed from equations (48) and (4) using values of ϵ , β , and α given above are shown in tables 16 and 17 and plotted as curves in figures 25 through 28, where it can be seen that the predicted values are in close agreement with their finite difference counterparts ($(\Delta \ln \epsilon / \Delta P)_T$ and $(\Delta \ln \epsilon / \Delta T)_P$) calculated directly from the experimental data. Uncertainties in the values of $(\partial \ln \epsilon / \partial T)_P$ and $(\partial \ln \epsilon / \partial P)_T$ computed from equations (48) and (49) are of the order of a few percent or less, which corresponds to the uncertainties in the values of α and β employed in the calculations.

It can be seen in figure 26 that $(\partial \ln \epsilon / \partial P)_T$ like β decreases dramatically and monotonically with increasing pressure at constant temperature $\cong 200^\circ\text{C}$, but unlike β , $(\partial \ln \epsilon / \partial P)_T$ increases monotonically with increasing temperature at all (constant) pressures (fig. 25). At high pressures, $(\partial \ln \epsilon / \partial P)_T \rightarrow (\partial^2 \ln \epsilon / \partial P^2)_T \rightarrow 0$ as pressure increases at any given temperature (figs. 26 and 29). Similarly, as temperature decreases below $\sim 100^\circ\text{C}$ at all pressures, $(\partial \ln \epsilon / \partial P)_T \rightarrow (\partial(\partial \ln \epsilon / \partial P)_T / \partial T)_P \rightarrow 0$ (figs. 25 and 33).

The strong influence of the critical phenomenon on the temperature and pressure dependence of $(\partial \ln \epsilon / \partial T)_P$ is apparent in figures 27 and 28. Note that the isobars for pressures ≤ 2 kb in the steam phase region pass through a minimum with increasing temperature, as do the isotherms for temperatures above the critical temperature. In the vicinity of the critical point, $(\partial \ln \epsilon / \partial P)_T$ is large and positive and $(\partial \ln \epsilon / \partial T)_P$ is large and negative. At the critical point, $(\partial \ln \epsilon / \partial P)_T = -(\partial \ln \epsilon / \partial T)_P = \infty$, but as the thermodynamic behavior of H_2O approaches ideality with decreasing pressure, $\epsilon \rightarrow 1$.

Partial differentiation of equations (48) and (49) leads to

$$\left(\frac{\partial^2 \epsilon}{\partial P^2}\right)_T = \epsilon \left(\frac{\partial \ln \epsilon}{\partial P}\right)_T \left(\frac{\partial \ln \beta}{\partial P}\right)_T + \beta^2 \sum_{i=0}^4 \sum_{j=0}^{4-i} j^2 e_{ij} T^i \rho^j \quad (50)$$

and

$$\begin{aligned} \left(\frac{\partial^2 \epsilon}{\partial T^2}\right)_P &= \sum_{i=0}^4 \sum_{j=0}^{4-i} e_{ij} \rho^j \left(j\alpha(j\alpha T^i - 2i T^{i-1}) \right. \\ &\quad \left. + i(i-1)T^{i-2} - jT^i \left(\frac{\partial \alpha}{\partial T}\right)_P \right) \end{aligned} \quad (51)$$

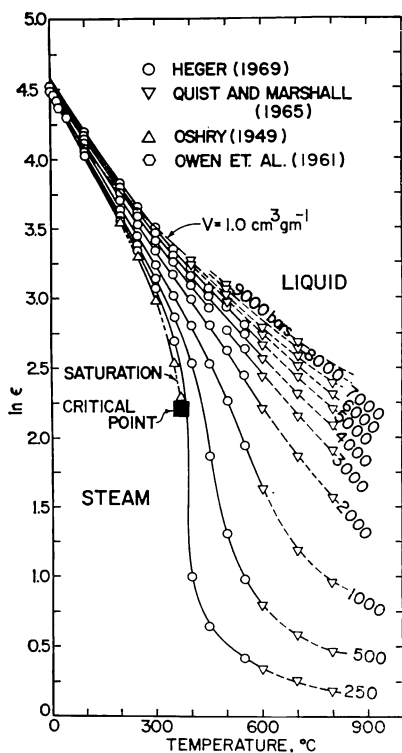


Fig. 22

Fig. 22. Logarithm of the dielectric constant (table 15) as a function of temperature at constant pressure (labeled in bars) computed from equations (19) through (21) and (47) and coefficients in tables 4, 5, 6, and 14 (solid curves). The symbols correspond to values taken from the literature and the dashed curves represent graphic interpolation of Quist and Marshall's (1965) values at pressures > 600°C.

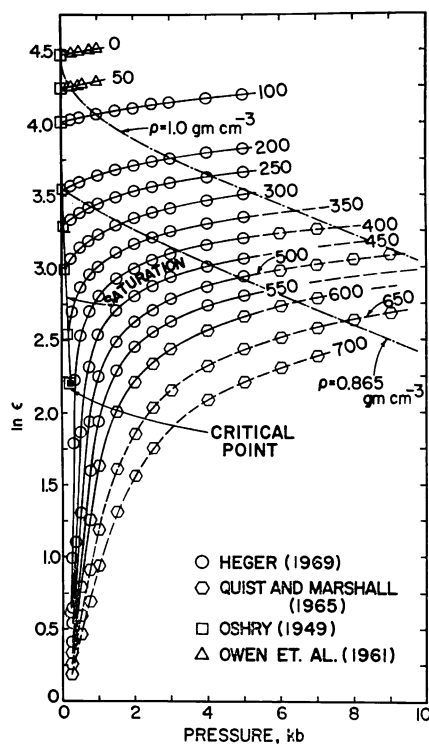


Fig. 23

Fig. 23. Logarithm of the dielectric constant (table 15) as a function of pressure at constant temperature (labeled in °C) computed from equations (19) through (21) and (47) and coefficients in tables 4, 5, 6, and 14 (solid curves). The symbols correspond to values taken from the literature, and the dashed curves represent graphic interpolation of Quist and Marshall's (1965) values at pressures > 5 kb and temperatures > 600°C.

which were used together with equations (47) through (49), values of V , α , β , $(\partial\alpha/\partial T)_P$, $(\partial\beta/\partial P)_T$, $(\partial \ln \varepsilon/\partial P)_T$, and $(\partial \ln \varepsilon/\partial T)_P$ given above, and the identities,

$$\left(\frac{\partial^2 \ln \varepsilon}{\partial P^2}\right)_T = \frac{1}{\varepsilon} \left(\frac{\partial^2 \varepsilon}{\partial P^2}\right)_T - \frac{1}{\varepsilon^2} \left(\frac{\partial \varepsilon}{\partial P}\right)_T^2 \quad (52)$$

and

$$\left(\frac{\partial^2 \ln \varepsilon}{\partial T^2}\right)_P = \frac{1}{\varepsilon} \left(\frac{\partial^2 \varepsilon}{\partial T^2}\right)_P - \frac{1}{\varepsilon^2} \left(\frac{\partial \varepsilon}{\partial T}\right)_P^2 \quad (53)$$

to compute the curves shown in figures 29 through 32 and the partial derivatives in tables 18 and 19. The close agreement of the values of $(\partial \ln \varepsilon/\partial P)_T$ and $(\partial \ln \varepsilon/\partial T)_P$ computed from equations (48) and (49) with their finite difference counterparts in figures 25 through 28 suggests that the partial derivatives computed from equations (50) through (53) are reasonably accurate representations of $(\partial^2 \ln \varepsilon/\partial P^2)_T$ and $(\partial^2 \ln \varepsilon/\partial T^2)_P$ within the fit region shown in figure 18. This conclusion is further substantiated below (fig. 33) by the agreement of computed values of $(\partial(\partial \ln \varepsilon/\partial P)_T/\partial T)_P$ with finite difference derivatives calculated directly from the curves in figures 25 and 28.

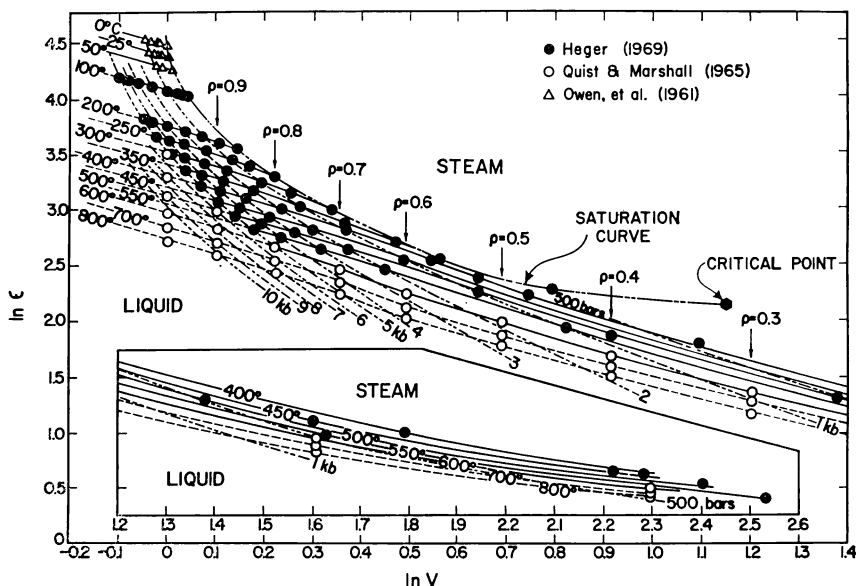


Fig. 24. Logarithm of the dielectric constant as a function of $\ln V$ at constant temperature (solid curves) and constant pressure (dashed curves) computed from equations (19) through (21) and (47) and coefficients in tables 4, 5, 6, and 14. The symbols correspond to values taken from the literature, and the dashed curves represent smooth graphic interpolation of Quist and Marshall's (1965) values at pressures > 5 kb and temperatures $> 600^\circ\text{C}$.

It can be seen in figure 32 that a large discrepancy in $(\partial^2 \ln \epsilon / \partial T^2)_T$ arises between 1 and 2 kb at 25°C, which is outside the fit region in figure 18. Similar discrepancies occur above $\sim 500^\circ\text{C}$, which is near the upper limit of the fit region. Erroneous values of $(\partial^2 \ln \epsilon / \partial T^2)_P$ and $(\partial^2 \ln \epsilon / \partial P^2)_P$ may arise from errors in $(\partial \alpha / \partial T)_P$ and $(\partial \beta / \partial P)_T$, which is apparently the case at 25°C above a kilobar in figure 32. Although comparative calculations for pressures and temperatures within the fit region indicate that errors of the order of 5 to 20 percent in $(\partial \alpha / \partial T)_P$ and $(\partial \beta / \partial P)_T$ have a minor effect on $(\partial^2 \ln \epsilon / \partial T^2)_P$ and $(\partial^2 \ln \epsilon / \partial P^2)_T$, the second partial derivatives of $\ln \epsilon$ are nevertheless highly uncertain near the boundaries of the fit region. For this reason, equations (52) and (53) as well as equations (56) and (57), which are derived below, should not be used for temperatures above $\sim 500^\circ\text{C}$ or pressures above ~ 500 bars at temperatures $\leq 100^\circ\text{C}$.

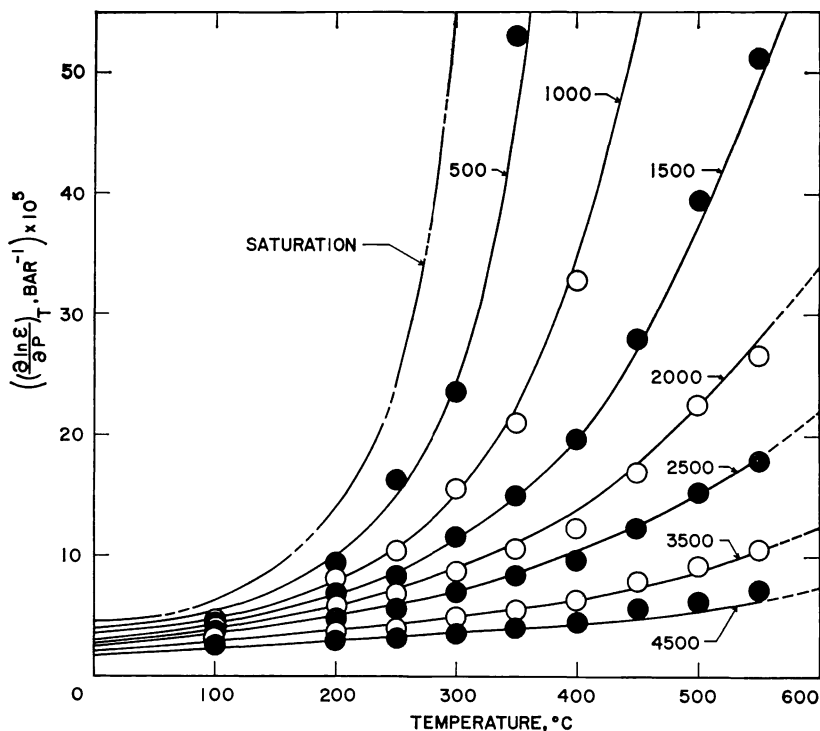


Fig. 25. Partial derivative of $\ln \epsilon$ with respect to pressure at constant temperature (table 16) as a function of temperature at constant pressure (labeled in bars) computed from equations (19) through (22), (32), (38), (47), and (48) and coefficients in tables 4, 5, 6, 9, 10, and 14 (curves). The symbols represent corresponding finite difference derivatives computed from data given by Oshry (ms), Owen and others (1961), and/or Heger (ms).

TABLE 15
Dielectric constant (ϵ) computed from equation (47) and the values
of V in table 3—see figures 19 through 21

t (°C)	PRESSURE, KB										
	SAT	0.5	1	1.5	2	2.5	3	3.5	4	4.5	5
25	78.47	80.20	81.78	(83.05)	(84.38)	(85.56)	(86.63)	(87.62)	(88.57)	(89.48)	(90.35)
50	69.96	71.59	73.09	(74.23)	(75.51)	(76.64)	(77.65)	(78.58)	(79.48)	(80.34)	(81.18)
75	62.30	63.91	65.38	(66.56)	(67.78)	(68.87)	(69.84)	(70.72)	(71.57)	(72.38)	(73.17)
100	55.47	57.10	58.55	59.78	60.98	62.06	63.00	63.85	64.65	65.43	66.17
125	49.37	51.05	52.53	53.76	54.97	56.04	56.98	57.82	58.60	59.34	60.05
150	43.91	45.68	47.19	48.42	49.64	50.73	51.68	52.52	53.28	54.00	54.68
175	39.02	40.90	42.46	43.69	44.92	46.03	47.00	47.85	48.61	49.31	49.96
200	34.60	36.63	38.27	39.51	40.75	41.88	42.87	43.73	44.48	45.17	45.81
225	30.58	32.79	34.54	35.82	37.06	38.20	39.21	40.07	40.83	41.51	42.13
250	26.87	29.31	31.20	32.55	33.79	34.94	35.95	36.83	37.58	38.25	38.86
275	23.38	26.12	28.20	29.63	30.88	32.03	33.04	33.92	34.67	35.33	35.92
300	19.99	23.15	25.46	27.00	28.27	29.41	30.43	31.30	32.05	32.70	33.27
325	16.58	20.32	22.94	24.61	25.90	27.05	28.05	28.92	29.66	30.29	30.85
350	12.87	17.57	20.58	22.40	23.74	24.88	25.88	26.74	27.47	28.09	28.63
375		14.86	18.37	20.35	21.74	22.89	23.89	24.74	25.45	26.06	26.58
400		(12.13)	16.27	18.42	19.88	21.06	22.05	22.88	23.59	24.18	24.68
425		(9.38)	14.30	16.63	18.16	19.35	20.34	21.17	21.86	22.44	22.92
450		(6.80)	12.46	14.95	16.56	17.78	18.77	19.59	20.27	20.84	21.31
475		(4.98)	10.78	13.41	15.08	16.33	17.34	18.16	18.83	19.39	19.85
500		(3.94)	9.27	12.01	13.75	15.03	16.05	16.88	17.56	18.11	18.56
525		(3.30)	7.97	10.78	12.57	13.90	14.94	15.78	16.46	17.02	17.48
550		(2.87)	6.89	9.74	11.58	12.95	14.03	14.90	15.59	16.16	16.63
575		(2.56)	(6.08)	(8.91)	(10.81)	(12.24)	(13.36)	(14.26)	(14.99)	(15.58)	(16.06)
600		(2.39)	(5.53)	(8.33)	(10.30)	(11.80)	(12.98)	(13.93)	(14.70)	(15.32)	(15.83)

TABLE 16
Partial derivative of the natural logarithm of the dielectric constant
with respect to pressure at constant temperature in $\text{bar}^{-1} \times 10^5$
computed from equations (47) and (48) and the values of V and β
in tables 3 and 8—see figures 25 and 26

t (°C)	PRESSURE, KB										
	SAT	0.5	1	2	2.5	3	3.5	4	4.5	5	
25	4.67	4.1	3.8	(3.1)	(2.8)	(2.6)	(2.3)	(2.1)	(2.0)	(1.8)	
50	4.94	4.3	4.0	(3.3)	(3.0)	(2.7)	(2.5)	(2.3)	(2.1)	(1.9)	
75	5.50	4.8	4.3	(3.5)	(3.2)	(2.9)	(2.6)	(2.4)	(2.2)	(2.0)	
100	6.34	5.4	4.8	3.8	3.4	3.1	2.8	2.6	2.4	(2.2)	
125	7.48	6.1	5.3	4.2	3.7	3.3	3.0	2.7	2.5	(2.3)	
150	9.02	7.1	6.0	4.6	4.0	3.6	3.2	2.9	2.7	(2.4)	
175	11.10	8.4	6.8	5.1	4.4	3.9	3.5	3.1	2.8	(2.6)	
200	14.00	10.0	7.8	5.7	4.9	4.2	3.7	3.3	3.0	(2.7)	
225	18.20	12.1	9.0	6.4	5.4	4.6	4.0	3.5	3.2	(2.9)	
250	24.66	14.9	10.6	7.1	5.9	5.0	4.3	3.8	3.3	(3.0)	
275	35.40	18.8	12.5	8.0	6.5	5.4	4.6	4.0	3.5	(3.1)	
300	55.52	24.5	15.0	8.9	7.2	5.9	4.9	4.2	3.7	(3.2)	
325	101.95	33.0	18.3	10.0	7.9	6.4	5.3	4.5	3.8	(3.4)	
350	274.99	46.4	22.5	11.1	8.6	6.9	5.6	4.7	4.0	(3.5)	
375		69.1	28.0	12.5	9.5	7.4	6.0	5.0	4.2	(3.6)	
400		111.5	34.9	14.0	10.4	8.0	6.4	5.2	4.4	(3.7)	
425		197.2	43.5	15.7	11.4	8.7	6.8	5.5	4.6	(3.9)	
450		319.6	54.0	17.7	12.6	9.4	7.3	5.9	4.8	(4.0)	
475		349.5	66.5	20.1	14.0	10.3	7.9	6.3	5.1	(4.2)	
500		309.1	80.5	22.8	15.5	11.2	8.5	6.7	5.4	(4.4)	
525			(94.7)	(25.0)	(16.4)	(12.4)	(9.8)	(7.6)	(5.9)	(4.7)	
550			(106.7)	(28.0)	(18.3)	(13.6)	(10.6)	(8.2)	(6.3)	(5.1)	
575			(114.7)	(31.0)	(20.3)	(14.9)	(11.5)	(8.8)	(6.8)	(5.4)	
600			(118.2)	(33.9)	(22.2)	(16.2)	(12.4)	(9.5)	(7.4)	(5.9)	

TABLE 17

Partial derivative of the natural logarithm of the dielectric constant with respect to temperature at constant pressure in $(^{\circ}\text{K})^{-1} \times 10^3$ computed from equations (47) and (49) and the values of V and α in tables 3 and 7—see figures 27 and 28

t (°C)	PRESSURE, KB									
	SAT	0.5	1	2	2.5	3	3.5	4	4.5	5
25	-4.55	-4.5	-4.5	(-4.4)	(-4.4)	(-4.4)	(-4.4)	(-4.4)	(-4.3)	(-4.3)
50	-4.62	-4.5	-4.5	(-4.4)	(-4.3)	(-4.3)	(-4.3)	(-4.3)	(-4.2)	(-4.2)
75	-4.64	-4.5	-4.4	(-4.3)	(-4.2)	(-4.2)	(-4.2)	(-4.1)	(-4.1)	(-4.1)
100	-4.66	-4.5	-4.4	-4.2	-4.1	-4.1	-4.1	-4.0	-4.0	(-4.0)
125	-4.67	-4.5	-4.3	-4.1	-4.0	-4.0	-3.9	-3.9	-3.9	(-3.8)
150	-4.71	-4.4	-4.3	-4.0	-3.9	-3.9	-3.8	-3.8	-3.7	(-3.7)
175	-4.78	-4.4	-4.2	-3.9	-3.8	-3.7	-3.7	-3.6	-3.6	(-3.6)
200	-4.90	-4.4	-4.1	-3.8	-3.7	-3.6	-3.5	-3.5	-3.5	(-3.4)
225	-5.12	-4.4	-4.1	-3.7	-3.6	-3.5	-3.4	-3.4	-3.3	(-3.3)
250	-5.50	-4.5	-4.0	-3.6	-3.5	-3.4	-3.3	-3.3	-3.2	(-3.2)
275	-6.18	-4.7	-4.1	-3.6	-3.4	-3.3	-3.2	-3.2	-3.1	(-3.1)
300	-7.42	-5.0	-4.1	-3.5	-3.4	-3.2	-3.2	-3.1	-3.1	(-3.0)
325	-10.02	-5.5	-4.2	-3.5	-3.3	-3.2	-3.1	-3.1	-3.0	(-3.0)
350	-18.24	-6.2	-4.4	-3.5	-3.3	-3.2	-3.1	-3.0	-3.0	(-3.0)
375		-7.3	-4.7	-3.5	-3.3	-3.2	-3.1	-3.0	-3.0	(-3.0)
400		-9.0	-5.0	-3.6	-3.3	-3.2	-3.1	-3.0	-3.0	(-2.9)
425		-11.7	-5.3	-3.6	-3.4	-3.2	-3.1	-3.0	-3.0	(-2.9)
450		-13.5	-5.7	-3.7	-3.4	-3.2	-3.1	-3.0	-2.9	(-2.9)
475		-11.0	-5.9	-3.7	-3.3	-3.1	-3.0	-2.9	-2.8	(-2.8)
500		-8.0	-6.1	-3.6	-3.2	-3.0	-2.8	-2.7	-2.6	(-2.6)
525			(-6.0)	(-3.5)	(-3.0)	(-2.7)	(-2.5)	(-2.4)	(-2.3)	(-2.2)
550			(-5.5)	(-3.1)	(-2.6)	(-2.3)	(-2.1)	(-1.9)	(-1.8)	(-1.7)
575			(-4.5)	(-2.4)	(-1.9)	(-1.6)	(-1.4)	(-1.2)	(-1.1)	(-1.0)
600			(-2.9)	(-1.4)	(-1.0)	(-0.7)	(-0.5)	(-0.3)	(-0.2)	(-0.1)

TABLE 18

Partial derivative of $(\partial \ln \epsilon / \partial P)_T$ with respect to pressure at constant temperature in $\text{bar}^{-2} \times 10^9$ computed from equation (50) and the values of V , β , $(\partial \beta / \partial P)_T$, ϵ , and $(\partial \ln \epsilon / \partial P)_T$ in tables 3, 8, 11, 15, and 16—see figures 29 and 30

t (°C)	PRESSURE, KB									
	SAT	0.5	1	2	2.5	3	3.5	4	4.5	5
25	-15.42	-8.4								
50	-16.66	-8.6								
75	-20.10	-10.8								
100	-26.41	-14.7	(-10.0)	(-8.8)	(-7.5)	(-6.4)	(-5.5)	(-4.7)	(-4.0)	(-3.5)
125	-36.64	-20.3	-14.1	-10.3	-8.6	-7.2	-6.1	-5.2	-4.4	(-3.8)
150	-52.94	-28.3	-19.2	-12.3	-10.0	-8.2	-6.9	-5.8	-4.9	(-4.2)
175	-79.55	-39.7	-25.8	-15.0	-11.8	-9.5	-7.8	-6.5	-5.5	(-4.7)
200	-125.21	-56.5	-34.6	-18.4	-14.1	-11.1	-8.9	-7.4	-6.2	(-5.2)
225	-209.40	-81.9	-46.5	-22.7	-17.0	-13.0	-10.3	-8.3	-6.9	(-5.8)
250	-380.92	-122.2	-63.0	-28.1	-20.4	-15.2	-11.8	-9.4	-7.7	(-6.4)
275	-783.27	-189.3	-86.4	-34.7	-24.6	-17.9	-13.6	-10.7	-8.6	(-7.1)
300	-1953.83	-307.7	-119.9	-42.8	-29.4	-20.9	-15.5	-12.0	-9.6	(-7.9)
325	-6917.75	-532.3	-168.4	-52.6	-35.1	-24.4	-17.8	-13.5	-10.7	(-8.7)
350	-57594.10	-1000.3	-238.5	-64.5	-41.7	-28.3	-20.2	-15.2	-11.9	(-9.6)
375		-2108.2	-339.1	-79.0	-49.4	-32.8	-23.0	-17.0	-13.2	(-10.5)
400		-5157.3	-482.0	-96.6	-58.3	-37.8	-26.1	-19.0	-14.6	(-11.6)
425			(-682.7)	-117.9	-68.7	-43.5	-29.5	-21.3	-16.1	(-12.7)
450			(-958.4)	-143.6	-80.7	-49.9	-33.3	-23.7	-17.8	(-14.0)
475			(-1311.9)	(-174.2)	(-94.8)	(-57.2)	(-37.5)	(-26.4)	(-19.7)	(-15.4)
500			(-1695.6)	(-210.1)	(-111.0)	(-65.5)	(-42.3)	(-29.4)	(-21.7)	(-16.9)

It can be seen in figure 30 that $(\partial^2 \ln \epsilon / \partial P^2)_T$ increases rapidly with increasing pressure ≤ 2 kb at all (constant) temperatures $\geq 200^\circ\text{C}$, but like $(\partial\beta/\partial P)_T$ in figure 10, its isobaric dependence on temperature is characterized by minima in the low pressure isobars. Note also that $(\partial^2 \ln \epsilon / \partial T^2)_P$ minimizes as an isothermal function of pressure at high temperatures and low pressures (fig. 32). In contrast, the isobaric temperature dependence of $(\partial^2 \ln \epsilon / \partial T^2)_P$ depicted in figure 31 exhibits an extremum in the vicinity of 75° to 150°C , which is flanked by a minimum on either side at pressures < 2 kb; as pressure increases, the low-temperature minimum disappears and at high temperatures, $(\partial^2 \ln$

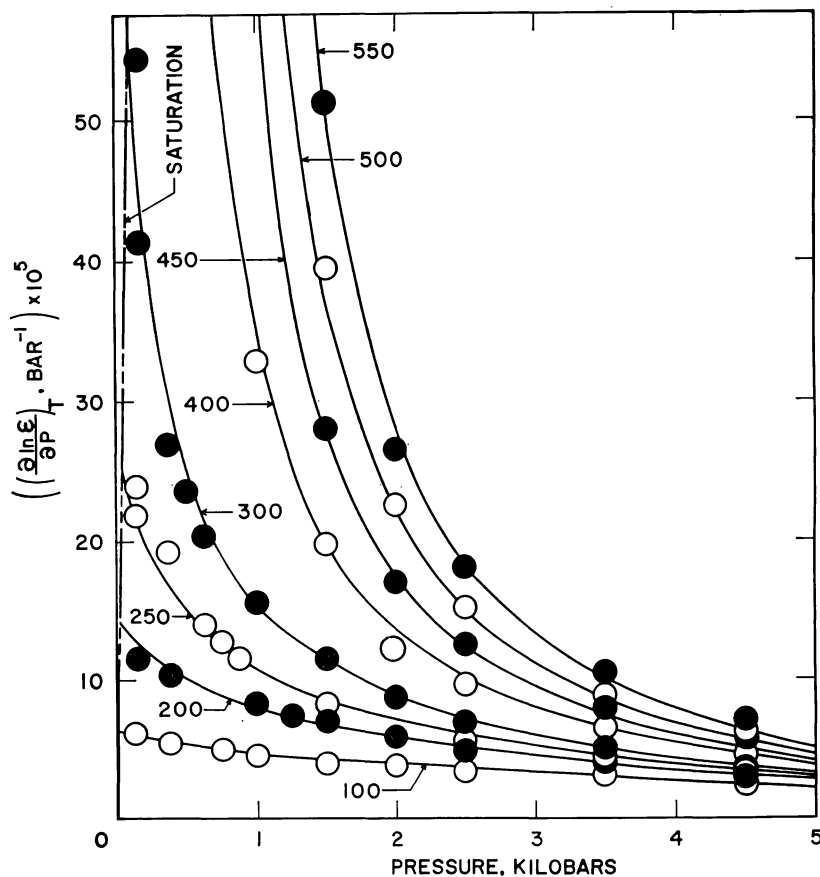


Fig. 26. Partial derivative of $\ln \epsilon$ with respect to pressure at constant temperature (table 16) as a function of pressure at constant temperature (labeled in $^\circ\text{C}$) computed from equations (19) through (22), (32), (38), (47), and (48) and coefficients in tables 4, 5, 6, 9, 10, and 14 (curves). The symbols represent corresponding finite difference derivatives computed from data given by Oshry (ms), Owen and others (1961), and/or Heger (ms).

$\epsilon/\partial T^2)_P$ increases dramatically with increasing temperature at constant pressure. Note that $(\partial^2 \ln \epsilon/\partial T^2)_P$ is negative at low pressures and positive at high pressures. As a consequence of the relations depicted in figure 24, the behavior of $(\partial^2 \ln \epsilon/\partial P^2)_T$ in figures 29 and 30 is similar to that exhibited by $(\partial\beta/\partial P)_T$ in figures 10 and 11, respectively.

Because

$$\left(\frac{\partial \left(\frac{\partial \epsilon}{\partial T} \right)_P}{\partial P} \right)_T = \left(\frac{\partial \left(\frac{\partial \epsilon}{\partial P} \right)_T}{\partial T} \right)_P \quad (54)$$

and

$$\left(\frac{\partial \left(\frac{\partial \ln \epsilon}{\partial T} \right)_P}{\partial P} \right)_T = \left(\frac{\partial \left(\frac{\partial \ln \epsilon}{\partial P} \right)_T}{\partial T} \right)_P \quad (55)$$

it follows that the partial derivative of equation (48) with respect to temperature at constant pressure is equivalent to that of equation (49)

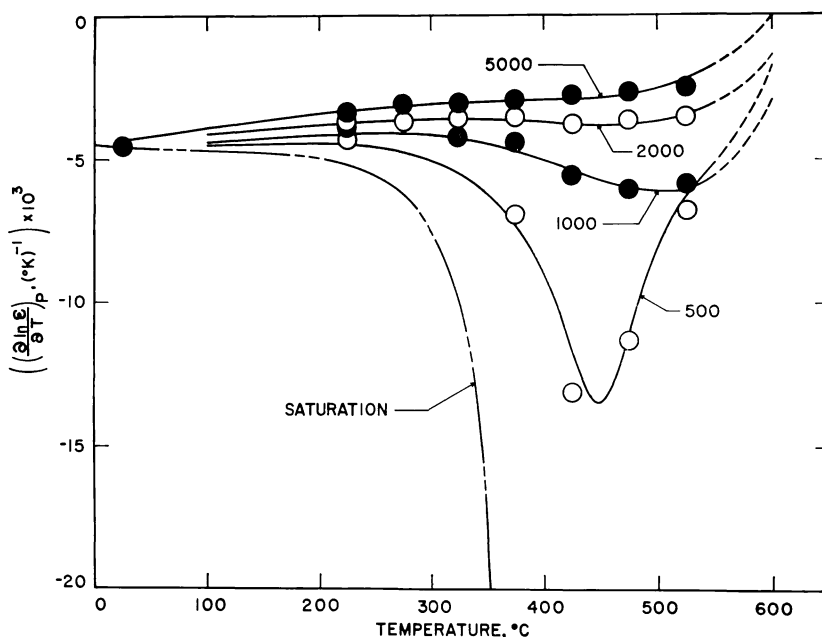


Fig. 27. Partial derivative of $\ln \epsilon$ with respect to temperature at constant pressure (table 17) as a function of temperature at constant pressure (labeled in bars) computed from equations (19) through (21), (25), (33), (39), (47), and (49) and coefficients in tables 4, 5, 6, 9, 10, and 14 (curves). The symbols represent corresponding finite difference derivatives computed from data given by Oshry (ms), Owen and others (1961), and/or Heger (ms).

TABLE 19

Partial derivative of $(\partial \ln \epsilon / \partial T)_P$ with respect to temperature at constant pressure in $(^\circ\text{K})^{-2} \times 10^6$ computed from equation (51) and the values of V , α , $(\partial\alpha/\partial T)_P$, ϵ , and $(\partial \ln \epsilon / \partial T)_P$ in tables 3, 7, 13, 15, and 17—see figures 31 and 32

t (°C)	PRESSURE, KB									
	SAT	0.5	1	2	2.5	3	3.5	4	4.5	5
25	-4.09	-1.3								
50	-1.57	0.3								
75	-9.57	1.2								
100	-0.55	1.3	(2.5)	(3.8)	(4.2)	(4.5)	(4.7)	(4.9)	(5.0)	(5.1)
125	-1.08	1.2	2.5	4.1	4.5	4.8	5.0	5.2	5.3	(5.3)
150	-2.09	0.9	2.5	4.3	4.7	5.0	5.2	5.3	5.4	(5.4)
175	-3.84	0.5	2.5	4.2	4.7	5.0	5.1	5.2	5.3	(5.3)
200	-6.93	-0.5	2.3	4.0	4.5	4.8	4.9	5.0	5.0	(5.0)
225	-12.41	-2.1	1.6	3.5	4.1	4.4	4.5	4.6	4.6	(4.6)
250	-22.30	-4.9	0.5	2.9	3.5	3.8	3.9	3.9	3.9	(3.9)
275	-41.38	-9.0	-1.2	2.1	2.7	3.0	3.1	3.2	3.2	(3.1)
300	-84.56	-15.0	-3.5	1.2	1.8	2.2	2.3	2.3	2.3	(2.3)
325	-222.63	-23.4	-6.2	0.2	0.9	1.3	1.4	1.5	1.5	(1.5)
350	-1232.61	-35.5	-9.1	-0.7	0.1	0.5	0.7	0.8	0.8	(0.8)
375		-54.4	-11.6	-1.5	-0.6	-0.1	0.2	0.3	0.4	(0.4)
400		-87.1	-13.2	-2.1	-0.9	-0.3	0.1	0.3	0.4	(0.6)
425			(-13.5)	-2.0	-0.7	0.1	0.6	0.9	1.2	(1.3)
450			(-12.4)	-1.2	0.4	1.4	2.0	2.5	2.8	(3.1)
475			(-9.0)	(0.9)	(2.8)	(4.0)	(4.7)	(5.3)	(5.7)	(6.1)
500			(-1.9)	(4.8)	(6.9)	(8.2)	(9.0)	(9.6)	(10.1)	(10.6)

TABLE 20

Partial derivative of $(\partial \ln \epsilon / \partial P)_T$ with respect to temperature at constant pressure in $\text{bar}^{-1} (^\circ\text{K})^{-1} \times 10^7$ computed from equation (56) and the values of V , α , β , $(\partial\beta/\partial T)_P$, ϵ , $(\partial \ln \epsilon / \partial P)_T$, and $(\partial \ln \epsilon / \partial T)_P$ in tables 3, 7, 8, 12, and 15 through 17—see figure 33

t (°C)	PRESSURE, KB									
	SAT	0.5	1	2	2.5	3	3.5	4	4.5	5
25	0.39	0.4								
50	1.69	1.3								
75	2.80	2.0								
100	3.94	2.7	(1.9)	(1.3)	(1.1)	(0.9)	(0.8)	(0.7)	(0.6)	(0.5)
125	5.32	3.5	2.4	1.5	1.2	1.0	0.9	0.8	0.7	(0.6)
150	7.17	4.4	3.0	1.8	1.4	1.2	1.0	0.8	0.7	(0.6)
175	9.89	5.6	3.6	2.1	1.6	1.3	1.0	0.9	0.7	(0.6)
200	14.17	7.3	4.4	2.4	1.8	1.4	1.1	0.9	0.7	(0.6)
225	21.45	9.7	5.5	2.8	2.0	1.5	1.1	0.9	0.7	(0.6)
250	35.00	13.2	6.9	3.2	2.2	1.6	1.2	0.9	0.7	(0.5)
275	63.63	18.7	8.8	3.6	2.4	1.7	1.2	0.9	0.7	(0.5)
300	137.25	27.4	11.4	4.0	2.6	1.8	1.3	0.9	0.7	(0.5)
325	407.74	41.9	14.8	4.5	2.9	1.9	1.3	0.9	0.7	(0.5)
350	2716.07	68.0	19.2	5.0	3.1	2.0	1.4	1.0	0.7	(0.4)
375		119.8	24.6	5.7	3.5	2.2	1.5	1.0	0.7	(0.5)
400		235.9	31.0	6.4	3.8	2.4	1.6	1.1	0.7	(0.5)
425			(38.2)	7.3	4.3	2.7	1.8	1.2	0.8	(0.5)
450			(46.0)	8.5	4.9	3.1	2.0	1.4	0.9	(0.6)
475			(53.5)	(9.8)	(5.6)	(3.5)	(2.3)	(1.6)	(1.1)	(0.8)
500			(57.6)	(11.3)	(6.4)	(4.0)	(2.6)	(1.8)	(1.3)	(1.0)

TABLE 21
Finite difference partial derivative of $(\partial(\partial \ln \varepsilon/\partial P)_T/\partial T)_P$ with respect to temperature at constant pressure in $\text{bar}^{-1} (\text{°K})^{-2} \times 10^9$

t (°C)	PRESSURE, KB									
	SAT	0.5	1	2	2.5	3	3.5	4	4.5	5
25	5.85	4.8								
50	4.65	3.0								
75	4.35	2.7								
100	4.91	2.8	(1.8)	(0.9)	(0.7)	(0.5)	(0.4)	(0.3)	(0.2)	(0.2)
125	6.31	3.3	2.0	1.0	0.7	0.5	0.3	0.2	0.2	(0.1)
150	8.92	4.2	2.4	1.1	0.7	0.5	0.3	0.2	0.1	(0.1)
175	13.66	5.6	2.9	1.3	0.8	0.5	0.3	0.1	0.1	(0.0)
200	22.60	7.9	3.7	1.4	0.8	0.4	0.2	0.1	0.0	(-0.1)
225	40.78	11.5	4.9	1.5	0.8	0.4	0.2	0.1	0.0	(-0.1)
250	82.44	17.3	6.5	1.6	0.8	0.4	0.2	0.0	-0.1	(-0.1)
275	196.55	27.1	8.8	1.7	0.9	0.4	0.2	0.0	-0.1	(-0.1)
300	612.38	44.1	11.9	1.8	0.9	0.4	0.2	0.0	-0.1	(-0.1)
325	3149.17	75.7	15.6	2.0	1.0	0.5	0.2	0.1	0.0	(-0.1)
350	22725.69	141.3	19.6	2.3	1.1	0.6	0.3	0.1	0.0	(-0.0)
375			(23.6)	2.8	1.4	0.8	0.4	0.3	0.1	(0.1)
400			(27.1)	3.3	1.7	1.0	0.6	0.4	0.3	(0.2)
425			(30.4)	4.1	2.1	1.2	0.8	0.6	0.4	(0.3)
450			(31.9)	4.9	2.6	1.6	1.0	0.8	0.6	(0.5)
475			(25.7)	(5.7)	(3.0)	(1.8)	(1.3)	(1.0)	(0.8)	(0.7)
500			(1.5)	(3.6)	(4.6)	(1.8)	(1.3)	(1.4)	(1.4)	(0.9)

TABLE 22
Y (eq 65) in $(\text{°K})^{-1} \times 10^5$ computed from values of ε and $(\partial \ln \varepsilon/\partial T)_P$ in tables 15 and 17—see figure 34

t (°C)	PRESSURE, KB									
	SAT	0.5	1	2	2.5	3	3.5	4	4.5	5
25	-5.80	-5.65	(-5.51)	(-5.27)	(-5.17)	(-5.07)	(-4.99)	(-4.91)	(-4.84)	(-4.77)
50	-6.60	-6.35	(-6.13)	(-5.80)	(-5.66)	(-5.55)	(-5.45)	(-5.35)	(-5.26)	(-5.18)
75	-7.45	-7.08	(-6.79)	(-6.34)	(-6.17)	(-6.03)	(-5.90)	(-5.79)	(-5.69)	(-5.59)
100	-8.39	-7.87	-7.48	-6.89	-6.68	-6.51	-6.36	-6.23	-6.11	(-5.99)
125	-9.47	-8.74	-8.22	-7.46	-7.20	-6.98	-6.81	-6.65	-6.51	(-6.38)
150	-10.73	-9.71	-9.01	-8.06	-7.73	-7.46	-7.25	-7.07	-6.91	(-6.76)
175	-12.25	-10.80	-9.87	-8.68	-8.26	-7.94	-7.68	-7.47	-7.29	(-7.13)
200	-14.17	-12.05	-10.79	-9.33	-8.82	-8.42	-8.12	-7.87	-7.67	(-7.49)
225	-16.75	-13.56	-11.81	-10.01	-9.39	-8.92	-8.56	-8.28	-8.05	(-7.85)
250	-20.48	-15.46	-12.99	-10.75	-10.01	-9.45	-9.03	-8.71	-8.45	(-8.24)
275	-26.42	-17.99	-14.40	-11.56	-10.68	-10.03	-9.55	-9.18	-8.90	(-8.67)
300	-37.09	-21.59	-16.18	-12.48	-11.44	-10.69	-10.13	-9.72	-9.41	(-9.16)
325	-60.43	-26.93	-18.48	-13.54	-12.32	-11.44	-10.81	-10.34	-9.99	(-9.72)
350	-141.66	-35.28	-21.53	-14.80	-13.34	-12.32	-11.60	-11.07	-10.68	(-10.38)
375		-49.15	-25.54	-16.29	-14.54	-13.34	-12.50	-11.90	-11.46	(-11.13)
400		-74.46	-30.74	-18.04	-15.91	-14.49	-13.51	-12.82	-12.32	(-11.94)
425		-124.64	-37.33	-20.05	-17.43	-15.74	-14.58	-13.77	-13.19	(-12.76)
450		-197.96	-45.46	-22.26	-19.01	-16.97	-15.61	-14.66	-13.98	(-13.48)
475		-220.61	-55.10	-24.51	-20.47	-18.02	-16.40	-15.28	-14.49	(-13.91)
500		-203.18	-65.64	-26.43	-21.47	-18.55	-16.65	-15.36	-14.44	(-13.78)
525			(-75.14)	(-27.55)	(-21.55)	(-18.14)	(-16.00)	(-14.56)	(-13.53)	(-12.78)
550			(-79.80)	(-26.53)	(-19.90)	(-16.16)	(-13.84)	(-12.28)	(-11.18)	(-10.37)
575			(-74.23)	(-22.35)	(-15.71)	(-11.98)	(-9.68)	(-8.16)	(-7.09)	(-6.30)
600			(-53.20)	(-13.98)	(-8.38)	(-5.23)	(-3.33)	(-2.07)	(-1.19)	(-0.54)

with respect to pressure at constant temperature. Hence,

$$\begin{aligned}
 \left(\frac{\partial \left(\frac{\partial \varepsilon}{\partial \mathbf{P}} \right)_{\mathbf{T}}}{\partial \mathbf{T}} \right)_{\mathbf{P}} &= \left(\frac{\partial \left(\frac{\partial \varepsilon}{\partial \mathbf{T}} \right)_{\mathbf{P}}}{\partial \mathbf{P}} \right)_{\mathbf{T}} \\
 &= \varepsilon \left(\left(\frac{\partial \left(\frac{\partial \ln \varepsilon}{\partial \mathbf{P}} \right)_{\mathbf{T}}}{\partial \mathbf{T}} \right)_{\mathbf{P}} \right. \\
 &\quad \left. + \left(\frac{\partial \ln \varepsilon}{\partial \mathbf{T}} \right)_{\mathbf{P}} \left(\frac{\partial \ln \varepsilon}{\partial \mathbf{P}} \right)_{\mathbf{T}} \right) \\
 &= \left(\frac{\partial \varepsilon}{\partial \mathbf{P}} \right)_{\mathbf{T}} \left(\frac{\partial \ln \beta}{\partial \mathbf{T}} \right)_{\mathbf{P}} \\
 &\quad + \beta \sum_{i=0}^4 \sum_{j=0}^{4-i} j e_{ij} \rho^j (i \mathbf{T}^{i-1} - j \alpha \mathbf{T}^i) \quad (56)
 \end{aligned}$$

from which it follows that

$$\begin{aligned}
 \left(\frac{\partial^2 \left(\frac{\partial \varepsilon}{\partial \mathbf{P}} \right)_{\mathbf{T}}}{\partial \mathbf{T}^2} \right)_{\mathbf{P}} &= \varepsilon \left(\left(\frac{\partial^2 \left(\frac{\partial \ln \varepsilon}{\partial \mathbf{P}} \right)_{\mathbf{T}}}{\partial \mathbf{T}^2} \right)_{\mathbf{P}} \right. \\
 &\quad \left. + 2 \left(\frac{\partial \ln \varepsilon}{\partial \mathbf{T}} \right)_{\mathbf{P}} \left(\frac{\partial \left(\frac{\partial \ln \varepsilon}{\partial \mathbf{P}} \right)_{\mathbf{T}}}{\partial \mathbf{T}} \right)_{\mathbf{P}} \right. \\
 &\quad \left. + \left(\frac{\partial^2 \ln \varepsilon}{\partial \mathbf{T}^2} \right)_{\mathbf{P}} \left(\frac{\partial \ln \varepsilon}{\partial \mathbf{P}} \right)_{\mathbf{T}} + \left(\frac{\partial \ln \varepsilon}{\partial \mathbf{T}} \right)_{\mathbf{P}}^2 \right. \\
 &\quad \left. \left(\frac{\partial \ln \varepsilon}{\partial \mathbf{P}} \right)_{\mathbf{T}} \right) = \left(\frac{\partial \varepsilon}{\partial \mathbf{P}} \right)_{\mathbf{T}} \left(\frac{\partial^2 \ln \beta}{\partial \mathbf{T}^2} \right)_{\mathbf{P}} \\
 &\quad + 2 \left(\frac{\partial \left(\frac{\partial \varepsilon}{\partial \mathbf{P}} \right)_{\mathbf{T}}}{\partial \mathbf{T}} \right)_{\mathbf{P}} \left(\frac{\partial \ln \beta}{\partial \mathbf{T}} \right)_{\mathbf{P}} \\
 &\quad - \left(\frac{\partial \varepsilon}{\partial \mathbf{P}} \right)_{\mathbf{T}} \left(\frac{\partial \ln \beta}{\partial \mathbf{T}} \right)_{\mathbf{P}}^2 +
 \end{aligned}$$

$$\begin{aligned}
 & + \beta \sum_{i=0}^4 \sum_{j=0}^{4-i} j e_{ij} \rho^j \left(j \alpha (j \alpha T^i - 2i T^{i-1}) + \right. \\
 & \left. i(i-1) T^{i-2} - j T^i \left(\frac{\partial \alpha}{\partial T} \right)_P \right) \quad (57)
 \end{aligned}$$

It can be seen in figure 33 that the values of $(\partial(\partial \ln \epsilon / \partial P)_T / \partial T)_P$ in table 20, which were computed from equation (56) and values of V , α , β , $(\partial \beta / \partial T)_P$, $(\partial \ln \epsilon / \partial T)_P$, and $(\partial \ln \epsilon / \partial P)_T$ given above, are in close agreement with finite difference derivatives calculated from the values of $(\partial \ln \epsilon / \partial P)_T$ and $(\partial \ln \epsilon / \partial T)_P$ in figures 25 and 28. However (as noted above), for temperatures $\cong 500^\circ\text{C}$ and pressures $\cong 500$ bars at temperatures $\leq 100^\circ\text{C}$, the proximity of the fit region boundary in figure 18 introduces inconsistencies in the values of $(\partial(\partial \ln \epsilon / \partial P)_T / \partial T)_P$ computed from the values of V , α , β , $(\partial \beta / \partial T)_P$, ϵ , $(\partial \ln \epsilon / \partial T)_P$, and $(\partial \ln \epsilon / \partial P)_T$ in tables 3, 7, 8, 12, and 15 through 17. For this reason, equations (56) and (57) should not be used to calculate values of $(\partial(\partial \ln \epsilon / \partial P)_T / \partial T)_P$ and $(\partial^2(\partial \ln \epsilon / \partial P)_T / \partial T^2)_P$ for $T > 500^\circ\text{C}$ or $P > 500$ bars at $T < 100^\circ\text{C}$. Because

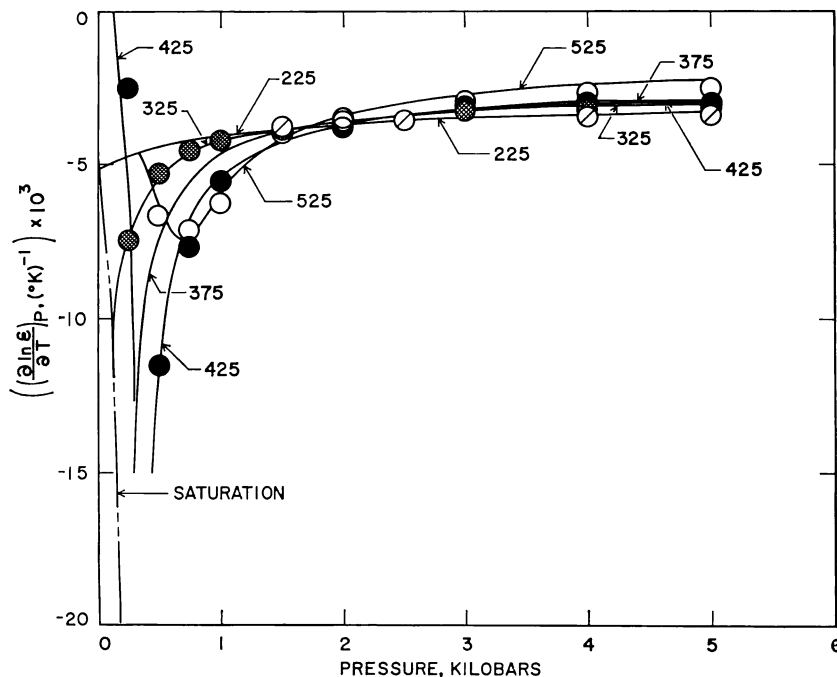


Fig. 28. Partial derivative of $\ln \epsilon$ with respect to temperature at constant pressure (table 17) as a function of pressure at constant temperature (labeled in $^\circ\text{C}$) computed from equations (19) through (21), (25), (33), (39), (47), and (49) and coefficients in tables 4, 5, 6, 9, 10, and 14. The symbols represent corresponding finite difference derivatives computed from data given by Oshry (ms), Owen and others (1961), and/or Heger (ms).

evaluation of equation (57) requires values of $(\partial^2 \ln \beta / \partial T^2)_P$, which cannot be computed with confidence from the partial derivatives of equations (36) and (42), the values of $(\partial^2(\partial \ln \epsilon / \partial P)_T / \partial T^2)_P$ given in table 21 correspond to finite difference derivatives calculated from the values of $(\partial(\partial \ln \epsilon / \partial P)_T / \partial T)_P$ in figure 33.

BORN FUNCTIONS

Continuum theories of liquid H₂O and electrostatic models of ion solvation in aqueous solution require values for the partial derivatives of ϵ^{-1} with respect to temperature and pressure. Because ϵ^{-1} and its partial derivatives, which are designated here as Born functions, are used extensively in solution chemistry, they are tabulated and plotted below as functions of pressure and temperature.

The Born equation (Born, 1920), which relates the effective electrostatic radius of an incompressible ion (with spherical charge symmetry)

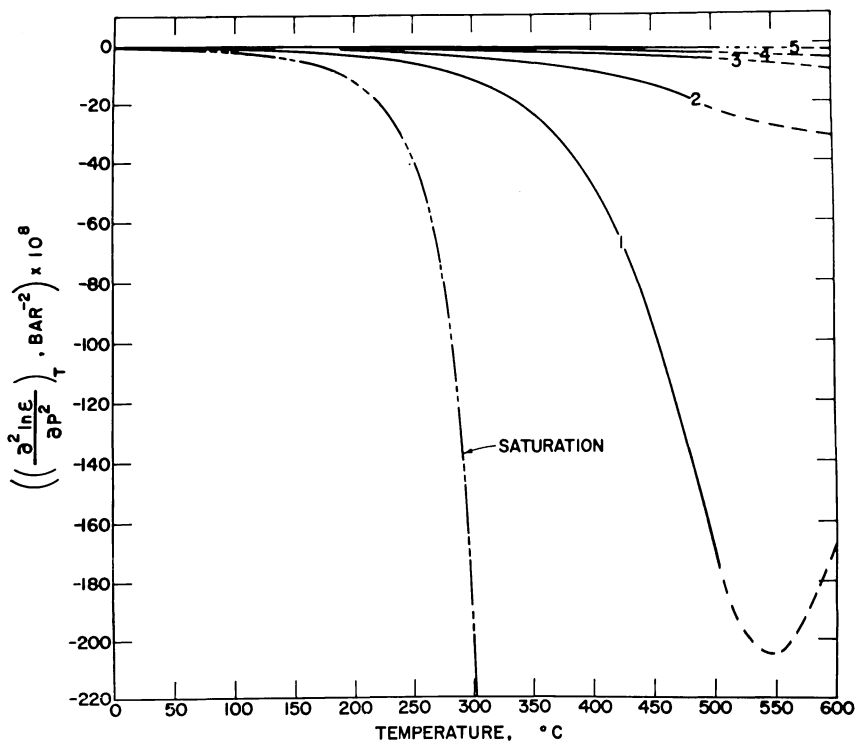


Fig. 29. Partial derivative of $(\partial \ln \epsilon / \partial P)_T$ with respect to pressure at constant temperature (table 18) as a function of temperature at constant pressure (labeled in kb) computed from equations (19) through (23), (32), (35), (38), (41), (47), (48), and (50) and coefficients in tables 4, 5, 6, 9, 10, and 14.

to the change in Gibbs free energy attending its transfer from a vacuum to a medium of dielectric constant ϵ , can be written as

$$\Delta G_{s,j} = \omega_j \left(\frac{1}{\epsilon} - 1 \right) \quad (58)$$

where

$$\omega_j = \frac{N^\circ Z_j^2 e^2}{2r_{e,j}} \quad , \quad (59)$$

$\Delta G_{s,j}$ denotes the molal Gibbs free energy of transfer for the j th ion, N° stands for Avogadro's number (6.02252×10^{23} mole⁻¹), e represents the

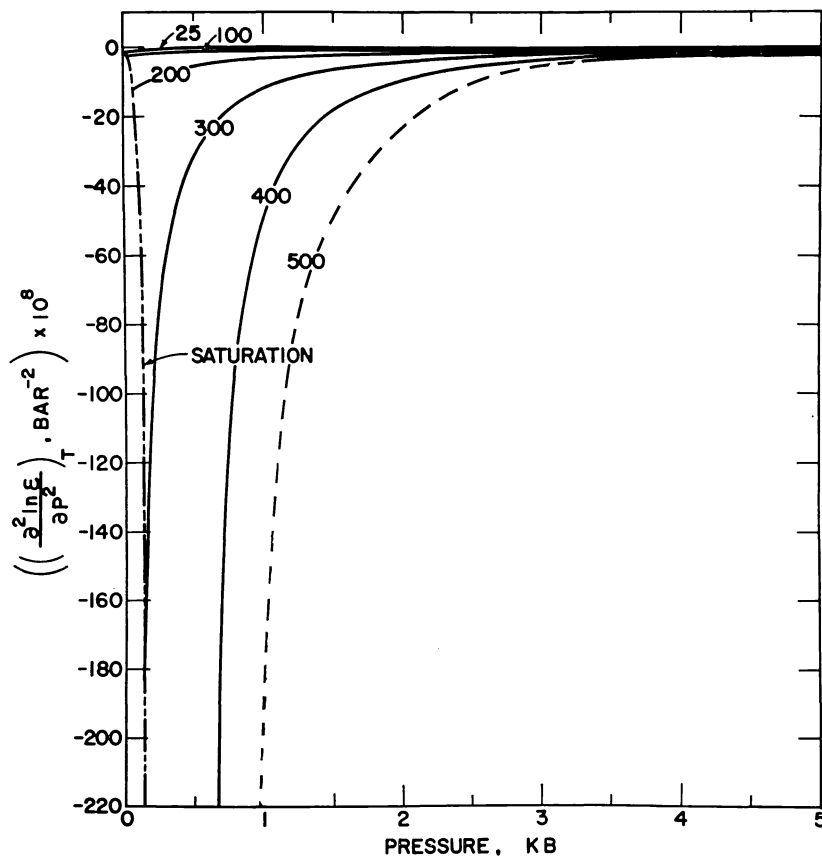


Fig. 30. Partial derivative of $(\partial \ln \epsilon / \partial P)_T$ with respect to pressure at constant temperature (table 18) as a function of pressure at constant temperature (labeled in °C) computed from equations (19) through (23), (32), (35), (38), (41), (47), (48), and (50) and coefficients in tables 4, 5, 6, 9, 10, and 14.

TABLE 23

X (eq 66) in $(^{\circ}\text{K})^{-2} \times 10^7$ computed from values of ε , $(\partial \ln \varepsilon / \partial T)_P$, and $(\partial^2 \ln \varepsilon / \partial T^2)_P$ in tables 15, 17, and 19—see figure 34

t ($^{\circ}\text{C}$)	PRESSURE, KB									
	SAT	0.5	1	2	2.5	3	3.5	4	4.5	5
25	-3.16	-2.7								
50	-3.28	-2.8								
75	-3.55	-3.0								
100	-4.01	-3.3	(-2.8)	(-2.3)	(-2.1)	(-1.9)	(-1.8)	(-1.7)	(-1.7)	(-1.6)
125	-4.65	-3.7	-3.1	-2.3	-2.1	-1.9	-1.8	-1.7	-1.6	(-1.6)
150	-5.53	-4.1	-3.3	-2.4	-2.1	-1.9	-1.8	-1.7	-1.6	(-1.5)
175	-6.84	-4.7	-3.5	-2.4	-2.1	-1.9	-1.7	-1.6	-1.5	(-1.5)
200	-8.95	-5.4	-3.9	-2.6	-2.2	-1.9	-1.8	-1.6	-1.5	(-1.5)
225	-12.63	-6.7	-4.3	-2.8	-2.3	-2.0	-1.8	-1.7	-1.6	(-1.5)
250	-19.57	-8.7	-5.1	-3.0	-2.5	-2.2	-1.9	-1.8	-1.7	(-1.6)
275	-34.02	-11.9	-6.3	-3.4	-2.8	-2.4	-2.2	-2.0	-1.9	(-1.8)
300	-69.80	-17.3	-8.0	-4.0	-3.2	-2.8	-2.5	-2.3	-2.2	(-2.1)
325	-194.82	-26.3	-10.6	-4.7	-3.8	-3.2	-2.9	-2.7	-2.5	(-2.4)
350	-1215.87	-42.0	-14.0	-5.5	-4.4	-3.7	-3.3	-3.1	-2.9	(-2.8)
375		-72.5	-18.3	-6.5	-5.1	-4.3	-3.8	-3.5	-3.3	(-3.1)
400		-139.1	-23.5	-7.5	-5.8	-4.8	-4.1	-3.7	-3.5	(-3.3)
425			(-29.4)	(-8.4)	(-6.2)	(-5.0)	(-4.2)	(-3.7)	(-3.4)	(-3.1)
450			(-35.7)	(-8.9)	(-6.2)	(-4.7)	(-3.7)	(-3.1)	(-2.7)	(-2.4)
475			(-41.1)	(-8.4)	(-5.1)	(-3.3)	(-2.3)	(-1.6)	(-1.1)	(-0.8)
500			(-42.0)	(-6.1)	(-2.3)	(-0.4)	(0.6)	(1.3)	(1.8)	(2.2)

TABLE 24

\hat{Q} (eq 67) in $\text{bar}^{-1} \times 10^6$ computed from values of ε and $(\partial \ln \varepsilon / \partial P)_T$ in tables 15 and 16—see figure 35

t ($^{\circ}\text{C}$)	PRESSURE, KB									
	SAT	0.5	1	2	2.5	3	3.5	4	4.5	5
25	0.60	0.51	0.46	(0.36)	(0.33)	(0.30)	(0.27)	(0.24)	(0.22)	(0.20)
50	0.71	0.61	0.55	(0.43)	(0.39)	(0.35)	(0.32)	(0.29)	(0.26)	(0.24)
75	0.88	0.75	0.66	(0.52)	(0.46)	(0.41)	(0.37)	(0.34)	(0.31)	(0.28)
100	1.14	0.94	0.81	0.62	0.55	0.49	0.44	0.40	0.36	(0.33)
125	1.52	1.20	1.01	0.76	0.66	0.58	0.52	0.47	0.42	(0.38)
150	2.05	1.56	1.26	0.92	0.79	0.69	0.61	0.55	0.49	(0.45)
175	2.85	2.05	1.60	1.14	0.96	0.83	0.72	0.64	0.57	(0.52)
200	4.05	2.72	2.03	1.40	1.16	0.98	0.85	0.75	0.66	(0.59)
225	5.95	3.68	2.61	1.72	1.41	1.17	1.00	0.87	0.76	(0.68)
250	9.18	5.09	3.39	2.12	1.70	1.39	1.17	1.00	0.87	(0.77)
275	15.14	7.22	4.44	2.59	2.04	1.64	1.36	1.15	0.99	(0.87)
300	27.77	10.59	5.90	3.16	2.44	1.93	1.57	1.32	1.12	(0.97)
325	61.49	16.25	7.97	3.85	2.91	2.27	1.82	1.50	1.27	(1.09)
350	213.62	26.41	10.94	4.69	3.47	2.66	2.10	1.71	1.43	(1.21)
375		46.50	15.23	5.73	4.14	3.11	2.42	1.95	1.61	(1.35)
400		91.93	21.45	7.03	4.94	3.64	2.80	2.22	1.81	(1.51)
425		210.24	30.44	8.66	5.91	4.28	3.23	2.53	2.04	(1.68)
450		469.90	43.37	10.72	7.10	5.03	3.75	2.90	2.31	(1.88)
475		702.10	61.73	13.32	8.55	5.93	4.35	3.33	2.62	(2.12)
500		785.14	86.87	16.57	10.30	7.00	5.06	3.82	2.99	(2.39)
525			(118.81)	(19.90)	(11.82)	(8.32)	(6.19)	(4.61)	(3.46)	(2.70)
550			(154.72)	(24.20)	(14.13)	(9.71)	(7.10)	(5.24)	(3.92)	(3.04)
575			(188.81)	(28.71)	(16.57)	(11.15)	(8.04)	(5.89)	(4.38)	(3.38)
600			(213.77)	(32.87)	(18.84)	(12.48)	(8.89)	(6.47)	(4.80)	(3.70)

TABLE 25
 U (eq 68) in $\text{bar}^{-1} (\text{°K})^{-1} \times 10^9$ computed from values of ϵ , $(\partial \ln \epsilon / \partial P)_T$,
 $(\partial \ln \epsilon / \partial T)_P$, and $(\partial(\partial \ln \epsilon / \partial P)_T) / \partial T)_P$ in tables 15 through 17
 and 20—see figure 35

t (°C)	PRESSURE, KB									
	SAT	0.5	1	2	2.5	3	3.5	4	4.5	5
25	3.20	2.9								
50	5.68	4.6								
75	8.59	6.6								
100	12.42	9.0	(6.8)	(4.7)	(4.0)	(3.5)	(3.0)	(2.7)	(2.4)	(2.1)
125	17.86	12.2	8.9	5.9	4.9	4.1	3.6	3.1	2.7	(2.4)
150	26.01	16.6	11.6	7.3	5.9	4.9	4.2	3.6	3.1	(2.7)
175	38.95	22.8	15.2	9.1	7.1	5.8	4.8	4.1	3.5	(3.0)
200	60.80	32.0	20.0	11.3	8.6	6.8	5.5	4.6	3.9	(3.3)
225	100.62	46.0	26.6	13.9	10.3	7.9	6.3	5.1	4.3	(3.6)
250	180.75	68.1	35.9	17.1	12.3	9.2	7.1	5.7	4.7	(3.9)
275	365.68	105.4	49.3	20.8	14.5	10.6	8.0	6.3	5.1	(4.1)
300	892.43	171.2	69.1	25.3	17.2	12.2	9.0	7.0	5.5	(4.4)
325	3075.19	295.2	98.4	30.8	20.4	14.1	10.2	7.7	6.0	(4.8)
350	24995.05	550.5	141.8	37.6	24.2	16.4	11.7	8.7	6.6	(5.2)
375		1146.1	205.5	46.3	28.9	19.2	13.4	9.8	7.4	(5.7)
400		2774.6	297.6	57.5	34.8	22.7	15.6	11.2	8.4	(6.4)
425			(429.4)	(71.9)	(42.2)	(27.0)	(18.4)	(13.1)	(9.7)	(7.3)
450			(615.1)	(90.6)	(51.5)	(32.3)	(21.7)	(15.4)	(11.2)	(8.5)
475			(863.2)	(114.1)	(62.8)	(38.6)	(25.6)	(18.0)	(13.1)	(9.8)
500			(1149.6)	(142.3)	(75.8)	(45.6)	(29.8)	(20.8)	(15.1)	(11.3)

TABLE 26
 N (eq 69) in $\text{bar}^{-2} \times 10^{10}$ computed from values of ϵ , $(\partial \ln \epsilon / \partial P)_T$,
 and $(\partial^2 \ln \epsilon / \partial P^2)_T$ in tables 15, 16, and 18—see figure 36

t (°C)	PRESSURE, KB									
	SAT	0.5	1	2	2.5	3	3.5	4	4.5	5
25	-2.24	-1.2								
50	-2.73	-1.5								
75	-3.71	-2.0								
100	-5.49	-3.1	(-2.1)	(-1.7)	(-1.4)	(-1.2)	(-1.0)	(-0.8)	(-0.7)	(-0.6)
125	-8.56	-4.7	-3.2	-2.1	-1.8	-1.5	-1.2	-1.0	-0.9	(-0.7)
150	-13.91	-7.3	-4.8	-2.9	-2.2	-1.8	-1.5	-1.2	-1.0	(-0.9)
175	-23.55	-11.4	-7.2	-3.9	-3.0	-2.3	-1.9	-1.5	-1.3	(-1.1)
200	-41.85	-18.1	-10.6	-5.3	-3.9	-3.0	-2.4	-1.9	-1.6	(-1.3)
225	-79.30	-29.4	-15.8	-7.2	-5.2	-3.9	-3.0	-2.3	-1.9	(-1.6)
250	-164.37	-49.3	-23.8	-9.8	-6.9	-4.9	-3.7	-2.9	-2.3	(-1.9)
275	-388.63	-86.1	-36.1	-13.3	-9.0	-6.3	-4.6	-3.5	-2.8	(-2.3)
300	-1131.44	-158.9	-56.0	-18.0	-11.7	-8.0	-5.7	-4.3	-3.4	(-2.7)
325	-4798.85	-315.6	-88.0	-24.2	-15.3	-10.1	-7.1	-5.2	-4.0	(-3.1)
350	-50615.56	-691.9	-140.5	-32.4	-19.8	-12.8	-8.7	-6.3	-4.8	(-3.8)
375		-1740.3	-227.3	-43.5	-25.5	-16.0	-10.8	-7.7	-5.7	(-4.5)
400		-5276.1	-371.1	-58.4	-32.8	-20.1	-13.2	-9.2	-6.8	(-5.3)
425			(-610.0)	(-78.6)	(-42.3)	(-25.1)	(-16.1)	(-11.1)	(-8.1)	(-6.2)
450			(-1003.5)	(-105.8)	(-54.4)	(-31.3)	(-19.7)	(-13.4)	(-9.7)	(-7.3)
475			(-1627.9)	(-142.3)	(-69.9)	(-39.1)	(-24.1)	(-16.1)	(-11.5)	(-8.6)
500			(-2528.7)	(-190.6)	(-89.8)	(-48.7)	(-29.3)	(-19.3)	(-13.6)	(-10.1)

electronic charge (4.80298 esu), and Z_j and $r_{e,j}$ refer to the charge and effective electrostatic radius of the subscripted ion. If $r_{e,j}$ is independent of temperature and pressure, it follows from equation (58) that the change in the molal entropy ($\Delta S_{s,j}$), heat capacity ($\Delta C_{P,s,j}$), volume ($\Delta V_{s,j}$), expansibility ($\Delta E_{x,s,j}$), and compressibility ($\Delta \kappa_{s,j}$) for the transfer process can be expressed as

$$\Delta S_{s,j} = \omega_j Y, \quad (60)$$

$$\Delta C_{P,s,j} = T \left(\frac{\partial \Delta S_{s,j}}{\partial T} \right)_P = \left(\frac{\partial \Delta H_{s,j}}{\partial T} \right)_P = \omega_j T X, \quad (61)$$

$$\Delta V_{s,j} = -\omega_j \hat{Q}, \quad (62)$$

$$\Delta E_{x,s,j} = \left(\frac{\partial \Delta V_{s,j}}{\partial T} \right)_P = -\omega_j U, \quad (63)$$

and

$$-\Delta \kappa_{s,j} = \left(\frac{\partial \Delta V_{s,j}}{\partial P} \right)_T = -\omega_j N, \quad (64)$$

where $\Delta H_{s,j}$ is the molal enthalpy change for the transfer process, and Y , X , \hat{Q} , U , and N stand for various Born functions given by

$$Y = \frac{1}{\epsilon} \left(\frac{\partial \ln \epsilon}{\partial T} \right)_P, \quad (65)$$

$$X = \frac{1}{\epsilon} \left(\left(\frac{\partial^2 \ln \epsilon}{\partial T^2} \right)_P - \left(\frac{\partial \ln \epsilon}{\partial T} \right)_P^2 \right), \quad (66)$$

$$\hat{Q} = \frac{1}{\epsilon} \left(\frac{\partial \ln \epsilon}{\partial P} \right)_T, \quad (67)$$

$$U = \frac{1}{\epsilon} \left(\left(\frac{\partial \left(\frac{\partial \ln \epsilon}{\partial P} \right)_T}{\partial T} \right)_P - \left(\frac{\partial \ln \epsilon}{\partial T} \right)_P \left(\frac{\partial \ln \epsilon}{\partial P} \right)_T \right) \quad (68)$$

and

$$N = \frac{1}{\epsilon} \left(\left(\frac{\partial^2 \ln \epsilon}{\partial P^2} \right)_T - \left(\frac{\partial \ln \epsilon}{\partial P} \right)_T^2 \right). \quad (69)$$

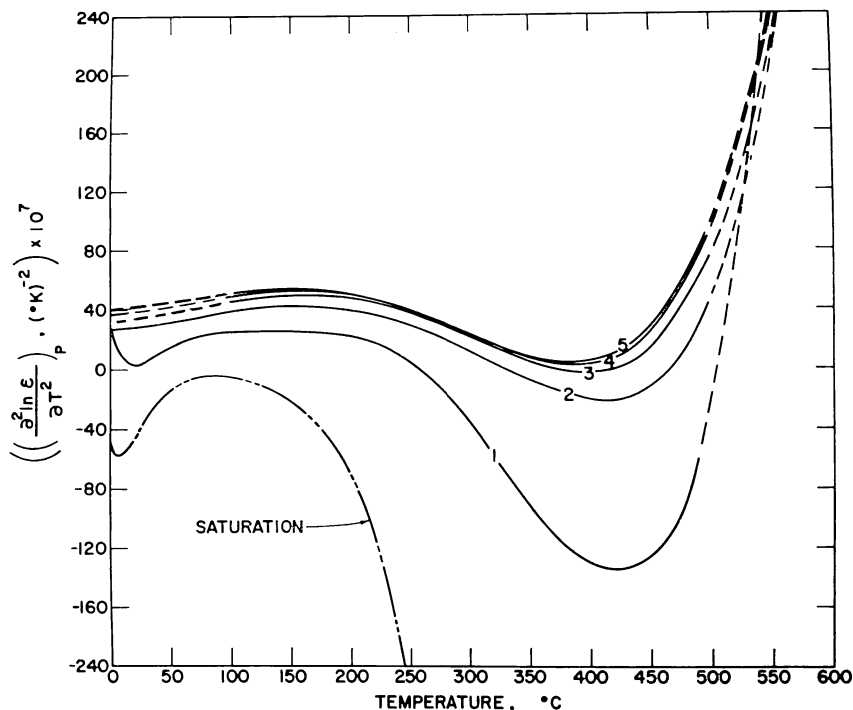


Fig. 31. Partial derivative of $(\partial \ln \epsilon / \partial T)_P$ with respect to temperature at constant pressure (table 19) as a function of temperature at constant pressure (labeled in kb) computed from equations (19) through (21), (25), (27), (33), (37), (39), (43), (47), (49), and (51) and coefficients in tables 4, 5, 6, 9, 10, and 14.

Values of Y , X , \hat{Q} , U , and N computed from equations (65) through (69) and values of $(\partial \ln \epsilon / \partial T)_P$, $(\partial^2 \ln \epsilon / \partial T^2)_P$, $(\partial \ln \epsilon / \partial P)_T$, $(\partial(\partial \ln \epsilon / \partial P)_T / \partial T)_P$, $(\partial \ln \epsilon / \partial T)_P$, and $(\partial^2 \ln \epsilon / \partial P^2)_T$ given above are shown in tables 22 through 26 and plotted in figures 34 through 36. Owing to the high sensitivity of X , U , and N to small errors in the partial derivatives of ϵ and V , values of these variables are not given in tables 23, 25, and 26 for temperatures $> 500^\circ\text{C}$ or pressures > 500 bars at temperatures $< 100^\circ\text{C}$.

It can be seen in figure 34 that the isobars for both Y and X exhibit minima at high temperatures. In contrast, \hat{Q} and U increase and N decreases monotonically with increasing temperature at constant pressure (figs. 35 and 36). Because each of the Born functions depends on the expansibility and/or compressibility of H_2O , $-Y$, $-X$, \hat{Q} , U , and $-N$ all approach ∞ at the critical point of H_2O . As a consequence, the standard thermodynamic partial molal properties of aqueous electrolytes also approach positive or negative infinity at the critical point of H_2O (Helgeson and Kirkham, 1974c).

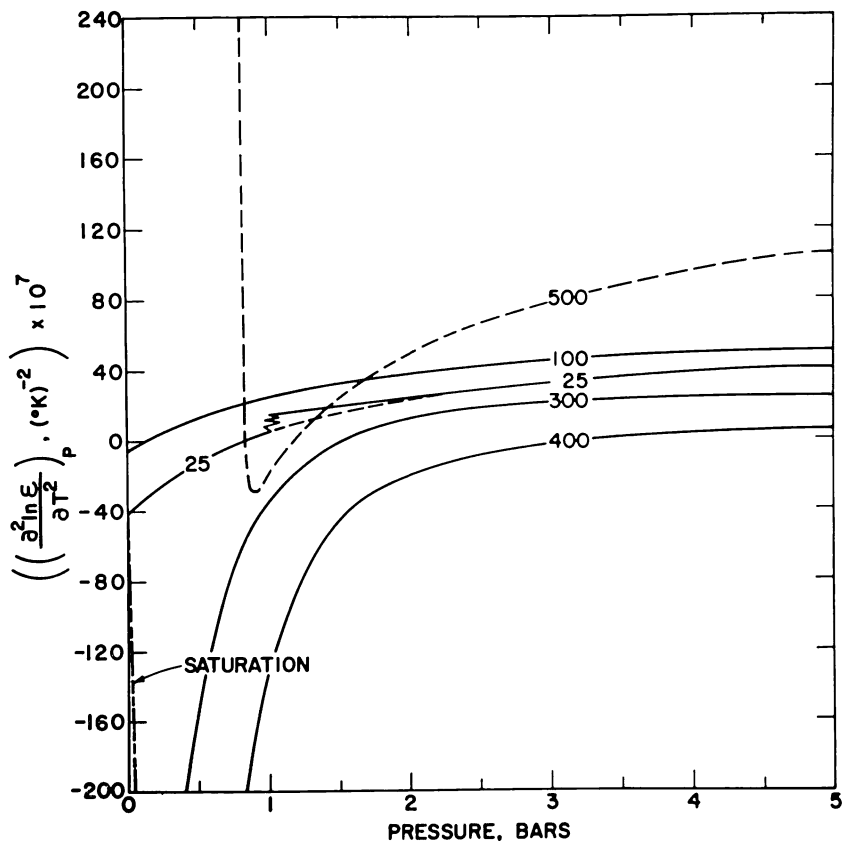


Fig. 32. Partial derivatives of $(\partial \ln \epsilon / \partial T)_P$ with respect to temperature at constant pressure (table 19) as a function of pressure at constant temperature (labeled in °C) computed from equations (19) through (21), (25), (27), (33), (37), (39), (43), (47), (49), and (51) and coefficients in tables 4, 5, 6, 9, 10, and 14.

ENTROPY

Computed values of the third law molal entropy of H_2O are given in table 27 and plotted in figures 37 and 38. Entropies for pressures \leq a kilobar were obtained by first evaluating the combined partial derivatives of equations (14) through (17) with respect to temperature at constant density; that is,

$$\begin{aligned}
 -\left(\frac{\partial \psi}{\partial T}\right)_\rho &= -\left(\frac{\partial A}{\partial T}\right)_\rho - S_{triple} = S - S_{triple} \\
 &= -\left(\frac{\partial \psi^\circ}{\partial T}\right)_\rho - R(\ln \rho + \rho Q) - RT_\rho \left(\frac{\partial Q}{\partial T}\right)_\rho \quad (70)
 \end{aligned}$$

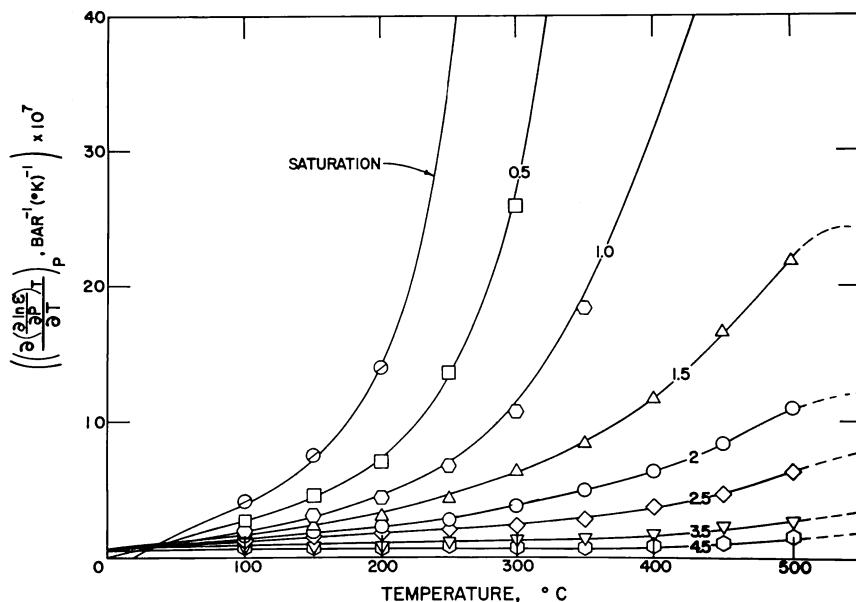


Fig. 33. Partial derivative of $(\partial \ln \epsilon / \partial T)_T$ with respect to temperature at constant pressure (table 20) as a function of temperature at constant pressure (labeled in kb) computed from equations (19) through (22), (24), (25), (32), (33), (36), (38), (39), (42), (47), (48), (49), (50) through (53), and (56) and coefficients in tables 4, 5, 6, 9, 10, and 14 (curves). The symbols represent corresponding finite difference derivatives computed from the finite difference derivatives of $\ln \epsilon$ plotted in figure 25.

where S_{triple} refers to the third law molal entropy of liquid H_2O at the triple point in joules g^{-1} (table 2), and $(\partial Q / \partial T)_P$ and $(\partial \psi_o / \partial T)_P$ represent partial derivatives of equations (15) and (16) given in the appendix (eqs A-43 and A-48, respectively). Entropies above a kilobar were computed from

$$S_{P,T} = S_{P=1000,T} - \left(\int_{P=1000}^P V \alpha dP \right)_T \quad (71)$$

where $S_{P,T}$ stands for the third law molal entropy at the pressure and temperature of interest, $S_{P=1000,T}$ refers to the corresponding entropy at 1 kb, and V and α represent the molal volume and coefficient of isobaric thermal expansion as a function of pressure at the temperature of interest. The integral in equation (71) for region A in figure 9 was evaluated numerically using equations (21), (33), and (39) together with an equal-interval integration routine adapted from Arden and Astill (1970).

For temperatures $> 550^{\circ}\text{C}$ in region B of figure 9, equation (71) was combined with the pressure integral of equation (39) to give

$$S_{P,T} = S_{P=1000,T} - \sum_{i=0}^5 \sum_{j=0}^{6-i} i \dot{D}_{ij} T^{i-1} ((1800)^{j+1} - (1000)^{j+1}) / (j+1) - \sum_{i=0}^9 \sum_{j=0}^{9-i} i D_{ij} T^{i-1} (P^{j+1} - (1800)^{j+1}) / (j+1) \quad (72)$$

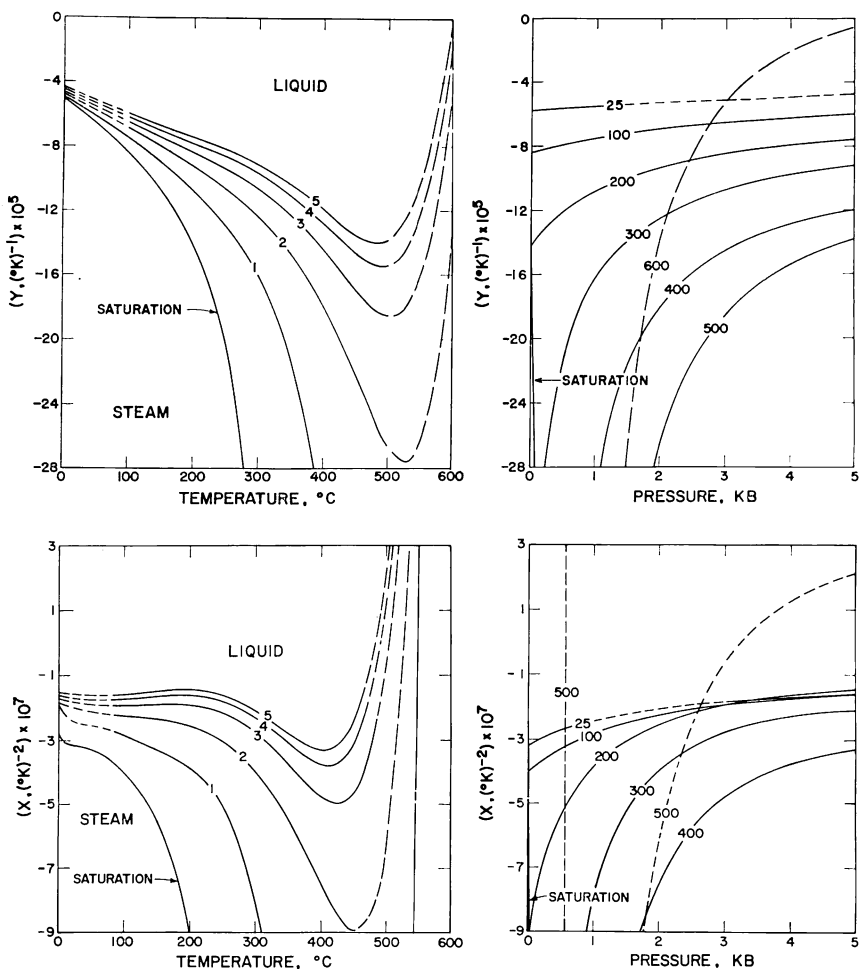


Fig. 34. Dependence of Y (table 22) and X (table 23) on temperature at constant pressure (labeled in kb) and pressure at constant temperature (labeled in $^{\circ}\text{C}$) computed from equations (65) and (66) and values of ϵ , $(\partial \ln \epsilon / \partial T)_P$, and $(\partial^2 \ln \epsilon / \partial T^2)_P$ in tables 15, 17, and 19.

where D_{ij} and \dot{D}_{ij} represent the arrays of fit coefficients for regions B and C, respectively, in table 10. For temperatures $\leq 550^\circ\text{C}$ in region B, \dot{D}_{ij} in equation (72) is set to zero, and $S_{P=1000,T}$ is replaced by $S_{P=1800,T}$ in region A. Similarly, for temperatures and pressures in region C, D_{ij} in equation (72) is set to zero, and (1800) is replaced by P.

The entropies computed in this study for pressures above a kilobar are generally in close agreement with those calculated by Burnham, Holloway, and Davis (1969b); those for pressures below a kilobar are identical (except for the unit conversion and difference in conventions) to those given by Keenan and others (1969). Estimated uncertainties in the entropies given in table 26 for pressures above a kilobar are of the order of 0.5 percent or less.

It can be seen in figure 37 that the entropy of H_2O in the liquid phase region decreases only slightly and exhibits a near-linear dependence

TABLE 27
Third law molal entropy (S) in $\text{cal mole}^{-1} (\text{K})^{-1}$ computed from equations (70) through (72), values of V and α in tables 3 and 7, and data in table 2—see figures 37 through 39

t (°C)	PRESSURE, KB									
	SAT	0.5	1	2	3	4	5	6	7	8
25	16.71	16.65	16.58	16.4	16.2	16.1	15.9	15.8	15.6	(15.5)
50	18.16	18.06	17.97	17.8	17.6	17.4	17.2	17.1	16.9	(16.8)
75	19.50	19.38	19.26	19.0	18.8	18.6	18.5	18.3	18.1	(17.9)
100	20.76	20.60	20.46	20.2	20.0	19.8	19.6	19.4	19.2	(19.0)
125	21.94	21.75	21.59	21.3	21.1	20.8	20.6	20.4	20.2	(20.1)
150	23.06	22.84	22.66	22.3	22.1	21.8	21.6	21.4	21.2	(21.0)
175	24.14	23.88	23.67	23.3	23.0	22.8	22.5	22.3	22.1	(21.9)
200	25.17	24.88	24.64	24.2	23.9	23.7	23.4	23.2	23.0	(22.8)
225	26.17	25.84	25.56	25.1	24.8	24.5	24.2	24.0	23.8	(23.6)
250	27.16	26.76	26.45	26.0	25.6	25.3	25.0	24.8	24.6	(24.4)
275	28.14	27.67	27.31	26.8	26.4	26.1	25.8	25.6	25.3	(25.1)
300	29.14	28.57	28.14	27.6	27.1	26.8	26.5	26.3	26.1	(25.8)
325	30.20	29.46	28.95	28.3	27.9	27.5	27.2	27.0	26.7	(26.5)
350	31.40	30.38	29.75	29.0	28.6	28.2	27.9	27.6	27.4	(27.2)
375		31.34	30.54	29.7	29.2	28.8	28.5	28.2	28.0	(27.8)
400		32.37	31.33	30.4	29.9	29.5	29.1	28.9	28.6	(28.4)
425		33.53	32.11	31.1	30.5	30.1	29.7	29.4	29.2	(29.0)
450		34.89	32.90	31.7	31.1	30.7	30.3	30.0	29.7	(29.5)
475		36.27	33.67	32.4	31.7	31.2	30.8	30.5	30.2	(30.0)
500		37.40	34.44	33.0	32.2	31.7	31.3	31.0	30.7	(30.5)
525		38.30	35.20	33.5	32.8	32.2	31.8	31.5	31.2	(30.9)
550		39.02	35.94	34.1	33.3	32.7	32.3	32.0	31.7	(31.4)
575		39.64	36.65	34.6	33.7	33.1	32.7	32.3	32.0	(31.8)
600		40.18	37.31	35.2	34.2	33.6	33.2	32.8	32.5	(32.3)
625		40.67	37.93	35.7	34.7	34.1	33.7	33.3	33.0	(32.7)
650		41.11	38.50	36.2	35.2	34.6	34.1	33.8	33.4	(33.2)
675		41.53	39.03	36.8	35.7	35.1	34.6	34.2	33.9	(33.6)
700		41.91	39.52	37.2	36.2	35.5	35.0	34.6	34.3	(34.0)
725		42.27	39.98	(37.7)	(36.6)	(35.9)	(35.4)	(35.0)	(34.7)	(34.4)
750		42.61	40.41	(38.1)	(37.0)	(36.3)	(35.8)	(35.4)	(35.1)	(34.8)
775		42.94	40.81	(38.5)	(37.4)	(36.7)	(36.2)	(35.8)	(35.4)	(35.1)
800		43.24	41.18	(38.9)	(37.8)	(37.1)	(36.5)	(36.1)	(35.8)	(35.5)
825		43.54	41.54							
850		43.82	41.87							
875		44.10	42.19							
900		44.36	42.50							

on pressure as pressure increases isothermally from 0.001 to 10 kb. In the steam phase region the entropy of H_2O increases rapidly and asymptotically with decreasing pressure at constant temperature. With increasing pressure above ~ 2 kb, the effect of the critical phenomenon on the entropy of H_2O diminishes and disappears (fig. 38). Isentropes are plotted in figure 39, where it can be seen that $(\partial P/\partial T)_S$ (which is equal to $C_P/TV\alpha$) at $25^\circ C$ decreases from ~ 550 bar $(^\circ K)^{-1}$ at low pressures to ~ 330 bar $(^\circ K)^{-1}$ at 5 kb, and then increases to ~ 380 bar $(^\circ K)^{-1}$ at 10 kb.

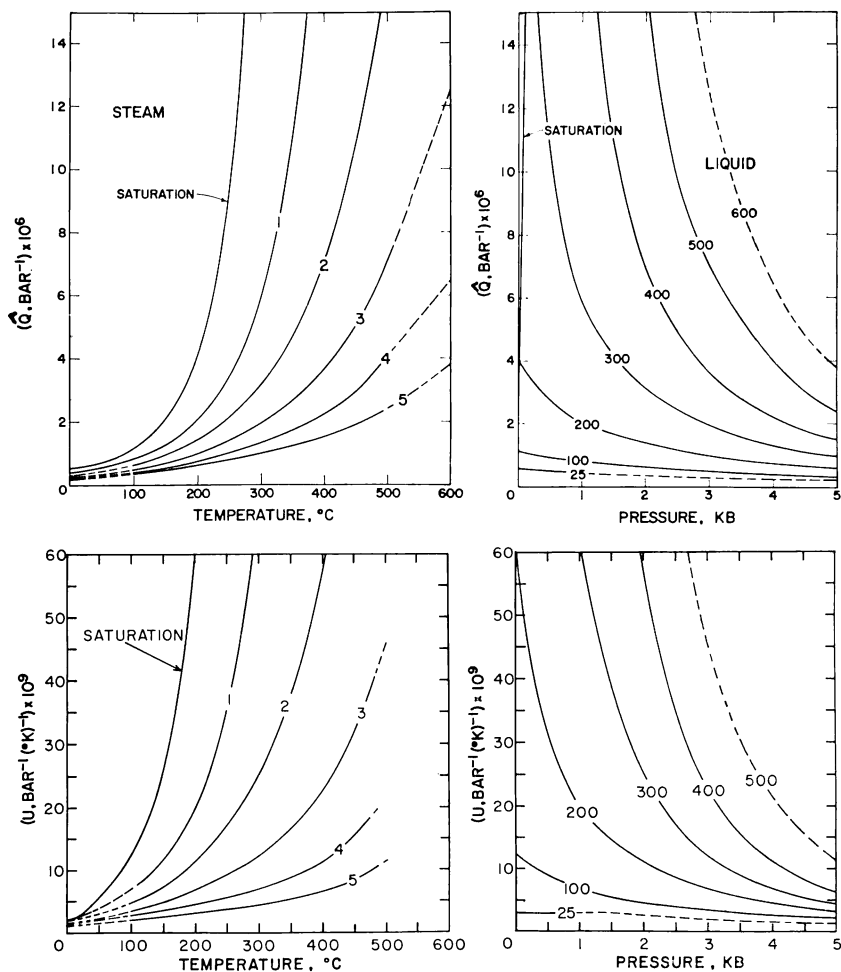


Fig. 35. Dependence of \hat{Q} (table 24) and U (table 25) on temperature at constant pressure (labeled in kb) and pressure at constant temperature (labeled in $^\circ C$) computed from equations (67) and (68) and values of ϵ , $(\partial \ln \epsilon / \partial P)_T$, $(\partial \ln \epsilon / \partial T)_P$, and $(\partial(\partial \ln \epsilon / \partial P)_T / \partial T)_P$ in tables 15 through 17 and 20.

As entropy and temperature increase at a given pressure, $(\partial P/\partial T)_S$ decreases asymptotically, reaching values $< 1 \text{ bar } (^{\circ}\text{K})^{-1}$ in the steam phase region.

HELMHOLTZ AND GIBBS FREE ENERGIES

The values of the apparent molal Helmholtz free energy of formation (ΔA) of H_2O for pressures \leq a kilobar in table 28 and figures 40 and 41 were computed from equations (9) and (14) through (17) using data given in table 2. Corresponding apparent molal Gibbs free energies of formation (table 29 and figs. 42 and 43) were then calculated from equations (3) and (8) using data in table 2, values of $A - A_{\text{triple}}$ computed from equations (14) through (17), and specific volumes calculated from equation (19). For pressures greater than a kilobar, apparent molal Gibbs free energies of formation were computed from

$$\Delta G_{P,T} = \Delta G_{P=1000,T} + \left(\int_{P=1000}^P V dP \right)_T \quad (73)$$

with the aid of equation (21), which can be integrated for region 1 in figure 3 to give

$$\begin{aligned} \left(\int_{P=1000}^P V dP \right)_T &= \sum_{i=0}^8 \left(\hat{a}_{i0} t^i \ln (P^*/1000) \right. \\ &\quad \left. - \sum_{j=1}^{8-i} \hat{a}_{ij} t^i (P^{*-j} - (1000)^{-j/j}) \right) \\ &+ \sum_{i=0}^9 \left(a_{i0} t^i \ln (P/P^*) + \sum_{j=1}^{9-i} a_{ij} t^i (P^j - P^{*j})/j \right) \end{aligned} \quad (74)$$

where a_{ij} designates the array of fit coefficients for region 1 (table 5), \hat{a}_{ij} stands for the array of fit coefficients for region 2 (designated as a_{ij} in table 6), and $P^* = 1000$ bars for temperatures $\leq 410^{\circ}\text{C}$ but corresponds to the upper pressure limit of region 2 in figure 3 for $410^{\circ}\text{C} \leq t < 800^{\circ}\text{C}$ where $P^* = 1300 + 1.22449(t - 410)$. For pressures and temperature in region 2 of figure 3, a_{ij} in equation (74) is set to zero and P^* is replaced by P . Values of ΔA at pressures above a kilobar were computed from

$$\begin{aligned} \Delta A_{P,T} &= \Delta A_{P=1000,T} + (\Delta G_{P,T} - \Delta G_{P=1000,T}) \\ &\quad - PV_{P,T} + 1000V_{P=1000,T} \end{aligned} \quad (75)$$

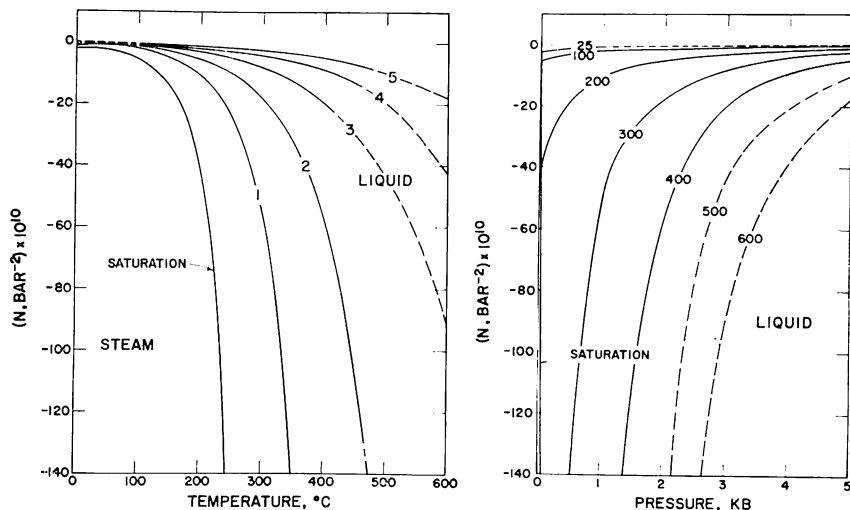


Fig. 36. Dependence of N (table 26) on temperature at constant pressure (labeled in kb) and pressure at constant temperature (labeled in °C) computed from equation (69) and values of ε , $(\partial \ln \varepsilon / \partial P)_T$ and $(\partial^2 \ln \varepsilon / \partial P^2)_T$ in tables 15, 16, and 18.

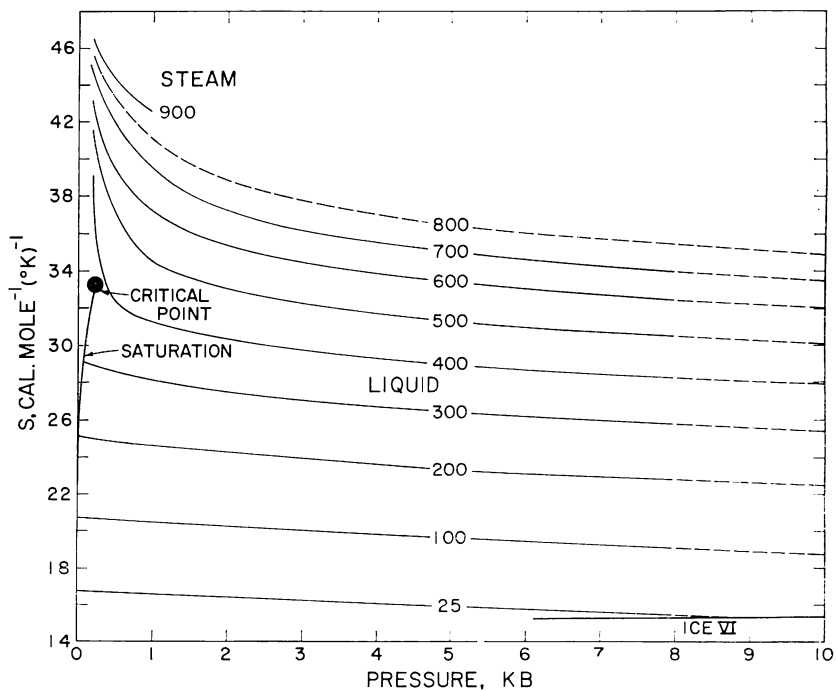


Fig. 37. Third law molal entropy (table 27) as a function of pressure at constant temperature (labeled in °C) computed from equations (19) through (21), (25), (33), and (70) through (72), data in table 2, and coefficients in tables 4, 5, 6, 9, and 10.

The results of the free energy calculations are summarized in tables 28 and 29 and figures 40 through 45. Estimated uncertainties in the values given in tables 28 and 29 for pressures > a kilobar are of the order of 0.1 percent or less.

As indicated above, the Gibbs free energies of H₂O calculated by Burnham, Holloway, and Davis (1969b) are not consistent with those computed in this study, which also differ from those reported by Pistorius and Sharp (1960, 1961). The latter authors referred their values to the internal energy of an ideal gas at absolute zero. Burnham, Holloway, and Davis used equation (4) to calculate Gibbs free energies for pressures below a kilobar from values of H and S given by Bain (1964), which are actually equal to H - H_{triple} and S - S_{triple}, respectively. The Gibbs free energy values reported by Burnham, Holloway, and Davis thus contravene the third law properties of H₂O in other compilations by requiring

$$G - G_{triple} = H - H_{triple} - T(S - S_{triple}) . \quad (76)$$

Equation (76) is valid only if temperature is held constant or S_{triple} = 0, which is the convention (S_{triple} = G_{triple} = 0) adopted by Bain in accord

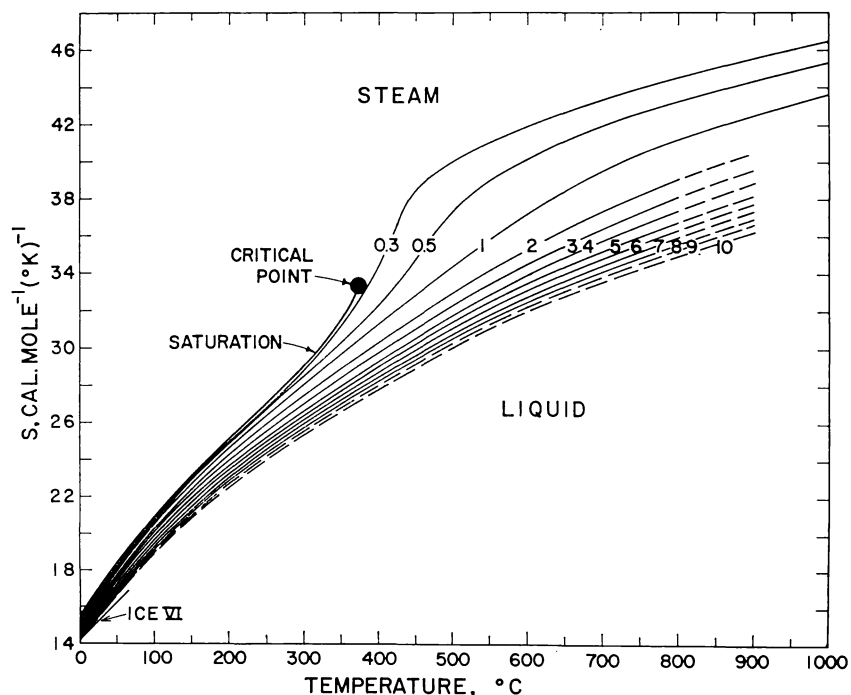


Fig. 38. Third law molal entropy (table 27) as a function of temperature at constant pressure (labeled in kb) computed from equations (19) through (21), (25), (33), and (70) through (72), data in table 2, and coefficients in tables 4, 5, 6, 9, and 10.

with the 5th International Conference on the Properties of Steam. Burnham, Holloway, and Davis then used equation (73) to compute Gibbs free energies of H₂O at higher pressures. The Gibbs free energies computed in this study differ from those given by Burnham, Holloway, and Davis by $\Delta G_{triple} - S_{triple} (T - T_{tr})$.

It can be seen in figure 40 that the apparent molal Helmholtz free energy of formation of H₂O is relatively insensitive to isothermal changes in pressure compared to its Gibbs counterpart (fig. 42), except in the steam phase region where the two variables decrease rapidly with decreasing pressure and approach each other at low pressures. At high pressures, both ΔG and ΔA approach linear functions of pressure at constant temperature, but as temperature increases at constant pressure, ΔA becomes increasingly more sensitive to pressure than ΔG (figs. 41 and 43). At 900°C, an increase in pressure from 1 to 10 kb causes a change of more than 7 kcal mole⁻¹ in ΔG compared to <5 kcal mole⁻¹ in ΔA ; in contrast, at 30°C the same pressure change results in ~ 3.5 kcal mole⁻¹ of change in ΔG but < 0.5 kcal mole⁻¹ in ΔA . Isopleths for these two functions are shown in figures 44 and 45 where $(\partial P/\partial T)_A$ (which is equal to $(S + PV_\alpha)/PV\beta$) can be compared with $(\partial P/\partial T)_G$ (that is, S/V), which is considerably more positive throughout the pressure-temperature range considered.

ACTIVITY AND FUGACITY

The activity (a) of H₂O is defined as

$$a = f/f^\circ \quad (77)$$

where f° stands for the fugacity of H₂O in the standard state (which is specified at 1 bar). The fugacity of H₂O is related to its pressure by

$$f = \chi P \quad (78)$$

where χ is the fugacity coefficient. Taking account of the relation,

$$\ln a = \frac{G - G^\circ}{RT} \quad (79)$$

it follows that

$$\left(\frac{\partial \ln a}{\partial P} \right)_T = \left(\frac{\partial \ln f}{\partial P} \right)_T = \frac{V}{RT} \quad (80)$$

and we can write

$$\left(\frac{\partial \ln \chi}{\partial P} \right)_T = \frac{V}{RT} - \frac{1}{P} \quad (81)$$

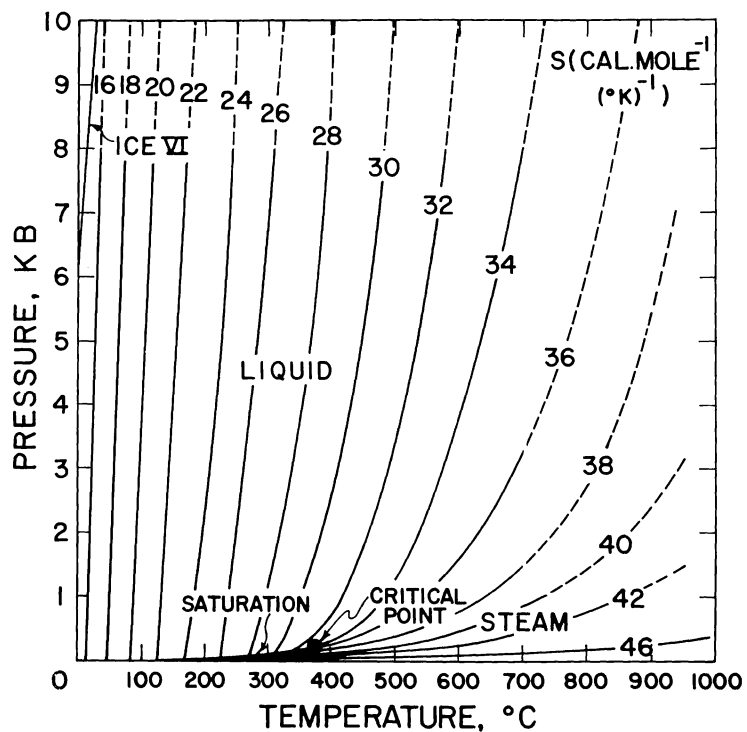


Fig. 39. Isentropes (labeled in $\text{cal mole}^{-1} (\text{°K})^{-1}$) as a function of temperature and pressure (table 27 and figs. 37 and 38).

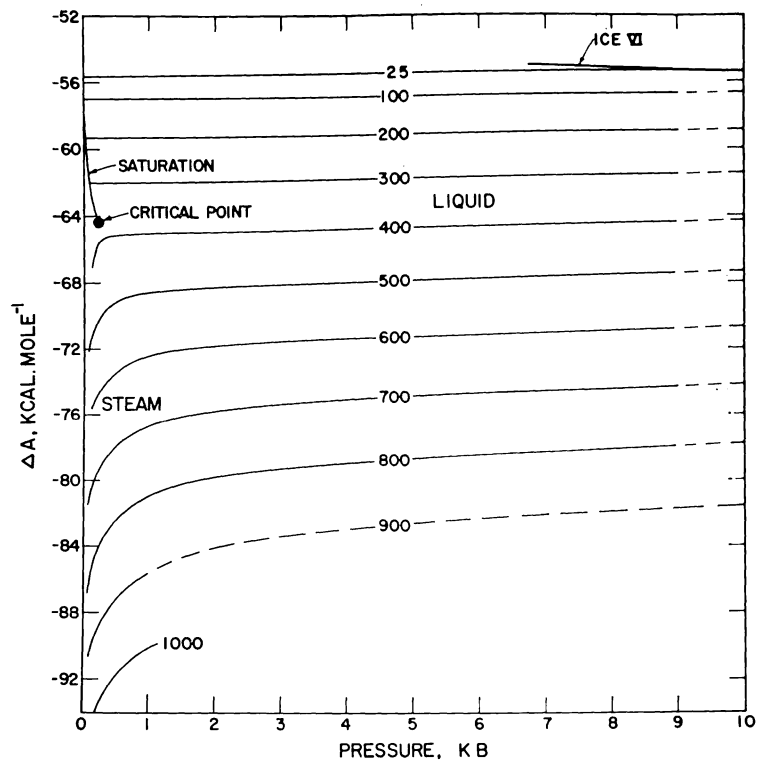


Fig. 40. Apparent molal Helmholtz free energy of formation (table 28) as a function of pressure at constant temperature (labeled in $^{\circ}\text{C}$) computed from equations (3), (8), (9), (14) through (17), (19), (20), and (73) through (75), data in table 2, and coefficients in tables 4, 5, and 6.

Hence, for a given temperature,

$$\ln \chi = \int_0^P \left(\frac{V}{RT} - \frac{1}{P} \right) dP = \int_0^P (z - 1) d \ln P \quad (82)$$

where z is the compressibility factor defined by

$$z = PV/RT \quad (83)$$

For pressures \leq a kilobar, the fugacity coefficient of H_2O can be computed by first rearranging equation (19) as

$$z - 1 = \rho Q + \rho^2 \left(\frac{\partial Q}{\partial \rho} \right)_T \quad (84)$$

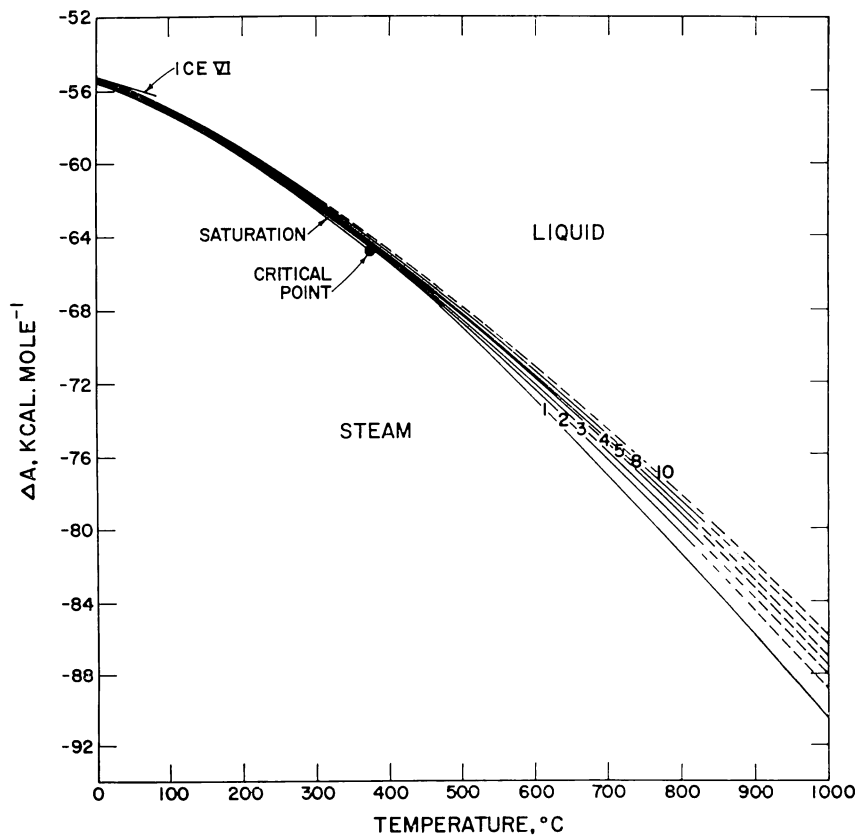


Fig. 41. Apparent molal Helmholtz free energy of formation (table 28) as a function of temperature at constant pressure (labeled in kb) computed from equations (3), (8), (9), (14) through (17), (19), (20), and (73) through (75), data in table 2, and coefficients in tables 4, 5, and 6.

TABLE 28
Apparent molal Helmholtz free energy of formation (ΔA)
in kcal mole⁻¹ computed from equations (3), (8), (9), (14) through (17),
and (73) through (75), data in table 2, and values of V in table 3—
see figures 40, 41, and 44

t (°C)	PRESSURE, KB										
	SAT	0.5	1	2	3	4	5	6	7	8	9
25	-55.812	-55.809	-55.804	-55.78	-55.76	-55.73	-55.69	-55.66	-55.62	-55.58	-55.54
50	-56.248	-56.246	-56.240	-56.22	-56.19	-56.16	-56.13	-56.09	-56.06	-56.02	-55.98
75	-56.719	-56.717	-56.711	-56.69	-56.66	-56.63	-56.60	-56.56	-56.52	-56.48	-56.44
100	-57.222	-57.220	-57.213	-57.19	-57.17	-57.13	-57.10	-57.06	-57.02	-56.98	-56.94
125	-57.756	-57.754	-57.747	-57.72	-57.69	-57.66	-57.63	-57.59	-57.54	-57.50	-57.46
150	-58.319	-58.316	-58.308	-58.28	-58.25	-58.22	-58.18	-58.14	-58.09	-58.05	-58.01
175	-58.909	-58.905	-58.897	-58.87	-58.83	-58.80	-58.76	-58.71	-58.67	-58.62	-58.58
200	-59.526	-59.521	-59.511	-59.48	-59.44	-59.40	-59.36	-59.31	-59.26	-59.22	-59.17
225	-60.168	-60.162	-60.150	-60.12	-60.07	-60.03	-59.98	-59.93	-59.88	-59.83	-59.78
250	-60.835	-60.828	-60.814	-60.78	-60.73	-60.68	-60.63	-60.58	-60.52	-60.47	-60.42
275	-61.528	-61.518	-61.500	-61.46	-61.40	-61.35	-61.29	-61.24	-61.18	-61.13	-61.07
300	-62.246	-62.233	-62.210	-62.16	-62.10	-62.04	-61.98	-61.92	-61.86	-61.81	-61.74
325	-62.994	-62.973	-62.943	-62.88	-62.82	-62.75	-62.69	-62.62	-62.56	-62.50	-62.44
350	-63.776	-63.740	-63.699	-63.63	-63.55	-63.48	-63.41	-63.34	-63.28	-63.21	-63.14
375		-64.537	-64.479	-64.39	-64.31	-64.23	-64.15	-64.08	-64.01	-63.94	-63.87
400		-65.370	-65.283	-65.17	-65.08	-64.99	-64.91	-64.83	-64.75	-64.68	-64.60
425		-66.253	-66.112	-65.98	-65.87	-65.77	-65.68	-65.58	-65.52	-65.44	-65.36
450		-67.211	-66.969	-66.80	-66.68	-66.57	-66.47	-66.38	-66.30	-66.21	-66.13
475		-68.249	-67.853	-67.64	-67.50	-67.38	-67.28	-67.18	-67.09	-67.00	-66.91
500		-69.325	-68.766	-68.50	-68.35	-68.21	-68.10	-67.99	-67.90	-67.80	-67.70
525		-70.411	-69.708	-69.38	-69.20	-69.06	-68.93	-68.82	-68.72	-68.61	-68.51
550		-71.502	-70.679	-70.28	-70.08	-69.92	-69.78	-69.66	-69.55	-69.44	-69.33
575		-72.597	-71.676	-71.20	-70.97	-70.79	-70.65	-70.52	-70.40	-70.28	-70.17
600		-73.697	-72.694	-72.14	-71.87	-71.68	-71.52	-71.39	-71.26	-71.14	-71.02
625		-74.803	-73.731	-73.08	-72.79	-72.58	-72.41	-72.27	-72.13	-72.00	-71.87
650		-75.914	-74.781	-74.05	-73.72	-73.49	-73.31	-73.16	-73.01	-72.88	-72.74
675		-77.031	-75.845	-75.03	-74.67	-74.42	-74.22	-74.06	-73.91	-73.76	-73.62
700		-78.154	-76.911	-76.03	-75.63	-75.36	-75.15	-74.97	-74.81	-74.66	-74.51
725		-79.283	-78.001	-77.04	-76.60	-76.30	-76.08	-75.90	-75.73	-75.57	-75.41
750		-80.418	-79.092	-78.06	-77.58	-77.27	-77.03	-76.83	-76.65	-76.49	-76.32
775		-81.558	-80.191	-79.09	-78.57	-78.24	-77.99	-77.78	-77.59	-77.41	-77.24
800		-82.705	-81.298	-80.13	-79.58	-79.22	-78.95	-78.73	-78.54	-78.35	-78.17
825		-83.857	-82.411								
850		-85.014	-83.530								
875		-86.177	-84.656								
900		-87.346	-85.788								

which can be combined with equation (82) to give

$$\ln \chi_{P,T} = \int_0^P \left(\rho Q + \rho^2 \left(\frac{\partial Q}{\partial \rho} \right)_T \right) d \ln P \quad (85)$$

The integral on the right side of equation (85) differs insignificantly from the corresponding integral for $P = 0.001$ to $P = 1$, which yields the values of $\chi_{1 \text{ bar}}$ shown in table 25. Below 100°C, the values of $\chi_{1 \text{ bar}}$ in table 30 correspond to those of metastable steam.

For the standard state adopted in this study, the fugacity coefficient of H₂O at 1 bar is related to the apparent molal Gibbs free energy of H₂O in the standard state (ΔG°) by³

$$\Delta G^\circ = \Delta G_{1 \text{ bar}} - RT \ln \chi_{1 \text{ bar}} \quad (86)$$

³The values of $\Delta G_{1 \text{ bar}}$ and $\chi_{1 \text{ bar}}$ in tables 29 and 31, respectively, are consistent with $\Delta G_{f, 25^\circ, 1 \text{ bar}}^\circ = 54,642$ cal mole⁻¹, which corresponds to the standard Gibbs free energy of formation of H₂O_{gas} from its elements in their stable form at 25°C and 1 bar. The value of $\Delta G_{f, 25^\circ, 1 \text{ bar}}^\circ$ computed in this study compares favorably with that given by Wagman and others (1968), who report $-54,634$ cal mole⁻¹.

which permits calculation of the fugacity and fugacity coefficient of H_2O at higher pressures from equations (78) and (79). Values of f and χ computed in this manner (tables 30 and 31) are in close agreement with corresponding values given by Burnham, Holloway, and Davis (1969b), Haas (1970), and Anderson (1964, 1967). Estimated uncertainties in the values of f and χ given in tables 30 and 31 are of the order of 1 percent or less.

The fugacity of H_2O is plotted in figures 46 and 47, where it can be seen that H_2O exhibits relatively large negative departures from ideality at low temperatures and pressures which diminish with increasing pressure and temperature toward line A' in figure 48. At pressures and temperatures along this line, H_2O behaves as an ideal supercritical phase, but at higher pressures and temperatures it exhibits positive departures from ideality which increase with increasing pressure and temperature. Although not shown in figure 48, line A' reverses its trend at higher temperatures and swings back toward the steam phase region at low pressures and high temperatures, where H_2O behaves as an ideal gas.

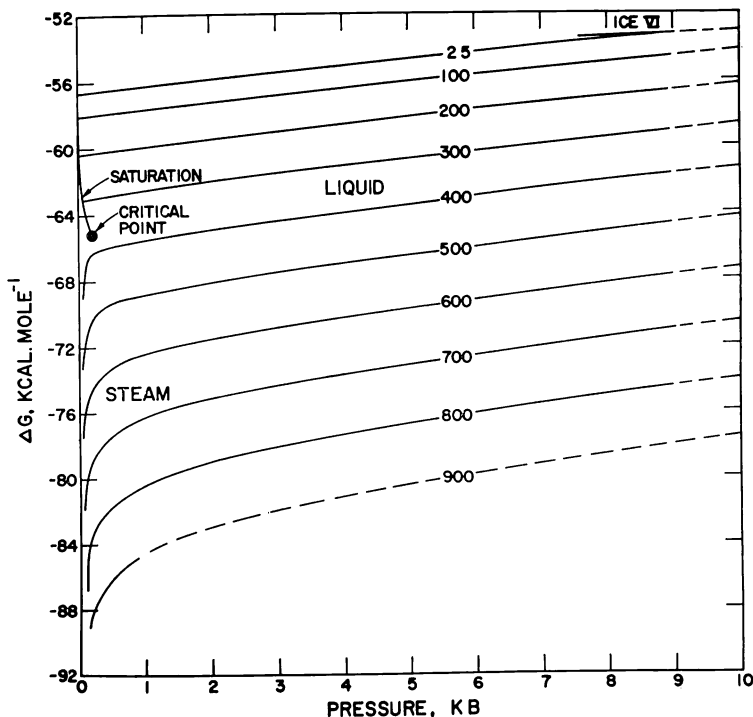


Fig. 42. Apparent molal Gibbs free energy of formation (table 29) as a function of pressure at constant temperature (labeled in $^{\circ}\text{C}$) computed from equations (3), (8), (9), (14) through (17), (19), (20), (73), and (74), data in table 2, and coefficients in tables 4, 5, and 6.

INTERNAL ENERGY AND ENTHALPY

The apparent molal internal energies of formation of H₂O (ΔE) given in table 32 and plotted in figures 49 and 50 were computed from

$$\Delta E = \Delta E_{triple} + (\Delta A - \Delta A_{triple}) + TS - T_{tr} S_{triple} \quad (87)$$

using data in table 2 and the values of S and ΔA computed above. Corresponding values of the apparent molal enthalpy of formation of H₂O (table 33) were then calculated in a similar manner from

$$\Delta H = \Delta H_{triple} + (\Delta E - \Delta E_{triple}) + PV - P_{tr} V_{triple} \quad (88)$$

It can be seen in figure 49 that $(\partial\Delta E/\partial P)_T$ is negative throughout the pressure-temperature region considered ($(\partial\Delta E/\partial P)_T = V(P\beta - T\alpha)$), which

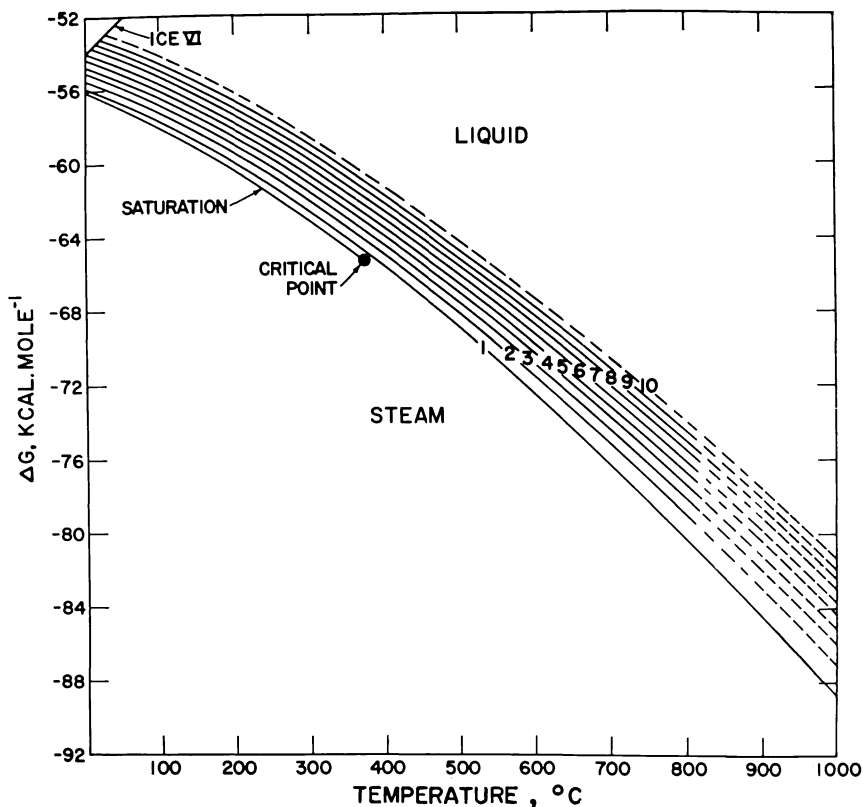


Fig. 43. Apparent molal Gibbs free energy of formation (table 29) as a function of temperature at constant pressure (labeled in kb) computed from equations (3), (8), (9), (14) through (17), (19), (20), (73), and (74), data in table 2, and coefficients in tables 4, 5, and 6.

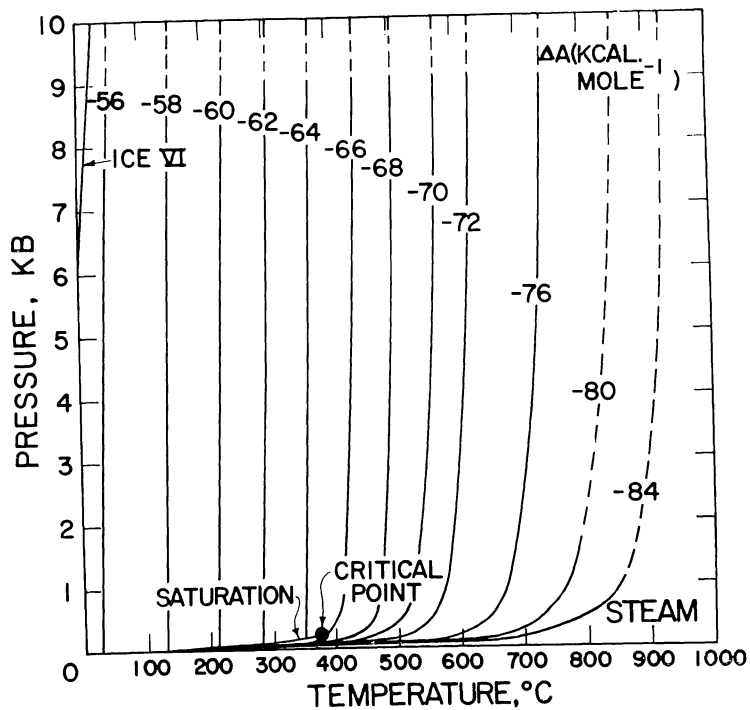


Fig. 44. Isopleths of the apparent molal Helmholtz free energy of formation (labeled in kcal mole⁻¹) as a function of temperature and pressure (table 28 and figs. 40 and 41).

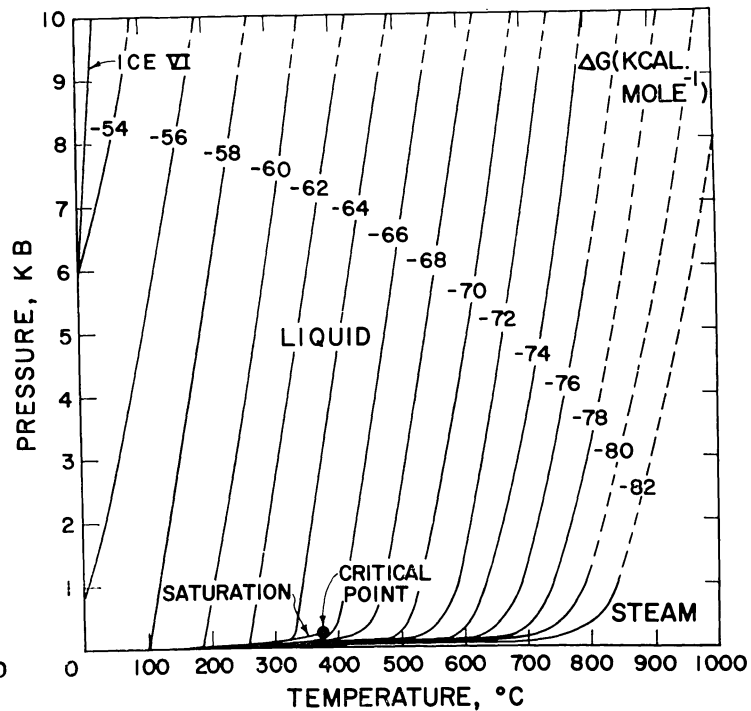


Fig. 45. Isopleths of the apparent molal Gibbs free energy of formation (labeled in kcal mole⁻¹) as a function of temperature and pressure (table 29 and figs. 42 and 43).

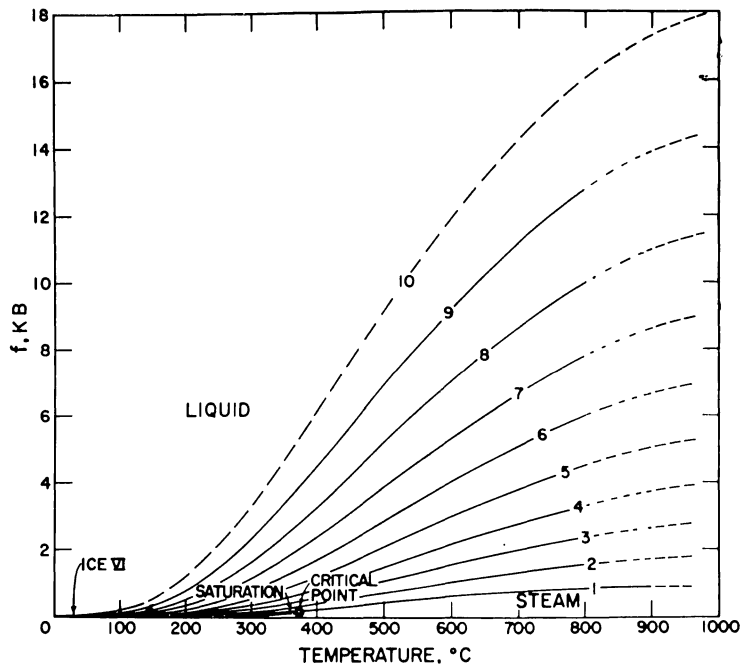


Fig. 46. Fugacity (table 31) as a function of temperature at constant pressure (labeled in kb) computed from equation (78) and the fugacity coefficients in table 30.

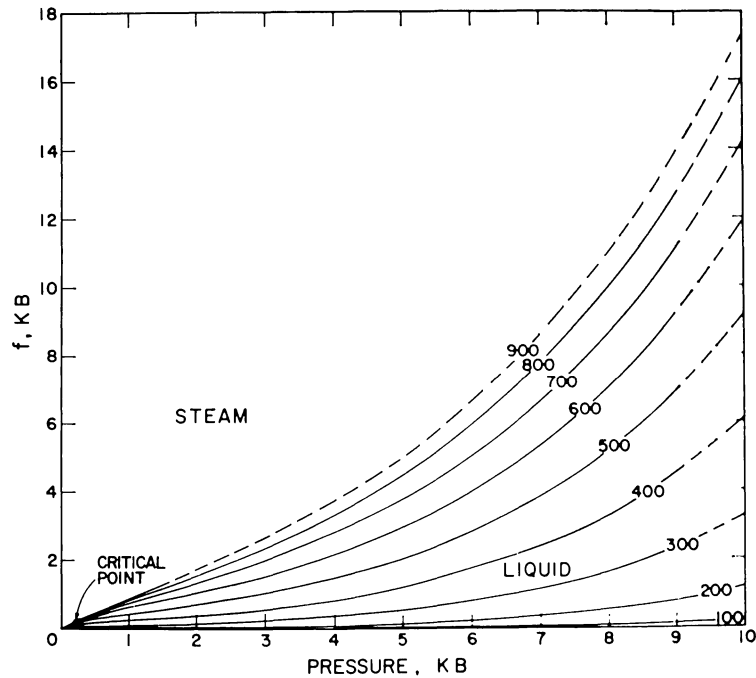


Fig. 47. Fugacity (table 31) as a function of pressure at constant temperature (labeled in kb) computed from equation (78) and the fugacity coefficients in table 30.

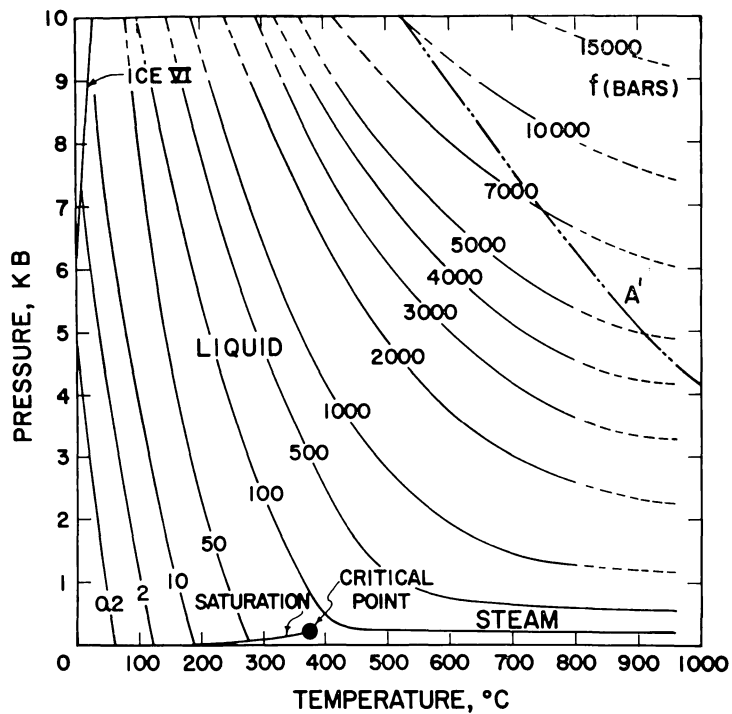


Fig. 48. Isopleths of fugacity (labeled in bars) as a function of temperature and pressure (table 31 and figs. 46 and 47).

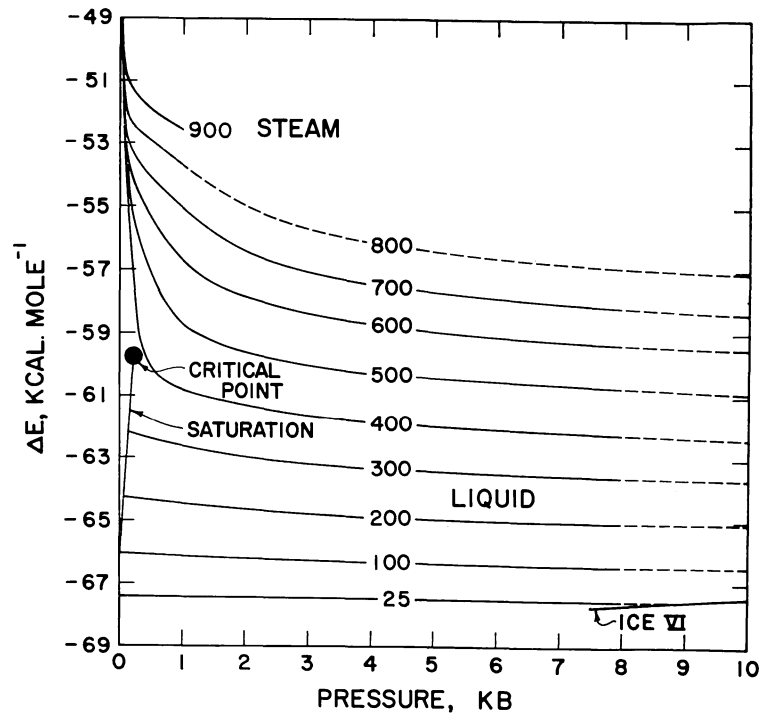


Fig. 49. Apparent molal internal energy of formation (table 32) as a function of pressure at constant temperature (labeled in °C) computed from equation (87), data in table 2, and the values of S and ΔA in tables 27 and 28 and figures 37, 38, 40, and 41.

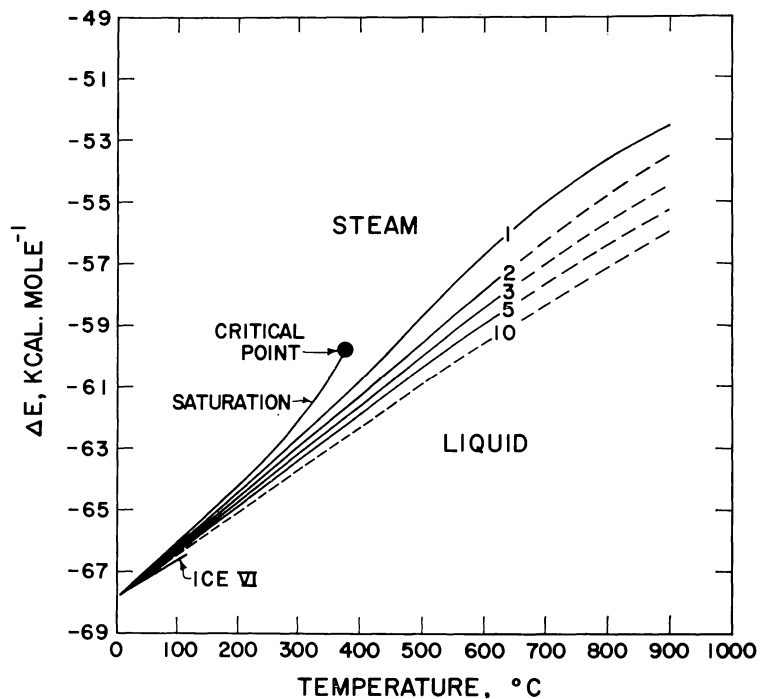


Fig. 50. Apparent molal internal energy of formation (table 32) as a function of temperature at constant pressure (labeled in kb) computed from equation (87), data in table 2, and the values of S and ΔA in tables 27 and 28 and figures 37, 38, 40, and 41.

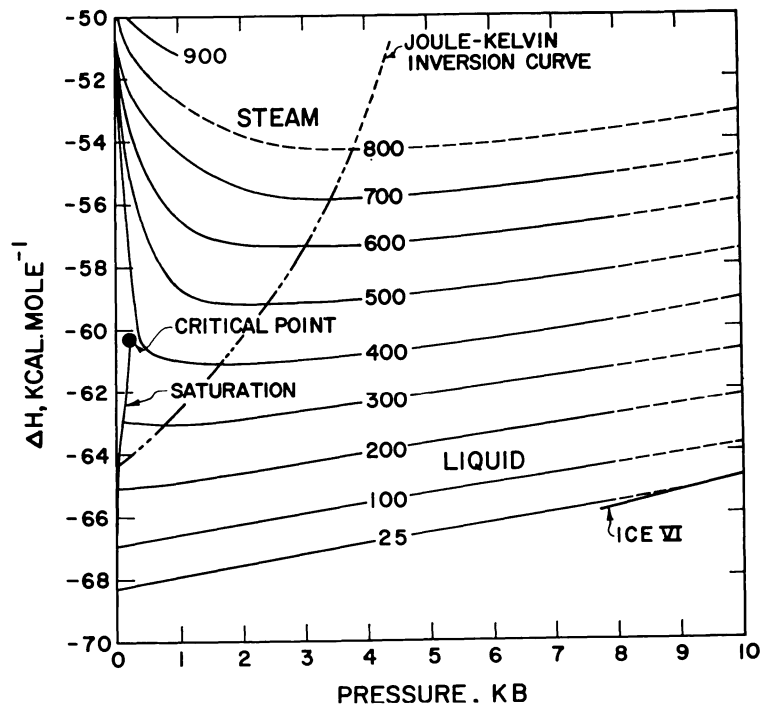


Fig. 51. Apparent molal enthalpy of formation (table 33) as a function of pressure at constant temperature (labeled in °C) computed from equation (88), data in table 2, and the values of V and ΔE in tables 3 and 32 and figures 1, 2, 49, and 50.

In contrast, the analogous curves for ΔE in figure 53 have positive slopes ($(\partial P/\partial T)_E = - (C_P - PV\alpha)/(PV\beta - TV\alpha)$) at all the pressures and temperatures considered. Taking account of the difference in units and conventions, the values of ΔH and ΔE computed in this study are closely consistent with the enthalpies and internal energies reported by Keenan and others (1969) and Burnham, Holloway, and Davis (1969b). Estimated uncertainties in the values of ΔH and ΔE given in tables 32 and 33 for pressures $>$ a kilobar are of the order of 0.2 percent or less.

HEAT CAPACITY

The heat capacity of H_2O at constant volume (C_V) or pressure (C_P) can be computed by first taking the partial derivative of equation (70) with respect to temperature at constant density, which leads to

$$\begin{aligned} C_V &= \left(\frac{\partial \Delta E}{\partial T} \right)_\rho = T \left(\frac{\partial S}{\partial T} \right)_\rho = -T \left(\frac{\partial^2 \psi}{\partial T^2} \right)_\rho \\ &= -T \left(\frac{\partial^2 \psi_0}{\partial T^2} \right)_\rho - 2RT\rho \left(\frac{\partial Q}{\partial T} \right)_\rho - RT^2\rho \left(\frac{\partial^2 Q}{\partial T^2} \right)_\rho \end{aligned} \quad (89)$$

where $(\partial Q/\partial T)_\rho$, $(\partial^2 Q/\partial T^2)_\rho$, and $(\partial^2 \psi_0/\partial T^2)$ refer to the partial derivatives of equations (15) and (16) numbered (A-43), (A-44), and (A-49) in the appendix. The heat capacity at constant volume is related to the heat capacity at constant pressure by

$$C_P = \left(\frac{\partial \Delta H}{\partial T} \right)_P = T \left(\frac{\partial S}{\partial T} \right)_P = C_V + \frac{\alpha^2 VT}{\beta}, \quad (90)$$

which was used together with equation (89) and the values of V , α , and β computed above to calculate the heat capacities given in tables 34 and 35 and those plotted in figures 55 and 56 for pressures \leq a kilobar. The values of C_P in the tables and diagrams for pressures above a kilobar were computed from

$$\begin{aligned} C_{P,T} &= C_{P=1000,T} - T \left(\int_{P=1000}^P \left(\frac{\partial^2 V}{\partial T^2} \right)_P dP \right)_T \\ &= C_{P=1000,T} - T \left(\int_{P=1000}^P V \left(\alpha^2 + \left(\frac{\partial \alpha}{\partial T} \right)_P \right) dP \right)_T \end{aligned} \quad (91)$$

which follows by partial differentiation of equation (80). The integral on the right side of equation (91) was evaluated for region A in figure 9 with the aid of equations (21), (33), and (37) and an equal-interval numerical integration routine adapted from Arden and Astill (1970). Corresponding calculations for regions B and C were carried out by first

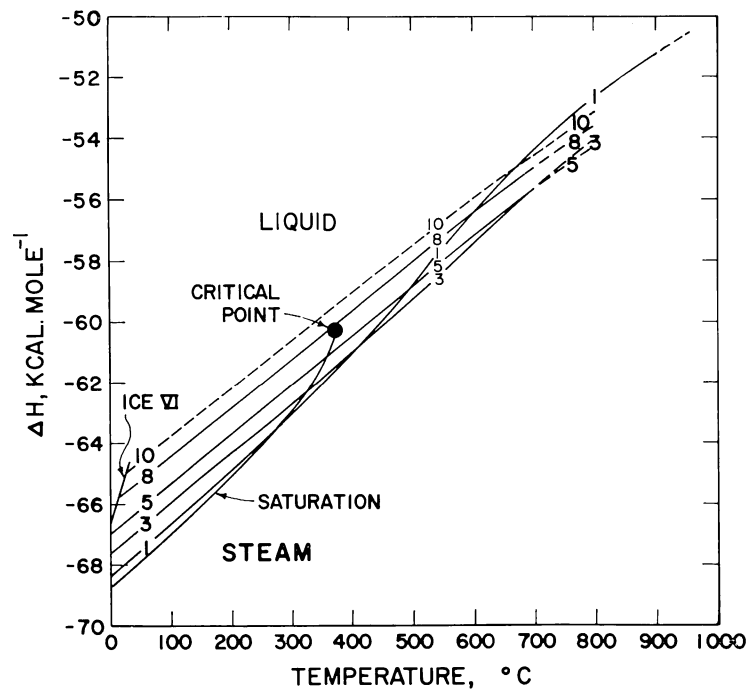


Fig. 52. Apparent molal enthalpy of formation (table 33) as a function of temperature at constant pressure (labeled in kb) computed from equation (88), data in table 2, and the values of V and ΔE in tables 3 and 32 and figures 1, 2, 49, and 50.

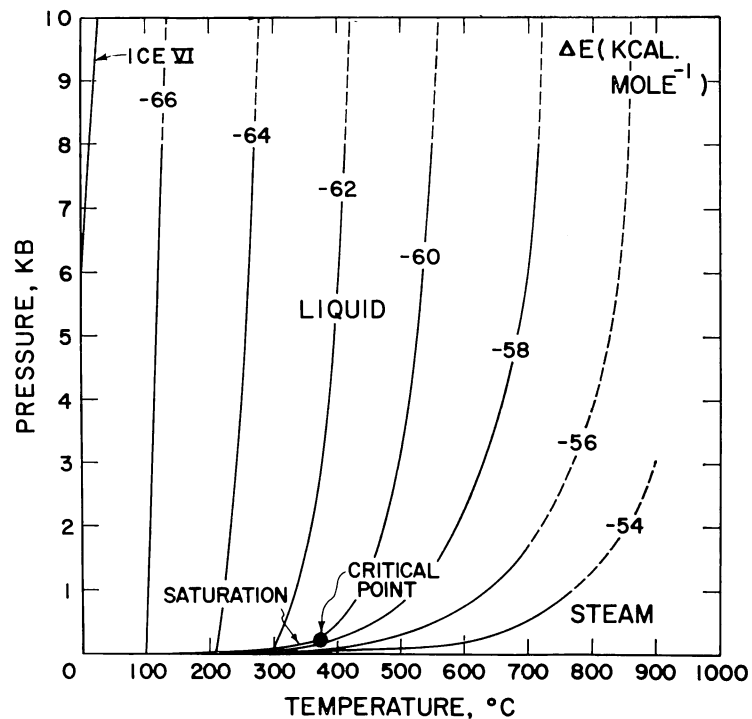


Fig. 53. Isopleths of the apparent molal internal energy of formation (labeled in kcal mole⁻¹) as a function of pressure and temperature (table 32 and figs. 49 and 50).

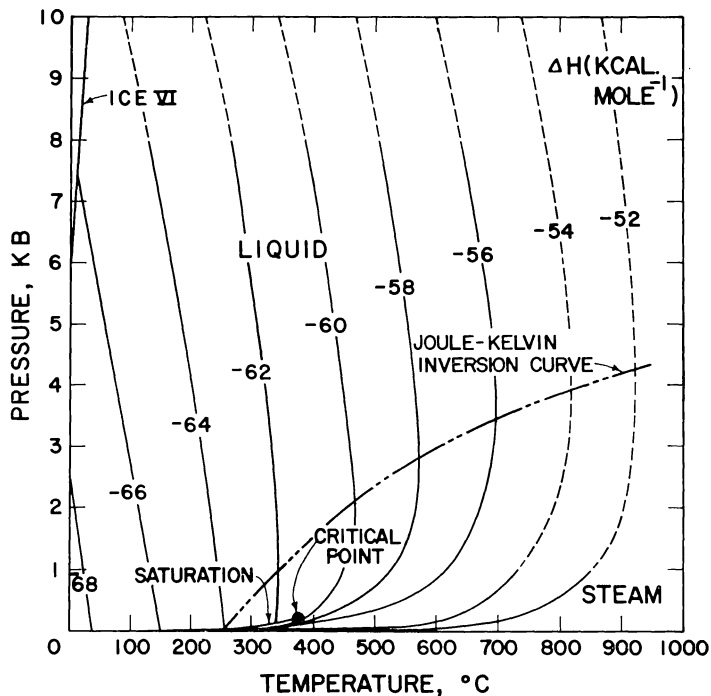


Fig. 54. Isenthalps (labeled in kcal mole⁻¹) as a function of pressure and temperature (table 33 and figs. 51 and 52).

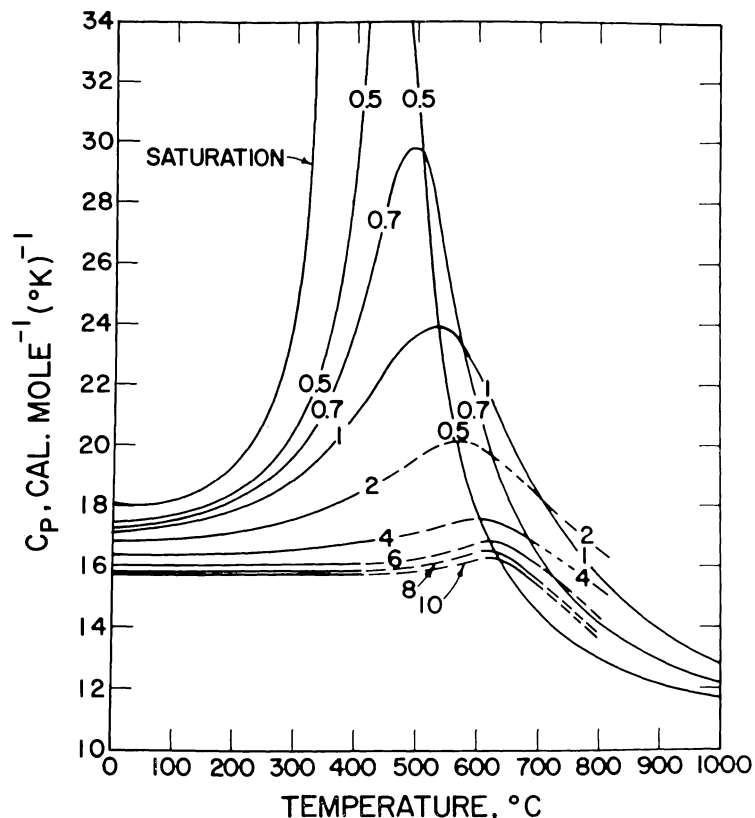


Fig. 55. Isobaric molal heat capacity (table 34) as a function of temperature at constant pressure (labeled in kilobars) computed from equations (19) through (21), (25), (27), (33), (37), (43), and (89) through (93) and coefficients in tables 4, 5, 6, 9, and 10 (solid curves). The dashed curves from 400° to 600°C represent graphic interpolation across the boundary between regions A and B in figure 9 (see text).

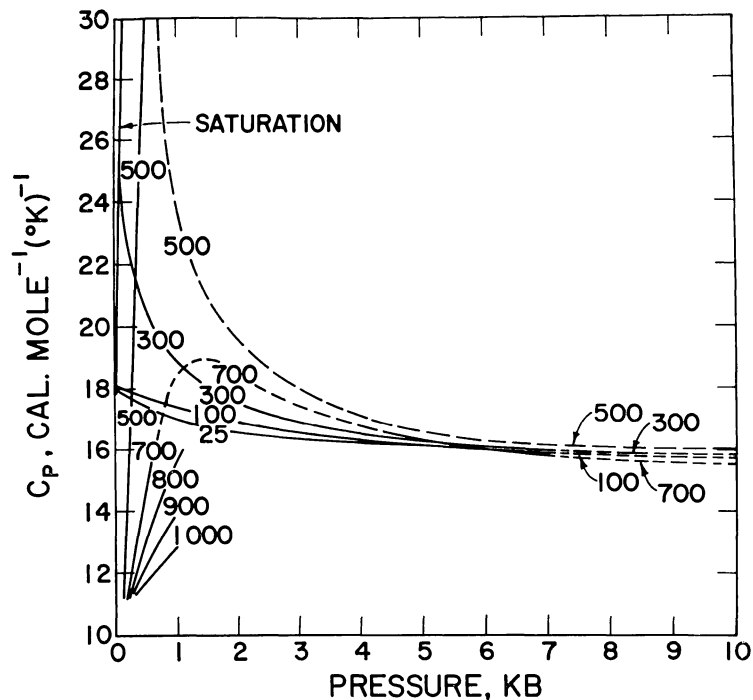


Fig. 56. Isobaric molal heat capacity (table 34) as a function of pressure at constant temperature (labeled in °C) computed from equations (19) through (21), (25), (27), (33), (37), (43), and (89) through (93) and coefficients in tables 4, 5, 6, 9, and 10 (solid curves). The dashed curve for 500°C represents graphic interpolation across the boundary between regions A and B in figure 9 (see text).

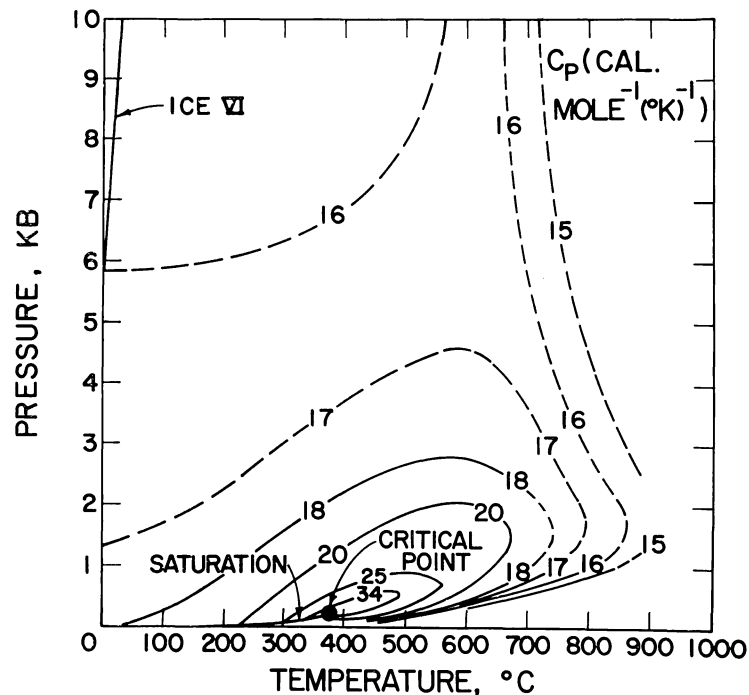


Fig. 57. Isoleths of the isobaric molal heat capacity (labeled in cal mole⁻¹ (°K)⁻¹) as a function of pressure and temperature (table 34 and figs. 55 and 56).

sensitivity of C_P to errors in $(\partial\alpha/\partial T)_P$ calculated from equation (37). Inter-regional discrepancies in the computed values of this derivative at the boundary separating regions A and B in figure 9 also preclude calculation of accurate values of C_P in the temperature interval $\sim 450^\circ$ to 550°C above a kilobar. The values of C_P given for this interval in table 29 were obtained by graphic interpolation of the dashed segments of the curves in figure 55. The heat capacities computed in this study for pressures $>$ a kilobar compare favorably with those reported by Jřza, Kmoniček, and řifner (1966) and Třdheide (1972).

Owing to the drastic effect of the critical phenomenon on the heat capacity of H_2O , the isobars in figure 55 exhibit extrema that dampen progressively and shift to higher temperatures as pressure increases from the critical point (where $C_P = \infty$). The amplitude of the extrema in the isobars for pressures $>$ 5 kb is $<$ 1 cal mole $^{-1}$ ($^\circ\text{K}$) $^{-1}$ (fig. 55), but at high temperatures C_P decreases rapidly with increasing temperature at all (constant) pressures. It is apparent in figure 56 that the high-temperature

TABLE 32
Apparent molal internal energy of formation (ΔE) in kcal mole $^{-1}$
computed from equation (87), data in table 2, and values of ΔA
in table 28—see figures 49, 50, and 53

t ($^\circ\text{C}$)	PRESSURE, KB									
	SAT	0.5	1	2	3	4	5	6	7	8
25	-67.436	-67.452	-67.466	-67.5	-67.5	-67.5	-67.5	-67.6	-67.6	(-67.6)
50	-66.986	-67.016	-67.041	-67.1	-67.1	-67.1	-67.2	-67.2	-67.2	(-67.2)
75	-66.536	-66.579	-66.614	-66.7	-66.7	-66.8	-66.8	-66.8	-66.8	(-66.8)
100	-66.084	-66.140	-66.186	-66.3	-66.3	-66.3	-66.4	-66.4	-66.5	(-66.5)
125	-65.628	-65.700	-65.758	-65.8	-65.9	-66.0	-66.0	-66.1	-66.1	(-66.1)
150	-65.168	-65.257	-65.329	-65.4	-65.5	-65.6	-65.6	-65.7	-65.7	(-65.8)
175	-64.701	-64.810	-64.897	-65.0	-65.1	-65.2	-65.3	-65.3	-65.4	(-65.4)
200	-64.225	-64.358	-64.463	-64.6	-64.7	-64.8	-64.9	-64.9	-65.0	(-65.0)
225	-63.738	-63.900	-64.025	-64.2	-64.3	-64.4	-64.5	-64.6	-64.6	(-64.7)
250	-63.236	-63.435	-63.584	-63.8	-63.9	-64.0	-64.1	-64.2	-64.3	(-64.3)
275	-62.711	-62.959	-63.138	-63.4	-63.5	-63.7	-63.8	-63.8	-63.9	(-64.0)
300	-62.152	-62.468	-62.688	-63.0	-63.1	-63.3	-63.4	-63.5	-63.5	(-63.6)
325	-61.539	-61.956	-62.231	-62.6	-62.8	-62.9	-63.0	-63.1	-63.2	(-63.2)
350	-60.818	-61.415	-61.766	-62.1	-62.4	-62.5	-62.7	-62.7	-62.8	(-62.9)
375		-60.832	-61.289	-61.7	-62.0	-62.1	-62.3	-62.4	-62.5	(-62.5)
400		-60.189	-60.800	-61.3	-61.6	-61.8	-61.9	-62.0	-62.1	(-62.2)
425		-59.450	-60.300	-60.9	-61.2	-61.4	-61.5	-61.7	-61.8	(-61.8)
450		-58.589	-59.788	-60.5	-60.8	-61.0	-61.2	-61.3	-61.4	(-61.5)
475		-57.724	-59.268	-60.0	-60.4	-60.6	-60.8	-61.0	-61.1	(-61.2)
500		-57.013	-58.743	-59.6	-60.0	-60.3	-60.5	-60.6	-60.7	(-60.8)
525		-56.453	-58.218	-59.2	-59.7	-59.9	-60.1	-60.3	-60.4	(-60.5)
550		-55.988	-57.702	-58.8	-59.3	-59.6	-59.8	-59.9	-60.1	(-60.2)
575		-55.584	-57.201	-58.5	-59.0	-59.3	-59.5	-59.7	-59.8	(-59.9)
600		-55.220	-56.724	-58.0	-58.6	-58.9	-59.1	-59.3	-59.4	(-59.6)
625		-54.884	-56.273	-57.6	-58.2	-58.5	-58.8	-58.9	-59.1	(-59.2)
650		-54.567	-55.848	-57.2	-57.8	-58.1	-58.4	-58.6	-58.7	(-58.9)
675		-54.266	-55.446	-56.8	-57.4	-57.8	-58.0	-58.2	-58.4	(-58.5)
700		-53.978	-55.066	-56.4	-57.0	-57.4	-57.7	-57.9	-58.0	(-58.2)
725		-53.698	-54.704	(-56.0)	(-56.7)	(-57.0)	(-57.3)	(-57.5)	(-57.7)	(-57.8)
750		-53.427	-54.359	(-55.6)	(-56.3)	(-56.7)	(-57.0)	(-57.2)	(-57.4)	(-57.5)
775		-53.163	-54.029	(-55.3)	(-55.9)	(-56.4)	(-56.7)	(-56.9)	(-57.0)	(-57.2)
800		-52.904	-53.711	(-54.9)	(-55.6)	(-56.0)	(-56.3)	(-56.5)	(-56.8)	(-56.9)
825		-52.650	-53.405							
850		-52.401	-53.108							
875		-52.155	-52.820							
900		-51.912	-52.541							

isotherms maximize between 1 and 2 kb. The relations shown in figures 55 and 56 lead to the configuration of isopleths depicted in figure 57, where it can be seen that the isopleths ring the "infinite peak" of the critical point in an elongated pattern.

SUMMARY OF THE PROPERTIES OF $\text{H}_2\text{O}_{\text{liquid}}$ AT SATURATION

The thermodynamic and electrostatic properties of steam-saturated liquid H_2O at closely spaced intervals from 0° to 350°C are given in tables 36 through 40. The numerical data in these tables were computed in the manner described above. The values of P , V , ΔE , ΔH , and S correspond (after unit and convention conversion) to those given by Keenan and others (1969). The fugacities and fugacity coefficients shown in the tables are in close agreement with those computed by Haas (1970), as are the values of α and β with those calculated for 1 atm by Kell (1967). The heat capacities are in accord with Schmidt's (1969) tabulation, and the values of the dielectric constant are consistent with those given by Oshry

TABLE 33
Apparent molal enthalpy of formation (ΔH) in kcal mole⁻¹
computed from equation (88), data in table 2, and values of ΔE
in table 32—see figures 51, 52, and 54

t (°C)	PRESSURE, KB									
	SAT	0.5	1	2	3	4	5	6	7	8
25	-68.315	-68.119	-67.930	-67.6	-67.2	-66.9	-66.5	-66.2	-65.9	(-65.6)
50	-67.865	-67.681	-67.501	-67.1	-66.8	-66.5	-66.1	-65.8	-65.5	(-65.2)
75	-67.415	-67.241	-67.069	-66.7	-66.4	-66.1	-65.7	-65.4	-65.1	(-64.8)
100	-66.962	-66.799	-66.635	-66.3	-66.0	-65.7	-65.3	-65.0	-64.7	(-64.4)
125	-66.506	-66.355	-66.199	-65.9	-65.6	-65.2	-64.9	-64.6	-64.3	(-64.0)
150	-66.044	-65.907	-65.761	-65.5	-65.1	-64.8	-64.5	-64.2	-63.9	(-63.6)
175	-65.575	-65.455	-65.320	-65.0	-64.7	-64.4	-64.1	-63.8	-63.5	(-63.2)
200	-65.096	-64.997	-64.875	-64.6	-64.3	-64.0	-63.7	-63.4	-63.1	(-62.8)
225	-64.604	-64.532	-64.426	-64.2	-63.9	-63.6	-63.3	-63.0	-62.7	(-62.4)
250	-64.093	-64.058	-63.971	-63.7	-63.5	-63.2	-62.9	-62.6	-62.3	(-62.0)
275	-63.556	-63.572	-63.512	-63.3	-63.1	-62.8	-62.5	-62.2	-61.9	(-61.6)
300	-62.979	-63.070	-63.045	-62.9	-62.6	-62.4	-62.1	-61.8	-61.5	(-61.2)
325	-62.338	-62.544	-62.569	-62.4	-62.2	-62.0	-61.7	-61.4	-61.1	(-60.8)
350	-61.573	-61.984	-62.081	-62.0	-61.8	-61.5	-61.3	-61.0	-60.7	(-60.4)
375		-61.375	-61.579	-61.5	-61.4	-61.1	-60.9	-60.6	-60.3	(-60.0)
400		-60.695	-61.059	-61.1	-60.9	-60.7	-60.5	-60.2	-59.9	(-59.6)
425		-59.896	-60.522	-60.6	-60.5	-60.3	-60.1	-59.8	-59.5	(-59.3)
450		-58.932	-59.966	-60.2	-60.1	-59.9	-59.7	-59.4	-59.1	(-58.9)
475		-57.919	-59.394	-59.7	-59.7	-59.5	-59.3	-59.0	-58.8	(-58.5)
500		-57.054	-58.808	-59.3	-59.2	-59.1	-58.9	-58.6	-58.4	(-58.1)
525		-56.354	-58.211	-58.8	-58.8	-58.7	-58.5	-58.3	-58.0	(-57.8)
550		-55.765	-57.613	-58.3	-58.4	-58.3	-58.1	-57.9	-57.6	(-57.4)
575		-55.249	-57.024	-57.9	-58.0	-58.0	-57.8	-57.6	-57.3	(-57.1)
600		-54.783	-56.453	-57.5	-57.6	-57.5	-57.3	-57.1	-56.9	(-56.8)
625		-54.352	-55.906	-57.0	-57.1	-57.1	-57.0	-56.7	-56.5	(-56.3)
650		-53.947	-55.385	-56.5	-56.7	-56.6	-56.5	-56.3	-56.1	(-55.9)
675		-53.562	-54.890	-56.0	-56.2	-56.2	-56.1	-55.9	-55.7	(-55.4)
700		-53.193	-54.418	-55.5	-55.8	-55.8	-55.7	-55.5	-55.3	(-55.0)
725		-52.837	-53.967	(-55.1)	(-55.4)	(-55.4)	(-55.3)	(-55.1)	(-54.9)	(-54.7)
750		-52.492	-53.536	(-54.6)	(-54.9)	(-55.0)	(-54.9)	(-54.7)	(-54.5)	(-54.3)
775		-52.157	-53.121	(-54.2)	(-54.5)	(-54.6)	(-54.5)	(-54.3)	(-54.2)	(-53.9)
800		-51.829	-52.722	(-53.8)	(-54.1)	(-54.2)	(-54.1)	(-54.0)	(-53.8)	(-53.6)
825		-51.508	-52.337							
850		-51.193	-51.963							
875		-50.883	-51.601							
900		-50.577	-51.248							

(ms) and Owen and others (1961). In contrast, the logarithmic partial derivatives of ϵ in table 36 differ from those computed for 1 atm by Owen and others, who derived their values by regressing dielectric constant data from 0° to 70°C and 1 to 1000 bars with a quadratic power function of temperature and pressure. The partial derivatives of $\ln \epsilon$ in table 36 also differ somewhat from the estimates computed by Sen and Cobble (1974).

CONCLUDING REMARKS

The equations presented above permit calculation of a large number of thermodynamic/electrostatic properties of H₂O in addition to those discussed in the foregoing pages. Owing to space limitations, many of these could not be included in this summary, but some are the subject of the following communication (Helgeson and Kirkham, 1974a). The calculations make it possible to predict the consequences of geochemical

TABLE 34
Isobaric molal heat capacity (C_p) in cal mole⁻¹ (°K)⁻¹ computed from equations (89) through (93) and values of V , α , β , and $(\partial\alpha/\partial T)_P$ in tables 3, 7, 8, and 13—see figures 55 through 57

t (°C)	PRESSURE, KB									
	SAT	0.5	1	2	3	4	5	6	7	8
25	18.01	17.46	17.09	16.7	16.5	16.3	16.2	16.2	16.2	(16.2)
50	17.99	17.56	17.24	16.8	16.5	16.3	16.2	16.1	16.1	(16.0)
75	18.05	17.65	17.35	16.9	16.6	16.4	16.2	16.1	16.0	(15.9)
100	18.15	17.72	17.39	16.9	16.6	16.3	16.1	16.0	15.9	(15.8)
125	18.32	17.83	17.46	16.9	16.6	16.3	16.1	16.0	15.9	(15.8)
150	18.57	17.99	17.57	17.0	16.6	16.3	16.1	16.0	15.9	(15.8)
175	18.90	18.20	17.72	17.1	16.7	16.4	16.2	16.0	15.9	(15.8)
200	19.35	18.45	17.89	17.1	16.7	16.4	16.2	16.0	15.9	(15.8)
225	19.97	18.76	18.07	17.2	16.7	16.4	16.2	16.1	15.9	(15.9)
250	20.89	19.16	18.27	17.3	16.8	16.4	16.2	16.1	16.0	(15.9)
275	22.34	19.72	18.52	17.4	16.8	16.5	16.2	16.1	15.9	(15.9)
300	24.78	20.51	18.84	17.5	16.9	16.5	16.2	16.1	15.9	(15.9)
325	29.52	21.65	19.26	17.7	17.0	16.5	16.3	16.1	16.0	(15.9)
350	43.45	23.25	19.79	17.9	17.1	16.6	16.3	16.1	16.0	(15.9)
375		25.57	20.43	18.1	17.2	16.7	16.4	16.1	16.0	(15.9)
400		29.18	21.13	18.3	17.3	16.7	16.3	16.1	15.9	(15.8)
425		35.15	21.86	(18.6)	(17.6)	(16.8)	(16.4)	(16.1)	(16.0)	(15.8)
450		41.20	22.56	(18.9)	(17.8)	(16.9)	(16.4)	(16.1)	(16.0)	(15.9)
475		38.26	23.19	(19.2)	(18.0)	(17.0)	(16.5)	(16.2)	(16.1)	(15.9)
500		30.98	23.70	(19.6)	(18.2)	(17.1)	(16.6)	(16.2)	(16.1)	(16.0)
525		25.46	23.96	(19.9)	(18.5)	(17.2)	(16.8)	(16.3)	(16.2)	(16.1)
550		21.89	23.83	(20.1)	(18.8)	(17.4)	(17.0)	(16.4)	(16.3)	(16.2)
575		19.52	23.26	(20.2)	(19.0)	(17.5)	(17.1)	(16.5)	(16.4)	(16.3)
600		17.88	22.38	(19.7)	(18.2)	(17.5)	(17.1)	(16.8)	(16.6)	(16.5)
625		16.68	21.36	(19.6)	(18.2)	(17.5)	(17.1)	(16.8)	(16.6)	(16.5)
650		15.77	20.32	(19.3)	(18.0)	(17.3)	(16.9)	(16.7)	(16.5)	(16.4)
675		15.05	19.33	(18.8)	(17.7)	(17.1)	(16.7)	(16.4)	(16.2)	(16.1)
700		14.47	18.43	(18.3)	(17.4)	(16.8)	(16.4)	(16.1)	(15.8)	(15.6)
725		14.00	17.63							
750		13.60	16.90							
775		13.26	16.26							
800		12.97	15.69							
825		12.72	15.17							
850		12.50	14.71							
875		12.32	14.30							
900		12.16	13.93							

reactions among minerals and aqueous electrolyte solutions at high pressures and temperatures (Helgeson and Kirkham, 1975a and b). The tables afford numerical values for such predictions, and the diagrams facilitate correlation of the thermodynamic/electrostatic behavior of H₂O with geologic observations and theoretical models of geochemical processes.

ACKNOWLEDGMENTS

During the course of this study, many people contributed helpful suggestions, discussion, programming expertise, and critical comment, but we are especially indebted to Philippe Lehot. We are also grateful to Professor J. H. Keenan and his colleagues for permission to program and publish calculations based on equation (14), to C. W. Burnham and A. J. Ellis for critical reviews of the manuscript, and to Scott Cornelius, Robin Reid, John Dalton, Yoshi Hidaka, Richard Weiss, David Bice, Robert

TABLE 35
Isochoric molal heat capacity (C_v) in cal mole⁻¹ (°K)⁻¹ computed from equation (89) and the values of V in table 3

t (°C)	PRESSURE, KB										
	SAT	100	200	300	400	500	600	700	800	900	1000
25	17.83	17.67	17.53	17.40	17.27	17.16	17.05	16.95	16.69	16.77	16.86
50	17.31	17.20	17.09	17.00	16.90	16.82	16.74	16.66	16.46	16.52	16.59
75	16.78	16.70	16.62	16.55	16.48	16.41	16.35	16.29	16.13	16.18	16.24
100	16.25	16.18	16.12	16.06	16.00	15.95	15.90	15.85	15.70	15.75	15.80
125	15.74	15.67	15.62	15.56	15.51	15.46	15.42	15.37	15.23	15.28	15.33
150	15.25	15.19	15.14	15.09	15.04	15.00	14.96	14.91	14.78	14.83	14.87
175	14.80	14.74	14.69	14.65	14.61	14.57	14.53	14.49	14.37	14.41	14.45
200	14.39	14.34	14.29	14.25	14.21	14.18	14.15	14.12	14.01	14.05	14.08
225	14.04	13.99	13.93	13.89	13.86	13.83	13.81	13.78	13.70	13.73	13.76
250	13.73	13.68	13.62	13.57	13.54	13.52	13.50	13.49	13.44	13.45	13.47
275	13.50	13.44	13.35	13.29	13.26	13.24	13.23	13.22	13.20	13.21	13.21
300	13.35	13.32	13.14	13.05	13.01	12.98	12.98	12.98	12.99	12.99	12.98
325	13.39	13.53	13.06	12.87	12.78	12.75	12.74	12.75	12.80	12.78	12.76
350	13.82	10.00	13.34	12.80	12.61	12.54	12.52	12.53	12.61	12.58	12.55
375		9.12	14.65	13.06	12.54	12.37	12.32	12.32	12.43	12.39	12.35
400		8.61	11.62	14.85	12.66	12.26	12.14	12.12	12.24	12.19	12.15
425		8.30	10.25	12.91	13.04	12.23	11.99	11.93	12.06	11.99	11.95
450		8.12	9.50	11.17	12.43	12.16	11.85	11.75	11.87	11.80	11.75
475		8.02	9.07	10.24	11.31	11.74	11.65	11.56	11.68	11.61	11.56
500		7.96	8.80	9.70	10.55	11.13	11.33	11.35	11.50	11.43	11.37
525		7.94	8.65	9.37	10.07	10.63	10.96	11.11	11.33	11.25	11.18
550		7.93	8.55	9.17	9.77	10.28	10.65	10.87	11.18	11.09	10.99
575		7.94	8.49	9.04	9.57	10.04	10.40	10.66	11.03	10.94	10.82
600		7.96	8.46	8.96	9.43	9.86	10.22	10.48	10.90	10.80	10.67
625		7.99	8.44	8.89	9.33	9.73	10.07	10.34	10.78	10.67	10.53
650		8.02	8.43	8.85	9.25	9.63	9.95	10.21	10.66	10.55	10.40
675		8.05	8.43	8.81	9.19	9.54	9.84	10.09	10.55	10.43	10.28
700		8.09	8.43	8.79	9.13	9.45	9.74	9.98	10.43	10.31	10.17
725		8.13	8.44	8.76	9.08	9.38	9.64	9.87	10.30	10.19	10.05
750		8.18	8.45	8.75	9.03	9.31	9.55	9.76	10.17	10.07	9.93
775		8.22	8.47	8.73	8.99	9.24	9.46	9.66	10.04	9.94	9.81
800		8.27	8.49	8.72	8.96	9.18	9.38	9.55	9.91	9.82	9.70
825		8.32	8.51	8.71	8.92	9.12	9.30	9.46	9.78	9.69	9.59
850		8.37	8.53	8.71	8.89	9.07	9.22	9.36	9.64	9.57	9.48
875		8.42	8.56	8.71	8.87	9.02	9.15	9.27	9.52	9.45	9.37
900		8.47	8.59	8.72	8.85	8.97	9.09	9.19	9.39	9.34	9.27

TABLE 36
Summary of the electrostatic properties of steam-saturated H₂O_{liquid}

$\frac{a}{t}$	$\frac{b}{P}$	$\frac{c}{V}$	$\frac{d}{\alpha}$ $\times 10^5$	$\frac{e}{\beta}$ $\times 10^6$	$\frac{f}{(\partial\beta/\partial P)_T}$ $\times 10^9$	$\frac{g}{(\partial\beta/\partial T)_P}$ $\times 10^9$	$\frac{h}{(\partial\alpha/\partial T)_P}$ $\times 10^8$
0	0.006	18.0194	-5.46	50.67	-11.93	-247.17	1320.85
5	0.009	18.0175	1.30	49.48	-14.48	-252.51	1362.61
10	0.012	18.0217	8.01	48.26	-15.57	-230.02	1310.78
15	0.017	18.0318	14.35	47.19	-15.89	-196.16	1219.72
20	0.023	18.0474	20.19	46.33	-15.87	-159.55	1118.08
25	0.032	18.0681	25.53	45.60	-15.66	-123.83	1019.58
30	0.042	18.0934	30.40	45.06	-15.44	-90.81	930.14
35	0.056	18.1230	34.85	44.69	-15.27	-60.85	851.81
40	0.074	18.1564	38.94	44.46	-15.16	-33.73	784.79
45	0.096	18.1935	42.72	44.35	-15.12	-9.13	728.42
50	0.123	18.2340	46.24	44.36	-15.17	13.32	681.71
55	0.158	18.2777	49.55	44.48	-15.30	34.02	643.55
60	0.199	18.3245	52.69	44.69	-15.52	53.28	612.84
65	0.250	18.3742	55.69	45.01	-15.82	71.42	588.57
70	0.312	18.4267	58.58	45.41	-16.20	88.68	569.80
75	0.386	18.4820	61.39	45.89	-16.66	105.28	555.69
80	0.474	18.5400	64.14	46.46	-17.20	121.40	545.51
85	0.578	18.6008	66.85	47.10	-17.83	137.22	538.64
90	0.701	18.6642	69.53	47.82	-18.53	152.90	534.53
95	0.845	18.7303	72.20	48.62	-19.32	168.57	532.73
100	1.013	18.7991	74.86	49.50	-20.20	184.37	532.88
105	1.208	18.8707	77.52	50.46	-21.18	200.44	534.66
110	1.433	18.9450	80.20	51.50	-22.26	216.90	537.87
115	1.691	19.0222	82.89	52.62	-23.44	233.88	542.32
120	1.985	19.1022	85.61	53.83	-24.75	251.51	547.92
125	2.321	19.1851	88.36	55.12	-26.18	269.95	554.60
130	2.701	19.2710	91.14	56.51	-27.75	289.32	562.35
135	3.130	19.3599	93.96	57.99	-29.47	309.78	571.21
140	3.613	19.4519	96.82	59.58	-31.36	331.52	581.25
145	4.154	19.5470	99.74	61.28	-33.43	354.70	592.59
150	4.758	19.6455	102.71	63.09	-35.71	379.53	605.37
155	5.431	19.7473	105.75	65.03	-38.22	406.23	619.76
160	6.178	19.8525	108.85	67.10	-40.99	435.06	635.97
165	7.004	19.9613	112.04	69.32	-44.05	466.28	654.25
170	7.916	20.0738	115.32	71.69	-47.43	500.22	674.86
175	8.920	20.1901	118.70	74.24	-51.18	537.23	698.09
180	10.021	20.3104	122.19	76.96	-55.35	577.72	724.30
185	11.226	20.4347	125.81	79.89	-60.00	622.15	753.84
190	12.543	20.5634	129.58	83.04	-65.19	671.06	787.13
195	13.978	20.6966	133.51	86.43	-71.02	725.08	824.63
200	15.537	20.8344	137.62	90.09	-77.56	784.91	866.87
225	25.476	21.6039	161.75	113.48	-126.08	1206.73	1172.77
250	39.728	22.5416	195.13	149.96	-225.07	1996.44	1736.78
275	59.415	23.7224	245.37	211.54	-458.96	3681.11	2854.08
300	85.805	25.2858	329.48	329.06	-1149.55	8089.35	5470.84
325	120.387	27.5307	499.05	607.65	-4157.99	24748.10	14159.30
350	165.125	31.3508	1038.30	1698.85	-36533.97	174219.75	80781.59

$a^{\circ}\text{C}$, b_{bar} , $c_{\text{cm}^3 \text{ mole}^{-1}}$, $d(^{\circ}\text{K})^{-1}$, $e_{\text{bar}^{-1}}$, $f_{\text{bar}^{-2}}$, $g_{\text{bar}^{-1} (^{\circ}\text{K})^{-1}}$, $h_{(^{\circ}\text{K})^{-2}}$

TABLE 37
Summary of thermodynamic properties of steam-saturated H₂O_{liquid}

$\frac{a}{t}$	$\frac{b}{P}$	$\frac{c}{S}$	$\frac{d}{\Delta A}$	$\frac{d}{\Delta G}$	$\frac{d}{\Delta E}$	$\frac{d}{\Delta H}$
0	0.006	15.13	-55.413	-56.288	-67.888	-68.766
5	0.009	15.46	-55.490	-56.364	-67.797	-68.676
10	0.012	15.78	-55.568	-56.442	-67.707	-68.585
15	0.017	16.10	-55.648	-56.522	-67.616	-68.495
20	0.023	16.41	-55.729	-56.603	-67.526	-68.405
25	0.032	16.71	-55.812	-56.686	-67.436	-68.315
30	0.042	17.01	-55.896	-56.770	-67.346	-68.225
35	0.056	17.31	-55.982	-56.856	-67.256	-68.135
40	0.074	17.60	-56.069	-56.944	-67.166	-68.045
45	0.096	17.88	-56.158	-57.032	-67.076	-67.955
50	0.123	18.16	-56.248	-57.122	-66.986	-67.865
55	0.158	18.44	-56.339	-57.214	-66.896	-67.775
60	0.199	18.71	-56.432	-57.307	-66.806	-67.685
65	0.250	18.98	-56.526	-57.401	-66.716	-67.595
70	0.312	19.24	-56.622	-57.496	-66.626	-67.505
75	0.386	19.50	-56.719	-57.593	-66.536	-67.415
80	0.474	19.76	-56.817	-57.691	-66.446	-67.324
85	0.578	20.02	-56.917	-57.791	-66.355	-67.234
90	0.701	20.27	-57.017	-57.891	-66.265	-67.143
95	0.845	20.51	-57.119	-57.993	-66.174	-67.053
100	1.013	20.76	-57.222	-58.096	-66.084	-66.962
105	1.208	21.00	-57.327	-58.201	-65.993	-66.871
110	1.433	21.24	-57.432	-58.306	-65.902	-66.780
115	1.691	21.48	-57.539	-58.413	-65.811	-66.689
120	1.985	21.71	-57.647	-58.521	-65.720	-66.598
125	2.321	21.94	-57.756	-58.630	-65.628	-66.506
130	2.701	22.17	-57.867	-58.740	-65.537	-66.414
135	3.130	22.40	-57.978	-58.851	-65.445	-66.322
140	3.613	22.62	-58.091	-58.963	-65.353	-66.230
145	4.154	22.84	-58.204	-59.077	-65.260	-66.137
150	4.758	23.06	-58.319	-59.191	-65.168	-66.044
155	5.431	23.28	-58.435	-59.307	-65.075	-65.951
160	6.178	23.50	-58.552	-59.423	-64.982	-65.858
165	7.004	23.71	-58.670	-59.541	-64.888	-65.764
170	7.916	23.92	-58.789	-59.660	-64.795	-65.670
175	8.920	24.14	-58.909	-59.779	-64.701	-65.575
180	10.021	24.34	-59.030	-59.900	-64.606	-65.480
185	11.226	24.55	-59.153	-60.022	-64.511	-65.385
190	12.543	24.76	-59.276	-60.144	-64.416	-65.289
195	13.978	24.96	-59.400	-60.268	-64.321	-65.193
200	15.537	25.17	-59.526	-60.392	-64.225	-65.096
225	25.476	26.17	-60.168	-61.029	-63.738	-64.604
250	39.728	27.16	-60.835	-61.688	-63.236	-64.093
275	59.415	28.14	-61.528	-62.369	-62.711	-63.556
300	85.805	29.14	-62.246	-63.069	-62.152	-62.979
325	120.387	30.20	-62.994	-63.789	-61.539	-62.338
350	165.125	31.40	-63.776	-64.527	-60.818	-61.573

$\frac{a}{t}$ —C. $\frac{b}{P}$ —bar. $\frac{c}{S}$ —cal mole⁻¹(°K)⁻¹. $\frac{d}{\Delta A}$ —kcal mole⁻¹.

TABLE 38
 Summary of thermodynamic properties of steam-saturated $\text{H}_2\text{O}_{\text{liquid}}$

$\frac{a}{t}$	$\frac{b}{P}$	$\frac{c}{\rho}$	$\frac{d}{C_P}$	$\frac{d}{C_V}$	X	$\frac{b}{f}$
0	0.006	0.9998	18.08	18.08	0.9996	0.0061
5	0.009	0.9999	18.10	18.10	1.0004	0.0087
10	0.012	0.9996	18.09	18.07	1.0000	0.0123
15	0.017	0.9991	18.06	18.01	1.0003	0.0171
20	0.023	0.9982	18.03	17.92	0.9995	0.0234
25	0.032	0.9971	18.01	17.83	0.9995	0.0317
30	0.042	0.9957	17.99	17.72	0.9986	0.0424
35	0.056	0.9941	17.98	17.62	0.9985	0.0562
40	0.074	0.9922	17.98	17.52	0.9977	0.0737
45	0.096	0.9902	17.98	17.41	0.9976	0.0957
50	0.123	0.9880	17.99	17.31	0.9968	0.1231
55	0.158	0.9856	17.99	17.20	0.9954	0.1568
60	0.199	0.9831	18.00	17.10	0.9948	0.1984
65	0.250	0.9805	18.02	16.99	0.9937	0.2487
70	0.312	0.9777	18.03	16.89	0.9934	0.3098
75	0.386	0.9747	18.05	16.78	0.9925	0.3829
80	0.474	0.9717	18.06	16.68	0.9911	0.4697
85	0.578	0.9685	18.08	16.57	0.9893	0.5721
90	0.701	0.9652	18.10	16.47	0.9883	0.6932
95	0.845	0.9618	18.13	16.36	0.9869	0.8344
100	1.013	0.9583	18.15	16.25	0.9838	0.9970
105	1.208	0.9547	18.18	16.15	0.9821	1.1865
110	1.433	0.9509	18.21	16.04	0.9801	1.4041
115	1.691	0.9471	18.25	15.94	0.9780	1.6533
120	1.985	0.9431	18.28	15.84	0.9758	1.9371
125	2.321	0.9390	18.32	15.74	0.9732	2.2584
130	2.701	0.9348	18.36	15.64	0.9707	2.6216
135	3.130	0.9305	18.41	15.54	0.9679	3.0295
140	3.613	0.9261	18.46	15.44	0.9650	3.4861
145	4.154	0.9216	18.51	15.34	0.9619	3.9955
150	4.758	0.9170	18.57	15.25	0.9587	4.5615
155	5.431	0.9123	18.63	15.15	0.9552	5.1878
160	6.178	0.9075	18.69	15.06	0.9516	5.8788
165	7.004	0.9025	18.76	14.97	0.9478	6.6388
170	7.916	0.8975	18.83	14.88	0.9439	7.4720
175	8.920	0.8923	18.90	14.80	0.9397	8.3819
180	10.021	0.8870	18.98	14.71	0.9355	9.3742
185	11.226	0.8816	19.06	14.63	0.9310	10.4516
190	12.543	0.8761	19.15	14.55	0.9263	11.6189
195	13.978	0.8704	19.25	14.47	0.9215	12.8806
200	15.537	0.8647	19.35	14.39	0.9165	14.2406
225	25.476	0.8339	19.97	14.04	0.8889	22.6454
250	39.728	0.7992	20.89	13.73	0.8572	34.0550
275	59.415	0.7594	22.34	13.50	0.8221	48.8462
300	85.805	0.7125	24.78	13.35	0.7840	67.2733
325	120.387	0.6544	29.52	13.39	0.7431	89.4572
350	165.125	0.5746	43.45	13.82	0.6990	115.4150

 $\frac{a}{t}$ °C. $\frac{b}{P}$ bar. $\frac{c}{\rho}$ g cm⁻³. $\frac{d}{C_P}$ cal mole⁻¹ (°K)⁻¹.

Turner, Joachim Hampel, David Pitou, and Joan Delany, who assisted at various times with plotting, drafting, and preparation of the manuscript. The work reported here was supported in part by NSF grants GA 25314, GA 36023, and GA 35888 in addition to funds received from the University of California Research Committee, the Anaconda Company, and the Kennecott Copper Corporation. Acknowledgment is also made with thanks to the donors of the Petroleum Research Fund, administered by the American Chemical Society, for support of this research under PRF #5356-AC2. Finally, we would like to express our appreciation to Debbie Aoki for contributing her expert talents in typing and retyping the manuscript.

TABLE 39
Summary of thermodynamic properties of steam-saturated H_2O_{liquid}

t	$\frac{b}{P}$	ϵ	$\frac{c}{\left(\frac{\partial \ln \epsilon}{\partial P}\right)_T}$ $\times 10^5$	$\frac{d}{\left(\frac{\partial \ln \epsilon}{\partial T}\right)_P}$ $\times 10^3$	$\frac{e}{\left(\frac{\partial^2 \ln \epsilon}{\partial P^2}\right)_T}$ $\times 10^9$	$\frac{f}{\left(\frac{\partial^2 \ln \epsilon}{\partial T^2}\right)_P}$ $\times 10^6$	$\frac{g}{\left(\frac{\partial (\partial \ln \epsilon / \partial P)}{\partial T}\right)_P}$ $\times 10^7$	$\frac{h}{\left(\frac{\partial^2 (\partial \ln \epsilon / \partial P)}{\partial T^2}\right)_P}$ $\times 10^8$
0	0.006	87.79	4.72	-4.42	-9.8	-4.79	-0.35	
5	0.009	85.86	4.70	-4.45	-12.6	-5.73	-0.52	-0.13
10	0.012	83.97	4.68	-4.48	-14.1	-5.75	-0.42	3.64
15	0.017	82.10	4.66	-4.50	-14.8	-5.34	-0.19	5.30
20	0.023	80.27	4.66	-4.53	-15.2	-4.74	0.09	5.84
25	0.032	78.47	4.67	-4.55	-15.4	-4.09	0.39	5.85
30	0.042	76.70	4.70	-4.57	-15.6	-3.47	0.67	5.63
35	0.056	74.96	4.74	-4.59	-15.7	-2.89	0.95	5.35
40	0.074	73.26	4.79	-4.60	-16.0	-2.38	1.21	5.08
45	0.096	71.59	4.86	-4.61	-16.3	-1.94	1.46	4.84
50	0.123	69.96	4.94	-4.62	-16.7	-1.57	1.69	4.65
55	0.158	68.36	5.03	-4.63	-17.2	-1.26	1.92	4.51
60	0.199	66.79	5.13	-4.63	-17.7	-1.02	2.15	4.41
65	0.250	65.26	5.24	-4.64	-18.4	-0.82	2.36	4.36
70	0.312	63.77	5.37	-4.64	-19.2	-0.67	2.58	4.34
75	0.386	62.30	5.50	-4.64	-20.1	-0.57	2.80	4.35
80	0.474	60.87	5.64	-4.65	-21.1	-0.51	3.02	4.41
85	0.578	59.48	5.80	-4.65	-22.2	-0.48	3.24	4.49
90	0.701	58.11	5.97	-4.65	-23.5	-0.47	3.47	4.60
95	0.845	56.77	6.15	-4.65	-24.9	-0.50	3.70	4.74
100	1.013	55.47	6.34	-4.66	-26.4	-0.55	3.94	4.91
105	1.208	54.19	6.54	-4.66	-28.1	-0.62	4.19	5.12
110	1.433	52.94	6.76	-4.66	-30.0	-0.71	4.45	5.36
115	1.691	51.73	6.98	-4.67	-32.0	-0.82	4.72	5.63
120	1.985	50.53	7.23	-4.67	-34.2	-0.94	5.01	5.95
125	2.321	49.37	7.48	-4.67	-36.6	-1.08	5.32	6.31
130	2.701	48.23	7.76	-4.68	-39.3	-1.24	5.64	6.72
135	3.130	47.11	8.04	-4.69	-42.3	-1.42	5.98	7.17
140	3.613	46.02	8.35	-4.69	-45.5	-1.62	6.35	7.69
145	4.154	44.96	8.68	-4.70	-49.0	-1.84	6.75	8.27
150	4.758	43.91	9.02	-4.71	-52.9	-2.09	7.17	8.92
155	5.431	42.89	9.39	-4.72	-57.2	-2.37	7.63	9.66
160	6.178	41.89	9.78	-4.73	-62.0	-2.68	8.13	10.48
165	7.004	40.91	10.19	-4.75	-67.3	-3.02	8.66	11.42
170	7.916	39.96	10.63	-4.76	-73.1	-3.41	9.25	12.47
175	8.920	39.02	11.10	-4.78	-79.6	-3.84	9.89	13.66
180	10.021	38.10	11.60	-4.80	-86.8	-4.33	10.59	15.01
185	11.226	37.20	12.14	-4.82	-94.8	-4.87	11.36	16.55
190	12.543	36.32	12.72	-4.85	-103.8	-5.48	12.20	18.30
195	13.978	35.45	13.33	-4.87	-113.9	-6.16	13.14	20.30
200	15.537	34.60	14.00	-4.90	-125.2	-6.91	14.17	22.60
225	25.476	30.58	18.20	-5.12	-209.4	-12.41	21.45	40.78
250	39.728	26.87	24.66	-5.50	-380.9	-22.30	35.00	82.44
275	59.415	23.38	35.40	-6.18	-783.3	-41.38	63.63	196.55
300	85.805	19.99	55.52	-7.42	-1953.8	-84.56	137.25	612.38
325	120.387	16.58	101.95	-10.02	-6917.8	-222.63	407.75	3149.17
350	165.125	12.87	274.99	-18.24	-57594.1	-1232.61	2716.08	45593.00

$\frac{a}{^\circ C}$, $\frac{b}{bar}$, $\frac{c}{bar^{-1}}$, $\frac{d}{(^\circ K)^{-1}}$, $\frac{e}{bar^{-2}}$, $\frac{f}{(^\circ K)^{-2}}$, $\frac{g}{bar^{-1} (^\circ K)^{-1}}$, $\frac{h}{bar^{-1} (^\circ K)^{-2}}$.

TABLE 40
Summary of Born functions (eqs 65 through 69)
for steam-saturated H₂O_{liquid}

$\frac{a}{t}$	$\frac{b}{P}$	$\frac{c}{Y} \times 10^5$	$\frac{d}{X} \times 10^7$	$\frac{e}{Q} \times 10^6$	$\frac{f}{U} \times 10^9$	$\frac{g}{N} \times 10^{10}$
0.00	.006	-5.04	-2.77	0.54	1.98	-1.37
5.00	.009	-5.18	-2.97	0.55	1.83	-1.73
10.00	.012	-5.33	-3.07	0.56	1.99	-1.94
15.00	.017	-5.49	-3.12	0.57	2.33	-2.07
20.00	.023	-5.64	-3.15	0.58	2.75	-2.17
25.00	.032	-5.80	-3.16	0.60	3.20	-2.24
30.00	.042	-5.96	-3.18	0.61	3.68	-2.32
35.00	.056	-6.12	-3.19	0.63	4.17	-2.40
40.00	.074	-6.28	-3.21	0.65	4.66	-2.49
45.00	.096	-6.44	-3.24	0.68	5.16	-2.60
50.00	.123	-6.60	-3.28	0.71	5.68	-2.73
55.00	.158	-6.77	-3.32	0.74	6.22	-2.88
60.00	.199	-6.94	-3.37	0.77	6.77	-3.05
65.00	.250	-7.11	-3.42	0.80	7.35	-3.24
70.00	.312	-7.28	-3.48	0.84	7.95	-3.46
75.00	.386	-7.45	-3.55	0.88	8.59	-3.71
80.00	.474	-7.63	-3.63	0.93	9.27	-3.99
85.00	.578	-7.82	-3.71	0.98	9.98	-4.31
90.00	.701	-8.00	-3.81	1.03	10.74	-4.66
95.00	.845	-8.20	-3.90	1.08	11.55	-5.05
100.00	1.013	-8.39	-4.01	1.14	12.42	-5.49
105.00	1.208	-8.60	-4.12	1.21	13.35	-5.98
110.00	1.433	-8.81	-4.24	1.28	14.36	-6.52
115.00	1.691	-9.02	-4.37	1.35	15.43	-7.13
120.00	1.985	-9.24	-4.50	1.43	16.60	-7.80
125.00	2.321	-9.47	-4.65	1.52	17.86	-8.56
130.00	2.701	-9.71	-4.80	1.61	19.22	-9.40
135.00	3.130	-9.95	-4.97	1.71	20.71	-10.34
140.00	3.613	-10.20	-5.14	1.81	22.32	-11.40
145.00	4.154	-10.46	-5.33	1.93	24.09	-12.58
150.00	4.758	-10.73	-5.53	2.05	26.01	-13.91
155.00	5.431	-11.01	-5.75	2.19	28.13	-15.40
160.00	6.178	-11.30	-5.99	2.33	30.45	-17.08
165.00	7.004	-11.61	-6.25	2.49	33.01	-18.98
170.00	7.916	-11.92	-6.53	2.66	35.83	-21.12
175.00	8.920	-12.25	-6.84	2.85	38.95	-23.55
180.00	10.021	-12.60	-7.18	3.05	42.42	-26.31
185.00	11.226	-12.96	-7.56	3.26	46.27	-29.45
190.00	12.543	-13.34	-7.98	3.50	50.58	-33.03
195.00	13.978	-13.75	-8.44	3.76	55.39	-37.13
200.00	15.537	-14.17	-8.95	4.05	60.80	-41.85
225.00	25.476	-16.75	-12.63	5.95	100.62	-79.30
250.00	39.728	-20.48	-19.57	9.18	180.75	-164.37
275.00	59.415	-26.42	-34.02	15.14	365.68	-388.63
300.00	85.805	-37.09	-69.80	27.77	892.43	-1131.44
325.00	120.387	-60.43	-194.82	61.49	3075.19	-4798.85
350.00	165.125	-141.66	-1215.87	213.62	24995.05	-50615.56

$\frac{a}{^\circ\text{C}}$, $\frac{b}{\text{bar}}$, $\frac{c}{(^\circ\text{K})^{-1}}$, $\frac{d}{(^\circ\text{K})^{-2}}$, $\frac{e}{\text{bar}^{-1}}$, $\frac{f}{\text{bar}^{-1} (^\circ\text{K})^{-1}}$, $\frac{g}{\text{bar}^{-2}}$.

APPENDIX

The partial derivatives of equation (16) can be expressed in simple notation by first writing

$$Q = x \sum_{j=1}^7 y_j z_j \tag{A-1}$$

where

$$x = \tau - \tau_c \tag{A-2}$$

$$y_j = (\tau - \tau_{aj})^{j-2} \tag{A-3}$$

and

$$z_j = u_j + v w_j \tag{A-4}$$

where

$$u_j = \sum_{i=1}^8 \frac{A_{ij}}{i-j} (\rho - \rho_{aj})^{i-1} \tag{A-5}$$

$$v = e^{-4.8\rho} \tag{A-6}$$

and

$$w_j = \sum_{i=9}^{10} \frac{A_{ij}}{i-j} \rho^{i-9} \tag{A-7}$$

It then follows that

$$\left(\frac{\partial Q}{\partial T}\right)_P = \frac{Q}{x} \left(\frac{\partial x}{\partial T}\right)_P + x \sum_{j=1}^7 \left(y_j \left(\frac{\partial z_j}{\partial T}\right)_P + z_j \left(\frac{\partial y_j}{\partial T}\right)_P \right) \tag{A-8}$$

and

$$\begin{aligned} \left(\frac{\partial^2 Q}{\partial T^2}\right)_P &= \frac{Q}{x} \left(\frac{\partial^2 x}{\partial T^2}\right)_P + \frac{2}{x} \left(\frac{\partial x}{\partial T}\right)_P \left(\left(\frac{\partial Q}{\partial T}\right)_P - \frac{Q}{x} \left(\frac{\partial x}{\partial T}\right)_P \right) \\ &+ x \sum_{j=1}^7 \left(y_j \left(\frac{\partial^2 z_j}{\partial T^2}\right)_P + 2 \left(\frac{\partial y_j}{\partial T}\right)_P \left(\frac{\partial z_j}{\partial T}\right)_P + z_j \left(\frac{\partial^2 y_j}{\partial T^2}\right)_P \right) \end{aligned} \tag{A-9}$$

where

$$\left(\frac{\partial x}{\partial T}\right)_P = -\frac{\tau}{T} \tag{A-10}$$

$$\left(\frac{\partial^2 x}{\partial T^2}\right)_P = \frac{2\tau}{T^2}, \quad (\text{A-11})$$

$$\left(\frac{\partial y_j}{\partial T}\right)_P = -\frac{(j-2)\tau y_j}{T(\tau - \tau_{aj})}, \quad (\text{A-12})$$

$$\left(\frac{\partial^2 y_j}{\partial T^2}\right)_P = \frac{1}{y_j} \left(\frac{\partial y_j}{\partial T}\right)_P^2 + \frac{y_j(j-2)\tau(\tau - 2\tau_{aj})}{T^2(\tau - \tau_{aj})^2}, \quad (\text{A-13})$$

$$\left(\frac{\partial z_j}{\partial T}\right)_P = \left(\frac{\partial u_j}{\partial T}\right)_P + v \left(\frac{\partial w_j}{\partial T}\right)_P + \frac{w_j}{z_j} \left(\frac{\partial v}{\partial T}\right)_P, \quad (\text{A-14})$$

and

$$\left(\frac{\partial^2 z_j}{\partial T^2}\right)_P = \left(\frac{\partial^2 u_j}{\partial T^2}\right)_P + v \left(\frac{\partial^2 w_j}{\partial T^2}\right)_P + 2 \left(\frac{\partial v}{\partial T}\right)_P \left(\frac{\partial w_j}{\partial T}\right)_P + \frac{w_j}{z_j} \left(\frac{\partial^2 v}{\partial T^2}\right)_P \quad (\text{A-15})$$

where

$$\left(\frac{\partial u_j}{\partial T}\right)_P = -\alpha \rho \sum_{i=1}^8 (i-1) A_{ij} (\rho - \rho_{aj})^{i-2}, \quad (\text{A-16})$$

$$\begin{aligned} \left(\frac{\partial^2 u_j}{\partial T^2}\right)_P &= \frac{1}{\alpha} \left(\frac{\partial u_j}{\partial T}\right)_P \left(\left(\frac{\partial \alpha}{\partial T}\right)_P - \alpha^2\right) \\ &+ \rho^2 \alpha^2 \sum_{i=1}^8 (i-1)(i-2) A_{ij} (\rho - \rho_{aj})^{i-3}, \end{aligned} \quad (\text{A-17})$$

$$\left(\frac{\partial v}{\partial T}\right)_P = 4.8 \rho \alpha v, \quad (\text{A-18})$$

$$\left(\frac{\partial^2 v}{\partial T^2}\right)_P = 4.8 \left(\rho \alpha \left(\frac{\partial v}{\partial T}\right)_P + \rho v \left(\frac{\partial \alpha}{\partial T}\right)_P - \rho v \alpha^2 \right), \quad (\text{A-19})$$

$$\left(\frac{\partial w_j}{\partial T}\right)_P = -\rho \alpha A_{10j} \quad (\text{A-20})$$

and

$$\left(\frac{\partial^2 w_{\underline{j}}}{\partial T^2}\right)_P = \rho_{\underline{1}0\underline{j}} \left(\alpha^2 - \left(\frac{\partial \alpha}{\partial T}\right)_P\right) \quad (\text{A-21})$$

Similarly, we can write

$$\left(\frac{\partial Q}{\partial \rho}\right)_T = \underline{x} \sum_{\underline{j}=1}^7 \underline{y}_{\underline{j}} \left(\frac{\partial z_{\underline{j}}}{\partial \rho}\right)_T \quad , \quad (\text{A-22})$$

$$\left(\frac{\partial^2 Q}{\partial \rho^2}\right)_T = \underline{x} \sum_{\underline{j}=1}^7 \underline{y}_{\underline{j}} \left(\frac{\partial^2 z_{\underline{j}}}{\partial \rho^2}\right)_T \quad (\text{A-23})$$

and

$$\left(\frac{\partial^3 Q}{\partial \rho^3}\right)_T = \underline{x} \sum_{\underline{j}=1}^7 \underline{y}_{\underline{j}} \left(\frac{\partial^3 z_{\underline{j}}}{\partial \rho^3}\right)_T \quad (\text{A-24})$$

where

$$\left(\frac{\partial z_{\underline{j}}}{\partial \rho}\right)_T = \left(\frac{\partial u_{\underline{j}}}{\partial \rho}\right)_T + \underline{v} \left(\frac{\partial w_{\underline{j}}}{\partial \rho}\right)_T + \underline{w}_{\underline{j}} \left(\frac{\partial v}{\partial \rho}\right)_T \quad , \quad (\text{A-25})$$

$$\left(\frac{\partial^2 z_{\underline{j}}}{\partial \rho^2}\right)_T = \left(\frac{\partial^2 u_{\underline{j}}}{\partial \rho^2}\right)_T + 2 \left(\frac{\partial v}{\partial \rho}\right)_T \left(\frac{\partial w_{\underline{j}}}{\partial \rho}\right)_T + \underline{w}_{\underline{j}} \left(\frac{\partial^2 v}{\partial \rho^2}\right)_T \quad (\text{A-26})$$

and

$$\left(\frac{\partial^3 z_{\underline{j}}}{\partial \rho^3}\right)_T = \left(\frac{\partial^3 u_{\underline{j}}}{\partial \rho^3}\right)_T + 3 \left(\frac{\partial^2 v}{\partial \rho^2}\right)_T \left(\frac{\partial w_{\underline{j}}}{\partial \rho}\right)_T + \underline{w}_{\underline{j}} \left(\frac{\partial^3 v}{\partial \rho^3}\right)_T \quad (\text{A-27})$$

where

$$\left(\frac{\partial u_{\underline{j}}}{\partial \rho}\right)_T = - \frac{1}{\rho \alpha} \left(\frac{\partial u_{\underline{j}}}{\partial T}\right)_P \quad (\text{A-28})$$

$$\left(\frac{\partial^2 u_{\underline{j}}}{\partial \rho^2}\right)_T = \sum_{\underline{i}=1}^8 (\underline{i}-1)(\underline{i}-2) \underline{A}_{\underline{i}\underline{j}} (\rho - \rho_{\underline{a}\underline{j}})^{\underline{i}-3} \quad (\text{A-29})$$

$$\left(\frac{\partial^3 u_{\underline{j}}}{\partial \rho^3}\right)_T = \sum_{\underline{i}=1}^8 (\underline{i}-1)(\underline{i}-2)(\underline{i}-3) \underline{A}_{\underline{i}\underline{j}} (\rho - \rho_{\underline{a}\underline{j}})^{\underline{i}-4} \quad , \quad (\text{A-30})$$

$$\left(\frac{\partial v}{\partial \rho}\right)_T = -4.8v \quad , \quad (A-31)$$

$$\left(\frac{\partial^2 v}{\partial \rho^2}\right)_T = -4.8\left(\frac{\partial v}{\partial \rho}\right)_T \quad , \quad (A-32)$$

$$\left(\frac{\partial^3 v}{\partial \rho^3}\right)_T = -4.8\left(\frac{\partial^2 v}{\partial \rho^2}\right)_T \quad , \quad (A-33)$$

and

$$\left(\frac{\partial w_j}{\partial \rho}\right)_T = A_{10j} \quad . \quad (A-34)$$

By cross partial differentiation it also follows that

$$\left(\frac{\partial\left(\frac{\partial Q}{\partial \rho}\right)}{\partial T}\right)_P = \frac{1}{x} \left(\frac{\partial Q}{\partial \rho}\right)_T \left(\frac{\partial x}{\partial T}\right)_P + x \sum_{j=1}^7 \left(\frac{\partial y_j}{\partial T}\right)_P \left(\frac{\partial z_j}{\partial \rho}\right)_T + y_j \left(\frac{\partial\left(\frac{\partial z_j}{\partial \rho}\right)}{\partial T}\right)_P \quad (A-35)$$

where

$$\left(\frac{\partial\left(\frac{\partial z_j}{\partial \rho}\right)}{\partial T}\right)_P = \left(\frac{\partial\left(\frac{\partial u_j}{\partial \rho}\right)}{\partial T}\right)_P + \frac{w_j}{x} \left(\frac{\partial\left(\frac{\partial v}{\partial \rho}\right)}{\partial T}\right)_P + 2\left(\frac{\partial w_j}{\partial \rho}\right)_T \left(\frac{\partial v}{\partial T}\right)_P \quad (A-36)$$

in which

$$\left(\frac{\partial\left(\frac{\partial u_j}{\partial \rho}\right)}{\partial T}\right)_P = -\rho\alpha \left(\frac{\partial^2 u_j}{\partial \rho^2}\right)_T \quad (A-37)$$

and

$$\left(\frac{\partial\left(\frac{\partial v}{\partial \rho}\right)}{\partial T}\right)_P = -4.8\left(\frac{\partial v}{\partial T}\right)_P \quad (A-38)$$

Also,

$$\left(\frac{\partial\left(\frac{\partial^2 Q}{\partial \rho^2}\right)}{\partial T}\right)_P = \frac{1}{x} \left(\frac{\partial^2 Q}{\partial \rho^2}\right)_T \left(\frac{\partial x}{\partial T}\right)_P + x \sum_{j=1}^7 \left(y_j \left(\frac{\partial\left(\frac{\partial^2 z_j}{\partial \rho^2}\right)}{\partial T}\right)_P + \left(\frac{\partial y_j}{\partial T}\right)_P \left(\frac{\partial^2 z_j}{\partial \rho^2}\right)_T\right) \quad (A-39)$$

where

$$\begin{aligned} \left(\frac{\partial \left(\frac{\partial^2 z_j}{\partial \rho^2} \right)}{\partial T} \right)_P &= \left(\frac{\partial \left(\frac{\partial^2 u_j}{\partial \rho^2} \right)}{\partial T} \right)_P + 2 \left(\frac{\partial \left(\frac{\partial v}{\partial \rho} \right)}{\partial T} \right)_P \left(\frac{\partial w_j}{\partial \rho} \right)_T \\ &+ w_j \left(\frac{\partial \left(\frac{\partial^2 v}{\partial \rho^2} \right)}{\partial T} \right)_P + \left(\frac{\partial w_j}{\partial T} \right)_P \left(\frac{\partial^2 v}{\partial \rho^2} \right)_T \end{aligned} \quad (\text{A-40})$$

in which

$$\left(\frac{\partial \left(\frac{\partial^2 u_j}{\partial \rho^2} \right)}{\partial T} \right)_P = - \rho \alpha \left(\frac{\partial^3 u_j}{\partial \rho^3} \right)_T \quad (\text{A-41})$$

and

$$\left(\frac{\partial \left(\frac{\partial^2 v}{\partial \rho^2} \right)}{\partial T} \right)_P = - 4.8 \left(\frac{\partial \left(\frac{\partial v}{\partial \rho} \right)}{\partial T} \right)_P \quad (\text{A-42})$$

The first and second isochoric partial derivatives of equation (16) can be written as

$$\left(\frac{\partial Q}{\partial T} \right)_\rho = \left(\frac{\partial Q}{\partial T} \right)_P - x \sum_{j=1}^7 y_j \left(\frac{\partial z_j}{\partial T} \right)_P \quad (\text{A-43})$$

and

$$\begin{aligned} \left(\frac{\partial^2 Q}{\partial T^2} \right)_\rho &= \frac{Q}{x} \left(\frac{\partial^2 x}{\partial T^2} \right)_P + \frac{2}{x} \left(\frac{\partial x}{\partial T} \right)_P \left(\left(\frac{\partial Q}{\partial T} \right)_\rho - \frac{Q}{x} \left(\frac{\partial x}{\partial T} \right)_P \right) \\ &+ x \sum_{j=1}^7 z_j \left(\frac{\partial^2 z_j}{\partial T^2} \right)_P \end{aligned} \quad (\text{A-44})$$

Further,

$$\begin{aligned} \left(\frac{\partial \left(\frac{\partial Q}{\partial T} \right)_\rho}{\partial T} \right)_P &= \left(\frac{\partial^2 Q}{\partial T^2} \right)_P + \frac{1}{x} \left(\frac{\partial x}{\partial T} \right)_P \left(\left(\frac{\partial Q}{\partial T} \right)_\rho - \left(\frac{\partial Q}{\partial T} \right)_P \right) \\ &- x \sum_{j=1}^7 \left(y_j \left(\frac{\partial^2 z_j}{\partial T^2} \right)_P + \left(\frac{\partial y_j}{\partial T} \right)_P \left(\frac{\partial z_j}{\partial T} \right)_P \right) \end{aligned} \quad (\text{A-45})$$

and

$$\left(\frac{\partial\left(\frac{\partial Q}{\partial \rho}\right)_T}{\partial T}\right)_\rho = \frac{1}{x} \left(\frac{\partial Q}{\partial \rho}\right)_T \left(\frac{\partial x}{\partial T}\right)_P + x \sum_{j=1}^7 \left(\frac{\partial y_j}{\partial T}\right)_P \left(\frac{\partial z_j}{\partial \rho}\right)_T, \quad (\text{A-46})$$

from which it follows that

$$\begin{aligned} \left(\frac{\partial\left(\frac{\partial\left(\frac{\partial Q}{\partial \rho}\right)_T}{\partial T}\right)_\rho}{\partial T}\right)_P &= \frac{1}{x} \left(\frac{\partial Q}{\partial \rho}\right)_T \left(\frac{\partial^2 x}{\partial T^2}\right)_P + \frac{1}{x} \left(\frac{\partial x}{\partial T}\right)_P \left(\frac{\partial\left(\frac{\partial Q}{\partial \rho}\right)_T}{\partial T}\right)_P \\ &\quad + \left(\frac{\partial\left(\frac{\partial Q}{\partial \rho}\right)_T}{\partial T}\right)_\rho - \frac{2}{x} \left(\frac{\partial x}{\partial T}\right)_P \left(\frac{\partial Q}{\partial \rho}\right)_T \\ &\quad + x \sum_{j=1}^7 \left(\left(\frac{\partial y_j}{\partial T}\right)_P \left(\frac{\partial\left(\frac{\partial z_j}{\partial \rho}\right)_T}{\partial T}\right)_P + \left(\frac{\partial z_j}{\partial \rho}\right)_T \left(\frac{\partial^2 y_j}{\partial T^2}\right)_P\right). \end{aligned} \quad (\text{A-47})$$

The first and second partial derivatives of equation (15) with respect to temperature can be written as

$$\left(\frac{\partial \psi_0}{\partial T}\right)_\rho = \sum_{i=1}^6 \left((i-1) \underline{c}_i / (T \tau^{(i-1)})\right) + (\underline{c}_7 + 2\underline{c}_8) / T \quad (\text{A-48})$$

and

$$\begin{aligned} \left(\frac{\partial^2 \psi_0}{\partial T^2}\right)_\rho &= \sum_{i=1}^6 \left(\frac{(i-1)(i-2)}{T^2 \tau^{(i-1)}} \underline{c}_i\right) \\ &\quad - (\underline{c}_7 + 2\underline{c}_8) / T^2. \end{aligned} \quad (\text{A-49})$$

REFERENCES

- Adams, L. H., 1931, Equilibrium in binary systems under pressure. I. An experimental and thermodynamic investigation of the system NaCl-H₂O at 25°: *Am. Chem. Soc. Jour.*, v. 53, p. 3769-3813.
- Åkerlof, G. C., 1932, Dielectric constants of some organic solvent-water mixtures at various temperatures: *Am. Chem. Soc. Jour.*, v. 54, p. 4125-4139.
- Åkerlof, G. C., and Oshry, H. I., 1950, The dielectric constant of water at high temperatures and in equilibrium with its vapor: *Am. Chem. Soc. Jour.*, v. 72, p. 2844-2847.
- Al'tshuler, L. V., Bakanova, A. A., and Trunin, R. F., 1958, Phase transformations of water compressed by strong shock waves: *Soviet Physics Doklady*, v. 3, p. 761-763.
- Amagat, E. N., 1893, Elasticite et dilatibilite des fluides: *Annales de Chimie et Physique*, ser. 6, v. 29, p. 68-136; 505-574.
- Anderson, G. M., 1964, The calculated fugacity of water to 1000°C and 10,000 bars: *Geochim. et Cosmochim. Acta*, v. 28, p. 713-715.
- 1967, Specific volumes and fugacities of water, in Barnes, H. L., ed., *Geochemistry of hydrothermal ore deposits*: San Francisco, Calif., Holt, Rinehart and Wilson, p. 632-635.
- Arden, B. W., and Astill, K. N., 1970, *Numerical algorithms: origins and applications*: Menlo Park, Calif., Addison-Wesley, 308 p.
- Bain, R. W., ed., 1964, *Steam Tables 1964*: Edinburgh, Her Majesty's Stationery Office, Natl. Eng. Lab., Dept. Sci. Indus. Research, 147 p.
- Barker, J. A., and Henderson, D., 1972, The structure and properties of water and aqueous solutions: Washington, D.C., Dept. Interior, Office of Saline Water, Resources and Devel. Prog. Rept. No. 773, 41 p.
- Benson, S. W., 1968, *Thermochemical Kinetics*: New York, John Wiley and Sons, 223 p.
- Born, M., 1920, Volumen und Hydratationswärme der Ionen: *Zeitschr. Physik*, v. 1, p. 45-48.
- Bridgeman, P. W., 1913, The thermodynamic properties of liquid water to 80°C and 12,000 KGM: *Am. Acad. Arts and Sci. Proc.*, v. 48, p. 307-362.
- 1931, The volume of 18 liquids as a function of pressure: *Am. Acad. Arts and Sci. Proc.*, v. 66, p. 185-233.
- 1935, The pressure-volume-temperature relations of the liquid and the phase diagram of heavy water: *Jour. Chem. Physics*, v. 3, p. 597-605.
- Burnham, C. W., Holloway, J. R., and Davis, N. F., 1969a, The specific volume of water in the range 1060 to 8900 bars, 20° to 900° C: *Am. Jour. Sci.*, v. 267-A, Schairer, p. 70-95.
- 1969b, Thermodynamic properties of water to 1,000°C and 10,000 bars: *Geol. Soc. America Spec. Paper* 132, 96 p.
- Callendar, G. S., and Egerton, A. C., 1944, *The 1939 Callendar steam tables*: London, 1973 p.
- 1958, *Tables of total heat of steam*: Leatherhead, Surrey, Elec. Research Assoc., ERA Rept. J/T 173, 72 p.
- Carnot, S., 1824, *Reflexions sur la puissance motrice du feu*: Paris, Chez Bachelier Libraire.
- Cole, R. H., 1960, Dielectric polarization and loss: *Ann. Rev. Physics Chemistry*, v. 11, p. 149-168.
- David, H. D., and Hamann, S. D., 1959, The chemical effects of pressure, Part 5.—The electrical conductivity of water at high shock pressures: *Faraday Soc. Trans.*, v. 55, p. 72-77.
- 1960, The chemical effects of pressure, Part 6.—The electrical conductivity of several liquids at high shock pressures: *Faraday Soc. Trans.*, v. 56, p. 1043-1050.
- Dorsey, N. E., 1940, *Properties of ordinary water substance*: New York, Reinhold Publishing Corp., 673 p.
- Dudziak, K. H., and Franck, E. U., 1966, Messungen der Viskosität des Wassers bis 560°C und 3500 bar: *Ber. Bunsengesellschaft für phys. Chemie*, v. 70, p. 1120-1128.
- Dzung, L. S., and Rohrbach, U. W., 1955, *Enthalpie-Entropie Diagramme für Wasserdampf und Wasser*: Berlin, Springer.
- Fine, R. A., and Millero, F. J., 1973, Compressibility of water as a function of temperature and pressure: *Jour. Chem. Physics*, v. 59, p. 5529-5536.

- Fisher, J. R., and Barnes, H. L., 1972, The ion-product constant of water to 350°: Jour. Phys. Chemistry, v. 76, p. 90-99.
- Fogo, J. K., Benson, S. W., and Copeland, C. S., 1954, The electrical conductivity of supercritical solutions of sodium chloride and water: Jour. Chem. Physics, v. 22, p. 212-217.
- Franck, E. U., 1956, Hochverdichteter Wasserdampf II. Ionendissoziation von KCl in H₂O bis 750°C: Zeitschr. Phys. Chemie, v. 8, p. 107-126.
- 1961, Überkritisches Wasser als electrolytisches Lösungsmittel: Angew. Chemie, v. 73, p. 309-322.
- 1969, Ions in aqueous solutions at high temperatures and pressures: Jour. Chem. Physics, p. 9-18.
- Franks, F., ed., 1972, Water Volume I, The physics and chemistry of water: New York, Plenum Press, 596 p.
- Gier, T. E., and Young, H. S., 1963, private communication cited by Lawson, A. W., and Hughes, A. J., "High pressure properties of water", in Bradley, R. S., ed., High pressure physics and chemistry, v. I: New York, Acad. Press, p. 207-225.
- Gildseth, W., Habenschuss, A., and Spedding, F. H., 1972, Precision measurements of densities and thermal dilation of water between 5° and 80°C: Jour. Chem. Eng. Data, v. 17, p. 402-409.
- Goranson, R. W., 1938, Silicate-water systems; phase equilibrium in the NaAlSi₃O₈-H₂O and KAlSi₃O₈-H₂O systems at high temperatures and pressures: Am. Jour. Sci., 5th ser., v. 35-A, p. 71-91.
- 1942, Temperature-pressure-volume and phase relations of water, in Birch, F., ed., Handbook of Physical Constants: Geol. Soc. America Spec. Paper 36, p. 203-212.
- Greene, F. T., Beachey, J., Milne, T. A., 1972, An experimental study of the structure, thermodynamics and kinetic behavior of water: Washington, D.C., Dept. Interior, Office of Saline Water, Resources Devel. Prog. Rept. 772, 33 p.
- Grindley, T., and Lind, J. E., Jr., 1971, PVT Properties of water and mercury: Jour. Chem. Physics, v. 54, p. 3983-3989.
- Gurney, R. W., 1953, Ions in solution: Dover, N.Y., McGraw-Hill, 206 p.
- Haas, J. L., Jr., 1970, Fugacity of H₂O from 0° to 350°C at the liquid-vapor equilibrium and at 1 atmosphere: Geochim. et Cosmochim. Acta, v. 34, p. 929-932.
- Harris, F. E., Haycock E. W., and Alder, B. J., 1953, Dielectric polarization and structure of polar liquids under pressure: Jour. Chem. Physics, v. 21, p. 1943-1948.
- Hasted, J. B., 1961, The dielectric properties of water, in Birks, J. B., and Hard, J., eds., Progress in dielectrics, v. 3: London, Heywood and Co., p. 101-147.
- 1972, Liquid water: dielectric properties, in Franks, F., ed., Water, v. I, The Physics and chemistry of water: New York, Plenum, p. 255-309.
- Heger, K., ms, 1969, Die statische Dielektrizitätskonstante von Wasser und Methylalkohol im überkritischen Temperatur- und Druckbereich: Ph.D. dissert., Univ. Karlsruhe, Karlsruhe, West Germany, 59 p.
- Helgeson, H. C., and Kirkham, D. H., 1974, Theoretical prediction of the thermodynamic behavior of aqueous electrolytes at high pressures and temperatures: II. Debye-Hückel parameters for activity coefficients and relative partial molal properties of the solute: Am. Jour. Sci., v. 274, p. 1199-1261.
- 1975a, Theoretical prediction of the thermodynamic behavior of aqueous electrolytes at high pressures and temperatures. III. Equation of state for aqueous species at infinite dilution: Am. Jour. Sci., v. 275.
- 1975b, Theoretical prediction of the thermodynamic behavior of aqueous electrolytes at high pressures and temperatures. IV. Calculation of the thermodynamic properties of aqueous species and electrolyte solutions to 5 kb and 600°C: Am. Jour. Sci., v. 275.
- Holloway, J. R., Egger, D. H., and Davis, N. F., 1971, Analytical expression for calculating the fugacity and free energy of H₂O to 10,000 bars and 1,300°C: Geol. Soc. America Bull., v. 82, p. 2639-2642.
- Holser, W. T., 1954, Fugacity of water at high temperatures and pressures: Jour. Phys. Chemistry, v. 58, p. 316-317.
- Holser, W. T., and Kennedy, G. C., 1958, Properties of water. Part IV. Pressure-volume-temperature relations of water in the range 100-400°C and 100-1400 bars: Am. Jour. Sci., v. 256, p. 744-753.
- 1959, Properties of water. Part V. Pressure-volume-temperature relations of water in the range 400-1000°C and 100-1400 bars: Am. Jour. Sci., v. 257, p. 71-77.

- Holzappel, W., and Franck, E. U., 1966, Leitfähigkeit und Ionendissoziation des Wassers bis 1000°C und 100 kbar: Ber. Bunsengesellschaft für phys. Chemie, v. 70, p. 1105-1112.
- Horne, R. A., 1969, Marine chemistry: New York, John Wiley & Sons, 568 p.
- ed., 1972, Water and aqueous solutions: New York, John Wiley & Sons, 837 p.
- Howard J. C., 1961, Thermodynamic Data for Water: Washington, D.C., U.S. Dept. Commerce, Office Tech. Services, 15 p.
- International Formulation Committee, 1967, The 1968 IFC formulation for Industrial use: Düsseldorf, Germany, IFC Secretariat, Ver. Deutscher Ingenieure.
- 1968, The 1968 IFC formulation for scientific and general use: New York, Am. Soc. Mechanical Engineers, Secretariat, Internat. Conf. Properties of Steam.
- Jansone, V. M., and Franck, E. U., 1972, The dielectric constant of water to high temperatures and pressures from the mean spherical model in the wertheim solution: Ber. der Bunsengesellschaft für phys. Chemie, v. 76, p. 945.
- Juza, J., Kmoníček, V., and Sifner, O., 1966, An equation of state for water and steam: Prague, Československé Akad. VED, Acad. Nakladatelství, p. 131-142.
- Kay, R. L., Vidulich, G. A., and Pribadi, K. S., 1969, A reinvestigation of the dielectric constant of water and its temperature coefficient: Jour. Phys. Chemistry, v. 73, p. 445.
- Keenan, J. H., 1930, Steam tables and Mollier diagram: New York, Am. Soc. Mechanical Eng.
- Keenan, J. H., and Keyes, F. G., 1936, Thermodynamic Properties of Steam: New York, N.Y., John Wiley and Sons, Inc., 89 p.
- Keenan, J. H., Keyes, F. G., Hill, P. G., and Moore, J. G., 1969, Steam Tables: New York, John Wiley and Sons, Inc., 162 p.
- Kell, G. S., 1967, Precise representation of the volume properties of water at 1 atmosphere: Jour. Chem. Eng. Data, v. 12, no. 1, p. 66-70.
- 1972, Thermodynamic and transport properties of fluid water, in Franks, F., ed., Water, Vol. 1, The physics and chemistry of water: New York, Plenum Press, p. 363-412.
- Kell, G. S., McLaurin, G. E., and Whalley, E., 1968, Properties of water. II. Virial coefficients in the range 150° to 450°C without independent measurement of vapor volumes: Jour. Chem. Physics, v. 48, p. 3805-3813.
- Kell, G. S., and Whalley, E., 1965, The PVT properties of water. I. Liquid water in the temperature range 0 to 150°C and at pressures up to 1 kb: Royal Soc. London Philos. Trans., ser. A, Math. Phys. Sci., v. 258, p. 565-617.
- Kennedy, G. C., 1950, Pressure-volume-temperature relations in water at elevated temperatures and pressures: Am. Jour. Sci., v. 248, p. 540-564.
- 1957, Properties of water Part I. Pressure-volume-temperature relations in steam to 100°C and 100 bars pressure: Am. Jour. Sci., v. 255, p. 724-730.
- Kennedy, G. C., Knight, W. L., and Holser, W. T., 1958, Properties of water. Part III. Specific volume of liquid water to 100°C and 1400 bars: Am. Jour. Sci., v. 256, p. 590-595.
- Keyes, F. G., Smith, L.B., and Gerry, H. T., 1936, The specific volume of steam in the saturated and superheated condition together with derived values of the enthalpy, heat capacity, and Joule-Thompson coefficients. Part IV. Steam research program: Am. Acad. Arts and Sci. Proc., v. 70, p. 319-364.
- Kirkwood, J. G., 1939, The dielectric polarization of polar liquids: Jour. Chem. Physics, v. 7, p. 911-919.
- Knoblauch, O., Raisch, E., Hausen, H., and Koch, W., 1932, Tabellen und Diagramme für Wasserdampf: Munich and Berlin.
- Köster, H., and Franck, E. U., 1969, Das spezifische Volumen des Wassers bei hohen Drucken bis 600°C und 10 kbar: Ber. der Bunsengesellschaft für phys. Chemie, v. 73, p. 716-722.
- Kyropoulos, S., 1926, Die Druckabhängigkeit der Dielektrizitätskonstante einiger Flüssigkeiten bis zu 3000 kg/cm²: Zeitschr. Physik., v. 40, p. 507-515.
- Latimer, W. M., 1952, The oxidation states of the elements and their potentials in aqueous solutions: Englewood Cliffs, N.J., Prentice Hall, 392 p.
- Lees, W. L., ms, 1949, Dielectric constants, as functions of pressure and temperature, of water and three alkyl halides: Ph.D. dissert., Harvard Univ., Dept. Physics, Cambridge, Mass.

- Maier, S., and Franck, E. U., 1966, Die dichte des wassers von 200 bis 850°C und von 1000 bis 6000 bar: *Ber. der Bunsengesellschaft für phys. Chemie*, v. 70, p. 639-645.
- Malmberg, C. G., and Maryott, A. A., 1956, Dielectric constant of water from 0° to 100°C: *Natl. Bur. Standards Jour. Research*, Research Paper 2641, v. 56, p. 1-8.
- Meyer, C. A., McClintock, R. B., Silvestri, G. J., and Spencer, R. C., Jr., eds., 1967, *Thermodynamic and Transport Properties of Steam*: New York, Am. Soc. Mechanical Eng., 328 p.
- Millero, F. J., Curry, R. W., and Drost-Hansen, W., 1969, Isothermal compressibility of water at various temperatures: *Jour. Chem. Eng. Data.*, v. 14, p. 422-425.
- Millero, F. J., Hoff, E. V., and Kahn, L., 1972, The effect of pressure on the ionization of water at various temperatures from molal-volume data: *Jour. Solution Chemistry*, v. 1, p. 309-327.
- Millero, F. J., Knox, J. H., and Emmet, R. T., 1972, A high-precision, variable-pressure magnetic float densimeter: *Jour. Solution Chemistry*, v. 1, p. 173-186.
- Mollier, R., 1932, *Neue Tabellen und Diagramme für Wasserdampf*: Berlin.
- Nowak, E. S., and Grosh, R. J., 1961, An analyses of specific heat data for water and water vapor in the critical region: Argonne Natl. Lab. Tech. Rept. 8, 79 p.
- Oshry, H. I., ms, 1949, The dielectric constant of saturated water from the boiling point to the critical point: Ph.D. dissert., Univ. Pittsburgh, Pittsburgh, Penn., 13 p.
- Oster G., and Kirkwood, J. G., 1943, The influence of hindered molecular rotation on the dielectric constants of water, alcohols, and other polar liquids: *Jour. Chem. Physics*, v. 11, p. 175-178.
- Owen, B. B., Miller, R. C., Milner, C. E., and Cogan, H. L., 1961, The dielectric constant of water as a function of temperature and pressure: *Jour. Phys. Chemistry*, v. 65, p. 2065-2070.
- Owen, B. B., White, J. R., and Smith, J. S., 1956, An evaluation of the density of water at 5° intervals between 45 and 85°: *Am. Chem. Soc. Jour.*, v. 78, p. 3561-3564.
- Papetti, R. A., and Fujisaki, M. C., 1971, Equation of state of water at high temperatures and pressures: U.S. Natl. Tech. Inf. Service, AD Rept. 729757, 77 p.
- Parker, V. B., Wagman, D. D., and Evans, W. H., 1971, Selected values of chemical thermodynamic properties, Part 6: *Natl. Bur. Standards Tech. Note* 270-6, 119 p.
- Pistorius, C. W. F. T., and Sharp, W. E., 1960, Properties of water. Pt. VI, Entropy and Gibbs free energy of water in the range 10-1000°C and 1-250,000 bars: *Am. Jour. Sci.*, v. 258, p. 757-768.
- 1961, Erratum—Properties of water. Pt. VI, Entropy and Gibbs free energy of water in the range 10-1000°C and 1-250,000 bars, a clarification: *Am. Jour. Sci.*, v. 259, p. 397-398.
- Quist, A. S., 1970, The ionization constant of water to 800° and 4000 bars: *Jour. Phys. Chemistry*, v. 74, p. 3396-3402.
- Quist, A. S., and Marshall, W. L., 1965, Estimation of the dielectric constant of water to 800°: *Jour. Phys. Chemistry*, v. 69, p. 3165-3167.
- Rice, M. H., and Walsh, J. M., 1957, Equation of state of water to 250 kilobars: *Jour. Chem. Physics*, v. 26, p. 824-830.
- Robie, R. A., and Waldbaum, D. R., 1968, Thermodynamic properties of minerals and related substances at 298.15°K (25°C) and one atmosphere (1.013 bars) pressure and at higher temperatures: U.S. Geol. Survey Bull. 1259, 256 p.
- Rowe, A. M., Jr., and Chou, J. C. S., 1970, Pressure-volume-temperature-concentration relation of aqueous NaCl solutions: *Jour. Chem. Eng. Data*, v. 15, p. 61-66.
- Scaife, B. K. P., 1955, Isothermal pressure dependence of the dielectric properties of eugenol, glycerol, and water: *Physics. Soc. (London) Proc.*, v. B 68, p. 790-799.
- Schall, R., 1950, Die Zustandsgleichung des Wassers bei hohen Drucken nach Röntgenblitzaufnahmen intensiver Stosswellen: *Zeitschr. angew. Physics*, v. 2, p. 252-254.
- Schmidt, E., 1969, *Properties of water and steam in SI units*: New York, Springer-Verlag, 205 p.
- Sen, U., and Cobble, J. W., ms, 1974, A unified approach to the theory of electrolytes in water (in preparation).
- Sengers, J. M. H., and Greer, S. C., 1972, Thermodynamic anomalies near the critical point of steam: *Jour. Heat and Mass Transfer*, v. 15, p. 1865-1886.
- Sharp, W. E., 1962, The thermodynamic functions for water in the range -10 to 1000°C and 1 to 250,000 bars: Livermore, Calif., Univ. California Lawrence Radiation Lab., UCRL-7118, 51 p.

- Smith, L. B., and Keyes, F. G., 1934, The volumes of unit mass liquid water and their correlation as a function of pressure and temperature. Part III. Steam Research Program: Am. Acad. Arts and Sci. Proc., v. 69, p. 285-312.
- Stull, D. R., and Prophet, H., 1971, JANAF thermochemical tables, 2d ed.: Natl. Bur. Standards, Natl. Standards Reference Data Ser., NBS 37, 1141 p.
- Tammann, G., and Rührenbeck, Ad., 1932, Die spezifischen Volumen des Wassers zwischen 20° und 650°, die des Äthyläthers und des Äthylalkohols zwischen 20° und 500° bei Drucken von 1-2500 Kg/cm²: Annalen Physik, v. 5, p. 63-79.
- Tödheide, K., 1972, Water at high temperatures and pressures, in Franks, F., ed., Water, v. I. The physics and chemistry of water: New York, Plenum, p. 463-514.
- Vidulich, G.A., Evans, D. F., and Kay, R. L., 1967, The dielectric constant of water and heavy water between 0° and 40°: Jour. Phys. Chemistry, v. 71, p. 656-662.
- Vidulich, G. A., and Kay, R. L., 1962, The dielectric constant of water between 0° and 40°: Jour. Phys. Chemistry, v. 66, p. 383.
- Vukalovich, M. P., 1958, Thermodynamische Eigenschaften des Wassers und des Wasserdampfes: Moscow and Berlin, VEB Verlag Technik.
- Vukalovich, M. P., Zubarev, V. N., Alexandrov, A. A., and Kalinin, Y. Y., 1959, Experimental determination of the specific volume of water under pressures up to 1200 kg/cm² at 300°C (in Russian): Teploenergetika, v. 6, no. 10, p. 74-102.
- Wagman, D. D., Evans, W. H., Halow, I., Parker, V. B., Bailey, S. M., and Schumm, R. H., 1965, Selected values of chemical thermodynamic properties Part I: Natl. Bur. Standards Tech. Note 270-1, 124 p.
- 1966, Selected values of chemical thermodynamic properties, Part 2: Natl. Bur. Standards Tech. Note 270-2, 62 p.
- 1968, Selected values of chemical thermodynamic properties, Part 3: Natl. Bur. Standards Tech. Note 270-3, 264 p.
- 1969, Selected values of chemical thermodynamic properties, Part 4: Natl. Bur. Standards Tech. Note 270-4, 152 p.
- Wagman, D. D., Evans, W. H., Parker, V. B., Halow, I., Bailey, S. M., Schumm, R. H., and Churney K. L., 1971, Selected values of chemical thermodynamic properties, Part 5: Natl. Bur. Standards Tech. Note 270-5, 49 p.
- Walsh, J. M., and Rice, M. H., 1957, Dynamic compression of liquids from measurements on strong shock waves: Jour. Chem. Physics, v. 26, p. 815-823.
- Wang, D. P., and Millero, F. J., 1973, Precise representation of the P-V-T properties of water and seawater determined from sound speeds: Jour. Geophys. Research, v. 78, p. 7122-7128.
- Whitfield, M., 1972, Self-ionization of water in dilute sodium chloride solutions from 5-35°C and 1-2000 bars: Jour. Chem. Eng. Data, v. 17, p. 124-128.
- Wyman, J. W., Jr., 1930, Measurements of the dielectric constants of conducting media: Phys. Rev., v. 35, p. 623-634.
- Wymann, J. W., and Ingalls, E. N., 1938, The dielectric constant of deuterium oxide: Am. Chem. Soc. Jour., v. 60, p. 1182-1184.